



THESIS

**SYNTHESIS, CHARACTERIZATION AND APPLICATION OF
COMPLEX BETWEEN 3-(2'-THIAZOLYLAZO)-2,6-
DIAMINOPYRIDINE AND RUTHENIUM(III)**

RATANON CHOTIMA

**GRADUATE SCHOOL, KASETSART UNIVERSITY
2008**



THESIS APPROVAL
GRADUATE SCHOOL, KASETSART UNIVERSITY

Master of Science (Chemistry)

DEGREE

Chemistry

FIELD

Chemistry

DEPARTMENT

TITLE: Synthesis, Characterization and Application of Complex between
3-(2'-Thiazolylazo)-2,6-Diaminopyridine and Ruthenium(III)

NAME: Mr. Ratanon Chotima

THIS THESIS HAS BEEN ACCEPTED BY

_____ **THESIS ADVISOR**

(Associate Professor Apisit Songsasen, Ph.D.)

_____ **THESIS CO-ADVISOR**

(Assistant Professor Waraporn Parasuk, Dr.rer.nat.)

_____ **DEPARTMENT HEAD**

(Assistant Professor Noojaree Prasitpan, Ph.D.)

APPROVED BY THE GRADUATE SCHOOL ON _____

_____ **DEAN**

(Associate Professor Gunjana Theeragool, D.Agr.)

THESIS

SYNTHESIS, CHARACTERIZATION AND APPLICATION OF
COMPLEX BETWEEN 3-(2'-THIAZOLYLAZO)-2,6-
DIAMINOPYRIDINE AND RUTHENIUM(III)

RATANON CHOTIMA

A Thesis Submitted in Partial Fulfillment of
the Requirements for the Degree of
Master of Science (Chemistry)
Graduate School, Kasetsart University

2008

Ratanon Chotima 2008: Synthesis, Characterization and Application of Complex between 3-(2'-Thiazolylazo)-2,6-Diaminopyridine and Ruthenium(III). Master of Science (Chemistry), Major Field: Chemistry, Department of Chemistry. Thesis Advisor: Associate Professor Apisit Songsasen, Ph.D. 141 pages.

3-(2'-thiazolylazo)-2,6-diaminopyridine (TADAP) was synthesized by diazotization of 2-aminothiazole and coupling with 2,6-diaminopyridine. FT-IR, ¹H-NMR, mass spectroscopy and elemental analysis were used to identify the structure of TADAP. The complex between TADAP and ruthenium(III) was prepared by refluxing TADAP and RuCl₃·xH₂O in tetrahydrofuran for 8 hours which gave red-brown complex at pH 7.0. The stoichiometric ratio of ruthenium(III) and TADAP was 1:2 with the stability constant 3.33×10⁸. FT-IR and ¹H-NMR were used to determine the structure of the complex which was confirmed by quantum chemical calculation at B3LYP level of theory using 6-31G* basis set for all atoms and SDD basis set with Stuttgart/Dresden electron core potential for ruthenium atom. It was found that [Ru(TADAP)₂Cl₂]⁺ was the most stable complex with the stabilization energy -1198.15 kcal/mol.

TADAP was immobilized on silica gel and gave the chelating resin (TADAP-SG) which had adsorption ability of ruthenium(III). The appropriate condition of the adsorption of ruthenium(III) was determined by batch equilibrium experiment. The capacity of TADAP-SG was 2.9022 mmol/g. 0.1 M thiourea was used as the eluent for the desorption of ruthenium(III) from TADAP-SG and TADAP-SG had an efficiency to reuse up to 3 times. TADAP-SG has great affinity for ruthenium(III) more than palladium(II), gold(III), iron(III) and copper(II). In addition, there might be an interaction between the complex and calf thymus DNA in Tris-HCl buffer pH 7.4 due to the precipitate and absorbance changing.

Student's signature

Thesis Advisor's signature

____ / ____ / ____

ACKNOWLEDGEMENTS

I wish to express my sincere gratitude to my supervisor, Associate Professor Dr. Apisit Songsasen for his unwavering support and continuously valuable guidance throughout the duration of my graduate study and research. I also wish to express my appreciation of my advisory committee Assistant Professor Dr. Waraporn Parasuk for her tremendous support and meticulous attention on the quantum chemical calculation part.

In addition, special thanks are extended to Dr. Pensri Bunsawansong for her kind to use nuclear magnetic resonance spectrometer and also Miss Praewpilin Kangvansura for her guidance to use atomic absorption spectrophotometer and mass spectrometer.

I would also like to thank all of staffs at Department of Chemistry, Faculty of Science, Kasetsart University for their kind helps in everything that they can.

Besides, I would like to thank the Thesis and Dissertation Support Fund, Graduate School of Kasetsart University, the Development and Promotion of Science and Technology Talents Project (DPST) and Center for Innovation in Chemistry: Postgraduate Education and Research Program in Chemistry (PERCH-CIC) for financial support and the Department of Chemistry, Faculty of Science, Kasetsart University for research facilities.

Last but not least, I wish to express my great appreciation and my gratitude to my family for their hard work, advice, encouragement, understanding and the financial assistance, which made my graduate study possible and I would like to thank all of my friends for their support and unconditional friendship.

Ratanon Chotima

April, 2008

TABLE OF CONTENTS

		Page
TABLE OF CONTENTS		i
LIST OF TABLES		ii
LIST OF FIGURES		v
LIST OF ABBREVIATIONS		x
INTRODUCTION		1
OBJECTIVES		16
LITERATURE REVIEW		17
MATERIALS AND METHODS		31
Materials		31
Methods		34
RESULTS AND DISCUSSION		44
CONCLUSION		94
LITERATURE CITED		95
APPENDICES		105
Appendix A	Calculation of stability constant by continuous variation method	106
Appendix B	Calculation of stability constant by Benesi-Hildebrand's equation	109
Appendix C	Determination of stabilization energies by quantum chemical calculation and the output data of all complexes optimized by Gaussian 03	112
Appendix D	Nucleic Acid Purity Assessment Using A260/A280 Ratios	133
Appendix E	Calculation of the percentage of elements of TADAP	139

LIST OF TABLES

Table		Page
1	Some properties of an element ruthenium.	2
2	The buffer solutions which were prepared and used in this work.	35
3	The elemental analysis of 3-(2'-thiazolylazo)-2,6-diaminopyridine (TADAP).	49
4	Complex formation between ruthenium(III) and TADAP at pH 3.0-7.0.	54
5	Conductance of mixture solution of 1000 ppm ruthenium(III) and TADAP at various mole ratios.	57
6	Hard and soft bases.	60
7	Hard and soft acids.	60
8	Data from the IR spectra of TADAP and ruthenium(III)-TADAP complex.	63
9	Data from the ¹ H NMR spectra of TADAP and ruthenium(III)-TADAP complex.	64
10	Selected bond lengths of TADAP and TADAP in [Ru(TADAP) ₂] ³⁺ , [Ru(TADAP) ₂ Cl ₂] ⁺ and [Ru(TADAP) ₂ (H ₂ O) ₂] ³⁺ .	68
11	Selected bond angles between ruthenium atom and donor atoms in [Ru(TADAP) ₂] ³⁺ , [Ru(TADAP) ₂ Cl ₂] ⁺ and [Ru(TADAP) ₂ (H ₂ O) ₂] ³⁺ .	69
12	Selected bond lengths of a ruthenium atom and a donor atom in [Ru(TADAP) ₂] ³⁺ , [Ru(TADAP) ₂ Cl ₂] ⁺ and [Ru(TADAP) ₂ (H ₂ O) ₂] ³⁺ .	70
13	Selected torsion angles of TADAP in [Ru(TADAP) ₂] ³⁺ , [Ru(TADAP) ₂ Cl ₂] ⁺ and [Ru(TADAP) ₂ (H ₂ O) ₂] ³⁺ .	70
14	Selected bond lengths of N–C, N=N, and N–H in TADAP and TADAP in complexes [Ru(TADAP) ₂] ³⁺ , [Ru(TADAP) ₂ Cl ₂] ⁺ and [Ru(TADAP) ₂ (H ₂ O) ₂] ³⁺ .	72

LIST OF TABLES (Continued)

Table		Page
15	Energies of atoms, molecules and possible structures of ruthenium(III)-TADAP complexes and stabilization energies of possible structures of ruthenium(III)-TADAP complexes obtained by the calculation on Gaussian03 at B3LYP level of theory using 6-31G* and SDD basis sets.	74
16	Energies of atoms, molecules, adenine base, guanine base, and compounds of $[\text{Ru}(\text{TADAP})_2]^{3+}$, $[\text{Ru}(\text{TADAP})_2\text{Cl}]^{2+}$ $[\text{Ru}(\text{TADAP})_2(\text{H}_2\text{O})]^{3+}$ with adenine and guanine base obtained by the calculation on Gaussian03 at B3LYP level of theory using 6-31G* and SDD basis sets.	85

Appendix Table

C1	Potential energies and stabilization energies of all species obtained at B3LYP level with 6-31G* and SDD basis sets.	114
C2	The standard orientation of TADAP.	116
C3	The optimized bond length of TADAP.	116
C4	The optimized bond angle of TADAP.	117
C5	The optimized torsion angle of TADAP.	117
C6	The standard orientation of adenine.	118
C7	The standard orientation of guanine.	119
C8	The standard orientation of $[\text{Ru}(\text{TADAP})\text{Cl}]^{2+}$.	120
C9	The optimized bond length of $[\text{Ru}(\text{TADAP})\text{Cl}]^{2+}$.	120
C10	The optimized bond angle of $[\text{Ru}(\text{TADAP})\text{Cl}]^{2+}$.	120
C11	The optimized torsion angle of $[\text{Ru}(\text{TADAP})\text{Cl}]^{2+}$.	121
C12	The standard orientation of $[\text{Ru}(\text{TADAP})\text{H}_2\text{O}]^{3+}$.	122
C13	The optimized bond length of $[\text{Ru}(\text{TADAP})\text{H}_2\text{O}]^{3+}$.	122

LIST OF TABLES (Continued)

Appendix Table		Page
C14	The optimized bond angle of $[\text{Ru}(\text{TADAP})\text{H}_2\text{O}]^{3+}$.	122
C15	The optimized torsion angle of $[\text{Ru}(\text{TADAP})\text{H}_2\text{O}]^{3+}$.	123
C16	The standard orientation of $[\text{Ru}(\text{TADAP})_2]^{3+}$.	124
C17	The optimized bond length of $[\text{Ru}(\text{TADAP})_2]^{3+}$.	124
C18	The optimized bond angle of $[\text{Ru}(\text{TADAP})_2]^{3+}$.	125
C19	The optimized torsion angle of $[\text{Ru}(\text{TADAP})_2]^{3+}$.	126
C20	The standard orientation of $[\text{Ru}(\text{TADAP})_2\text{Cl}_2]^+$.	127
C21	The optimized bond length of $[\text{Ru}(\text{TADAP})_2\text{Cl}_2]^+$.	128
C22	The optimized bond angle of $[\text{Ru}(\text{TADAP})_2\text{Cl}_2]^+$.	128
C23	The optimized torsion angle of $[\text{Ru}(\text{TADAP})_2\text{Cl}_2]^+$.	129
C24	The standard orientation of $[\text{Ru}(\text{TADAP})_2(\text{H}_2\text{O})_2]^{3+}$.	130
C25	The optimized bond length of $[\text{Ru}(\text{TADAP})_2(\text{H}_2\text{O})_2]^{3+}$.	131
C26	The optimized bond angle of $[\text{Ru}(\text{TADAP})_2(\text{H}_2\text{O})_2]^{3+}$.	131
C27	The optimized torsion angle of $[\text{Ru}(\text{TADAP})_2(\text{H}_2\text{O})_2]^{3+}$.	132

LIST OF FIGURES

Figure		Page
1	Examples of ruthenium anticancer complexes.	7
2	General structure of thiazolylazo dyes. G may be H, OH, NH ₂ , SO ₃ H, halogen atom or other groups.	8
3	The structure of 3-[<i>N,N</i> -ethyl-met-azo]-2,6-diaminopyridine (2,6-DAPEMA).	20
4	The five possible [Ru(azpy) ₂ Cl ₂] isomers, with a systematic three-letter code indicating the <i>cis</i> (<i>c</i>), or <i>trans</i> (<i>t</i>) geometries of the chlorides (Cl), the pyridine (N _p) and the azo nitrogen (N _a), respectively.	20
5	Three structures of [Ru(apy)(tpy)L ^{<i>n</i>-}](ClO ₄) _(2-<i>n</i>) ; L = Cl, H ₂ O, CH ₃ CN (1a-1c).	21
6	Structure of bis-[5-(4'-R-phenylazo)-8-hydroxyquinoline] ruthenium.	23
7	The schematic structure of α-[Ru(azpy) ₂ Cl ₂].	26
8	Synthesis pathway of 3-(2'-thiazolylazo)-2,6-diaminopyridine (TADAP).	44
9	IR spectrum of 3-(2'-thiazolylazo)-2,6-diaminopyridine (TADAP).	47
10	¹ H NMR spectrum of 3-(2'-thiazolylazo)-2,6-diaminopyridine (TADAP).	48
11	ESI-Mass spectrum of 3-(2'-thiazolylazo)-2,6-diaminopyridine (TADAP).	49
12	Pathway of the fragmentation of 3-(2'-thiazolylazo)-2,6-diaminopyridine (TADAP).	50
13	Absorption spectra of TADAP and Ru(III)-TADAP complex at pH 3.0.	51
14	Absorption spectra of TADAP and Ru(III)-TADAP complex at pH 4.0.	52
15	Absorption spectra of TADAP and Ru(III)-TADAP complex at pH 5.0.	52

LIST OF FIGURE (Continued)

Figure		Page
16	Absorption spectra of TADAP and Ru(III)-TADAP complex at pH 6.0.	53
17	Absorption spectra of TADAP and Ru(III)-TADAP complex at pH 7.0.	53
18	Tanabe-Sugano diagram of d^5 electron configuration (Kettle, 1998).	55
19	Absorption spectrum of 4.0×10^{-5} M ruthenium(III)-TADAP complex at pH 7.0.	55
20	Continuous variation plot of complex between ruthenium(III) and TADAP in phosphate buffer at pH 7.0.	57
21	The plot between conductances of mixture solution of 1000 ppm ruthenium(III) and TADAP at various mole ratios.	58
22	Postulated structures of complexes between ruthenium(III) and TADAP.	61
23	Infrared spectra of (a) TADAP and (b) ruthenium(III)-TADAP complex.	63
24	^1H NMR spectra (DMSO-d_6) of TADAP and ruthenium(III)-TADAP complex.	64
25	The optimized structure of TADAP (GaussView 3.09).	66
26	The optimized structure of $[\text{Ru}(\text{TADAP})_2]^{3+}$ (GaussView 3.09).	67
27	The optimized structure of $[\text{Ru}(\text{TADAP})_2\text{Cl}_2]^+$ (GaussView 3.09).	67
28	The optimized structure of $[\text{Ru}(\text{TADAP})_2(\text{H}_2\text{O})_2]^{3+}$ (GaussView 3.09).	68
29	Geometry of coordinated bond between ruthenium atom and donor atoms in (a) $[\text{Ru}(\text{TADAP})_2]^{3+}$, (b) $[\text{Ru}(\text{TADAP})_2\text{Cl}_2]^+$, and (c) $[\text{Ru}(\text{TADAP})_2(\text{H}_2\text{O})_2]^{3+}$.	72
30	The optimized structure of $[\text{Ru}(\text{TADAP})\text{Cl}]^{2+}$ (GaussView 3.09).	73
31	The optimized structure of $[\text{Ru}(\text{TADAP})\text{H}_2\text{O}]^{3+}$ (GaussView 3.09).	73

LIST OF FIGURE (Continued)

Figure		Page
32	Relationship between absorbance of ruthenium(III)-TADAP complex and time.	75
33	Absorption spectra of calf thymus DNA at various concentrations.	77
34	Absorption spectra of 4.0×10^{-5} M ruthenium(III)-TADAP complex in various concentrations of calf thymus DNA.	77
35	The five coordinated complex of $[\text{Ru}(\text{TADAP})_2]^{3+}$ by rotating the C–N bond.	79
36	The five coordinated complex of $[\text{Ru}(\text{TADAP})_2\text{Cl}_2]^+$ by removing Cl ⁻ ion.	79
37	The five coordinated complex of $[\text{Ru}(\text{TADAP})_2(\text{H}_2\text{O})_2]^{3+}$ by removing H ₂ O molecule.	80
38	The available donor atom of adenine base (the nitrogen atom in a circle).	80
39	The available donor atom of guanine base (the nitrogen atom in a circle).	81
40	The optimized structure of $[\text{Ru}(\text{TADAP})_2]^{3+}$ bonding with adenine base.	81
41	The optimized structure of $[\text{Ru}(\text{TADAP})_2\text{Cl}]^{2+}$ bonding with adenine base.	82
42	The optimized structure of $[\text{Ru}(\text{TADAP})_2\text{H}_2\text{O}]^{3+}$ bonding with adenine base.	82
43	The optimized structure of $[\text{Ru}(\text{TADAP})_2]^{3+}$ bonding with guanine base.	83
44	The optimized structure of $[\text{Ru}(\text{TADAP})_2\text{Cl}]^{2+}$ bonding with guanine base.	83
45	The optimized structure of $[\text{Ru}(\text{TADAP})_2\text{H}_2\text{O}]^{3+}$ bonding with guanine base.	84

LIST OF FIGURE (Continued)

Figure		Page
46	Stabilization energy of six, five coordinated complexes and the complexes with nucleobase adenine and guanine.	86
47	Synthesis pathway of 3-(2'-thiazolylazo)-2,6-diaminopyridine resin.	88
48	Effect of pH on the adsorption of ruthenium(III) by TADAP-SG.	89
49	Effect of shaking time on the adsorption of ruthenium(III) by TADAP-SG.	90
50	Desorption efficiency of ruthenium(III) from TADAP-SG by 8 eluents.	91
51	Adsorption efficiency (%) for ruthenium(III) of TADAP-SG that had been used 1 to 3 times.	92
52	Adsorption capacity of TADAP-SG of 20 ppm of each metal ion at pH 7.0.	93

Appendix Figure

A1	The relationship between $[\text{Ru(III)}]/A$ and $1/[\text{TADAP}]^2$.	111
C2	The optimized structure of TADAP.	116
C3	The optimized structure of adenine.	118
C4	The optimized structure of guanine.	119
C5	The optimized structure of $[\text{Ru(TADAP)Cl}]^{2+}$.	119
C6	The optimized structure of $[\text{Ru(TADAP)H}_2\text{O}]^{3+}$.	121
C7	The optimized structure of $[\text{Ru(TADAP)}_2]^{3+}$.	123
C8	The optimized structure of $[\text{Ru(TADAP)}_2\text{Cl}_2]^+$.	127
C9	The optimized structure of $[\text{Ru(TADAP)}_2(\text{H}_2\text{O})_2]^{3+}$.	130
D10	Absorbance profiles of DNA and protein samples from 240 nm to 290 nm.	135

LIST OF FIGURE (Continued)

Appendix Figure		Page
D11	A ₂₈₀ ratio of samples containing DNA and/or protein at wavelengths from 240 nm to 290 nm.	136
D12	Comparison of theoretical A ₂₆₀ /A ₂₈₀ ratios with those determined using the PowerWave 200 scanning microplate spectrophotometer.	136

LIST OF ABBREVIATIONS

B3LYP	=	Becke-Lee, Yang and Parr correlation functional
CT-DNA	=	Calf thymus DNA
DFT	=	Density Functional Theory
DMSO-d ⁶	=	Dimethylsulfoxide, D-6
ESI-MS	=	Electrospray Ionization Mass Spectroscopy
FT-IR	=	Fourier Transform Infrared Spectrophotometry
¹ H NMR	=	Proton Nuclear Magnetic Resonance Spectroscopy
KHP	=	Potassium Hydrogen Phthalate
SDD	=	Stuttgart/Dresden basis set
TADAP	=	3-(2'-thiazolylazo)-2,6-diaminopyridine
TADAP-SG	=	3-(2'-thiazolylazo)-2,6-diaminopyridine resin
Tris-HCl	=	trishydroxymethylaminomethane hydrochloride

SYNTHESIS, CHARACTERIZATION AND APPLICATION OF COMPLEX BETWEEN 3-(2'-THIAZOLYLAZO)-2,6- DIAMINOPYRIDINE AND RUTHENIUM(III)

INTRODUCTION

1. Ruthenium

Ruthenium was discovered by J. A. Sniadecki in 1808 in Poland, but not recognized as an element. K. K. Klaus, the Russian chemist, is generally recognized as the discoverer, as in 1844, he purified the metal from impure oxide. The name "Ruthenium" is derived from the Latin "Ruthenia". It is a member of group 8 metals triad which is considerable properties as borderline acid. The properties of ruthenium are shown in Table 1. The appearance of ruthenium is lustrous and silvery in color like iron and osmium in the same group. The solid ruthenium has hcp (hexagonal closed-pack) structure. Ruthenium, one of platinum group metals, is generally found with other platinum metals and coinage metals. It is the rare earth metal, its estimated abundance in the earth's crust is 0.0001 ppm.

The method for ruthenium preparation is usually removed by distillation of its tetroxide after the initial dissolution with hydrochloric acid and chlorine. Collection of the tetroxide in alcoholic sodium hydroxide and aqueous hydrochloric acid respectively yields $(\text{NH}_4)_3\text{RuCl}_6$ from which the metal is by ignition in H_2 . The metal is in the form of powder or sponge and is usually consolidated by powder-metallurgical techniques.

Table 1 Some properties of an element ruthenium.

Properties	Value
Atomic symbol	Ru
Atomic number	44
Atomic weight/g mol ⁻¹	101.07
Electronic configuration	[Kr]4d ⁷ 5s ¹
Density(20°C)/g cm ⁻³	12.37
Melting point/°C	2282(±20)
Boiling point/°C	extrap 4050(±100)
ΔH_{fus} / kJ mol ⁻¹	~25.5
ΔH_{vap} / kJ mol ⁻¹	--
ΔH_f (monoatomic gas)/ kJ mol ⁻¹	640
Electronegativity (Pauling Scale)	2.2
Electrical resistivity (20°C)/μΩ cm	6.71
Number of naturally occurring isotopes	7
Metal radius (12-coordinate)/pm	134
Effective ionic radius/pm	
VIII (6-coordinate)	36
VI (6-coordinate)	38
V (4-coordinate)	56.5
IV (4-coordinate)	62
III (4-coordinate)	68

Source: Greenwood (1997)

Ruthenium is not a reactive element of the triad, it virtually unaffected by non-oxidizing acids, or even aqua regia (conc. HNO₃ + conc. HCl). As same as iron, ruthenium reacts easily with most non-metals but only in high temperature, except in the case of oxidizing agents such as F₂ and Cl₂.

The known highest oxidation state of ruthenium is +8 in RuO_4 . But generally, the most common oxidation state for ruthenium is +3. The coordination numbers of ruthenium compounds are naturally 6 for octahedral compounds, 4 for tetrahedral and 5 for trigonal bipyramid.

2. Compounds of ruthenium

The lowest oxidation state of ruthenium in which they form oxides is +4. RuO_2 is a blue to black solid and has the rutile structure. The intense color arises from the presence of small amounts of ruthenium in another oxidation state, possibly +3. The most interesting oxide is the volatile and yellow RuO_4 with octahedral structure. It will be decomposed explosively to RuO_2 when heat above 100°C . In addition, ruthenium forms only a disulfide compound with the pyrite structure and diamagnetic semiconductor.

Ruthenium can be formed oxoanion compounds; $[\text{RuO}_4]^-$ and $[\text{RuO}_4]^{2-}$. The black crystal $\text{K}[\text{RuO}_4]$ (perruthenate) is synthesized by dissolving RuO_4 in cold dilute KOH or oxidizing aqueous K_2RuO_4 by chlorine. $\text{K}_2[\text{RuO}_4]$ (ruthenate) is obtained from fusing ruthenium metal with KOH and KNO_3 (Luoma and Brubaker, 1966). Moreover, mixed metal oxides of ruthenium can be made by heating the metal with appropriate alkali or alkali earth oxides such as “ruthenite” $\text{M}^{2+}\text{Ru}^{4+}\text{O}_3$. Ru(V) has been established by ^{99}Ru Mössbauer spectroscopy as a common stable oxidation state in mixed oxides such as $\text{Na}_3\text{Ru}^{5+}\text{O}_4$ and $\text{Na}_4\text{Ru}_2^{5+}\text{O}_7$ (Gibb *et al.*, 1980).

The well known halide compound of ruthenium is RuCl_3 which is the anhydrous compound. This compound exists in two forms: the α -form and the β -form. The β -form is prepared by heating ruthenium metal at 330°C in CO and Cl_2 which produces the dark-brown substance. The black α -form is formed when heated the β -form above 450°C in Cl_2 (Hyde *et al.*, 1965). Another type of ruthenium chloride compound is $\text{RuCl}_3 \cdot 3\text{H}_2\text{O}$ which prepared from evaporation of RuO_4 solution in hydrochloric acid (Goldberg *et al.*, 1968). In addition of halide compounds, the dark

brown RuF_6 has low melting point ($54\text{ }^\circ\text{C}$) and hydrolyze violently with water (Selig *et al.*, 1978). The tetrafluoride of ruthenium is yellow solid which obtained by reducing RuF_5 with I_2 (Aynsley *et al.*, 1952).

3. Complexes of ruthenium

In case of oxidation state VIII (d^0), Ru(VIII) complexes are confined to a few stable (sometimes explosive) amine adducts of RuO_4 . Ru(VII) (d^1) is mentioned as salt such as $(\text{R}_4\text{N})[\text{RuO}_4]$ ($\text{R} = n\text{-propyl}$ and $n\text{-butyl}$) which use as the reagent to oxidize a variety of organic materials without attacking double or allylic bonds. In the oxidation state IV (d^4), $[\text{RuX}_6]^{2-}$ ($\text{X} = \text{F}, \text{Cl}, \text{Br}$) is readily to reduce to ruthenium(III), it produces few other complexes of interest.

For complexes of ruthenium, the oxidation state III (d^5) is the best known oxidation state. Ruthenium(III) complexes are all octahedral and low-spin with one pair electron. It can also form extensive series of halide complexes, the aqua-chloro series being probably the best characterized of all its complexes. The Ru(III)/Cl/ H_2O system has received extensive study, especially by ion exchange technique. $\text{K}_3[\text{RuF}_6]$ can be synthesized from molten salt $\text{RuCl}_3/\text{KHF}_2$ (Goldberg *et al.*, 1968). The dimeric anion of bromo complexes were reported, for example, $[\text{Ru}_2\text{Br}_9]^{3-}$ which is composed of a pair of faced-sharing octahedra. Cyano complexes of ruthenium(III) were prepared, the parent $[\text{Ru}(\text{CN})_6]^{3-}$ was isolated as the brilliant yellow salt by aerial oxidation of dimethylsulfoxide solution of $[\text{Ru}(\text{CN})_6]^{2+}$. Ruthenium(III) is much more amenable in coordination with N-donor ligands than is iron(III), and forms amines with 3 to 6 NH_3 ligands (the extra ligands making up octahedral coordination are commonly H_2O or halides) as well as complexes with 2,2'-bipyridine and 1,10-phenanthroline (Dwyer *et al.*, 1963).

Treatment RuCl_3 with aqueous ammonia in air slowly yields an extremely intense red solution (call "ruthenium red") from which a diamagnetic solid can be

isolated. It is stable in acids and alkali and its solution can be used as a sensitive test for oxidizing agent (Fletcher *et al.*, 1960).

The oxidation state II (d^6) is the second common state for ruthenium, particularly with group 15 donor ligands. Ruthenium probably forms more nitrosyl complexes than any other metal. Ruthenium(II) compounds are octahedral and diamagnetic. $[\text{Ru}(\text{H}_2\text{O})_6]^{2+}$ can be prepared in aqueous solution by electrolytic reduction of $[\text{RuCl}_5(\text{H}_2\text{O})]^{2-}$ using Pt/H₂. The cyano complexes, $[\text{Ru}(\text{CN})_6]^{4-}$, and group 15 donor complexes (ammines and nitrosyls) are also known. $[\text{Ru}(\text{NH}_3)_6]^{2+}$ and corresponding tris chelates with en (ethylenediamine), bipy (2,2'-bipyridine) and phen (1,10-phenanthroline), etc., are obtained from RuCl₃ with Zn powder as reducing agent. The hexaammine is a strongly reducing substance and $[\text{Ru}(\text{bipy})_3]^{2+}$ thermally very stable, considerable to prepare suitable derivatives which could be used to catalyze the photolytic decomposition of water, with a view to the conversion of solar energy in hydrogen fuel. The pentaammine derivative, $[\text{Ru}(\text{NH}_3)_5\text{N}_2]^{2+}$ was prepared in 1965 by the reduction of aqueous RuCl₃ with N₂H₄. It was the first dinitrogen complex which contains the linear Ru-N-N group (Allen and Bottomley, 1968).

4. Biochemistry of ruthenium

Transition-metal-based compounds constitute a class of chemotherapeutics, which are widely used in clinic (Brabec and Nováková, 2006). Especially precious metals, for example, platinum compounds being used in the treatment of cancer, silver compounds being used for antimicrobial agents and gold compounds be used in the treatment of rheumatoid arthritis (Allardyce and Dyson, 2001).

In the 1960s, Rosenberg discovered the first transition metal anticancer compound, cisplatin [*cis*-diamminedichloroplatinum(II)]. This very simple inorganic molecule is highly effective for the treatment of testicular and ovarian cancer cell. Despite the success of platinum based anticancer compounds in clinic, there is still a

need for new and improved metal based anticancer drugs because of the toxic side effects of the current platinum compounds in clinical use.

Recently, ruthenium complexes have attracted as alternative drugs to cisplatin in cancer chemotherapy. Ruthenium complexes show lower toxicity than cisplatin and have the ability to mimic the binding of iron to biological molecule. In addition, all oxidation states of ruthenium, Ru(II), Ru(III) and Ru(IV), are accessible under physiological condition. Many ruthenium complexes with ammine, dimethylsulfoxide, imine and *N*-heterocyclic ligands have been found to bind to DNA.

One of the recent application usages of ruthenium complexes is the innovative of new metallopharmaceuticals, particularly with *N*-donor ligands such as ammine, bipy, and their derivatives. The advantages of using ruthenium in drugs development are the stability of complexes and the affinities of ligands. Both ruthenium(II) and ruthenium(III) complexes with *N*-donor ligands are selectively bind to biomolecules and inhibit growth of cancer and tumor cells. (Clarke, 2003)

There are several types of ruthenium anticancer complexes. The structures are shown in Figure 1.

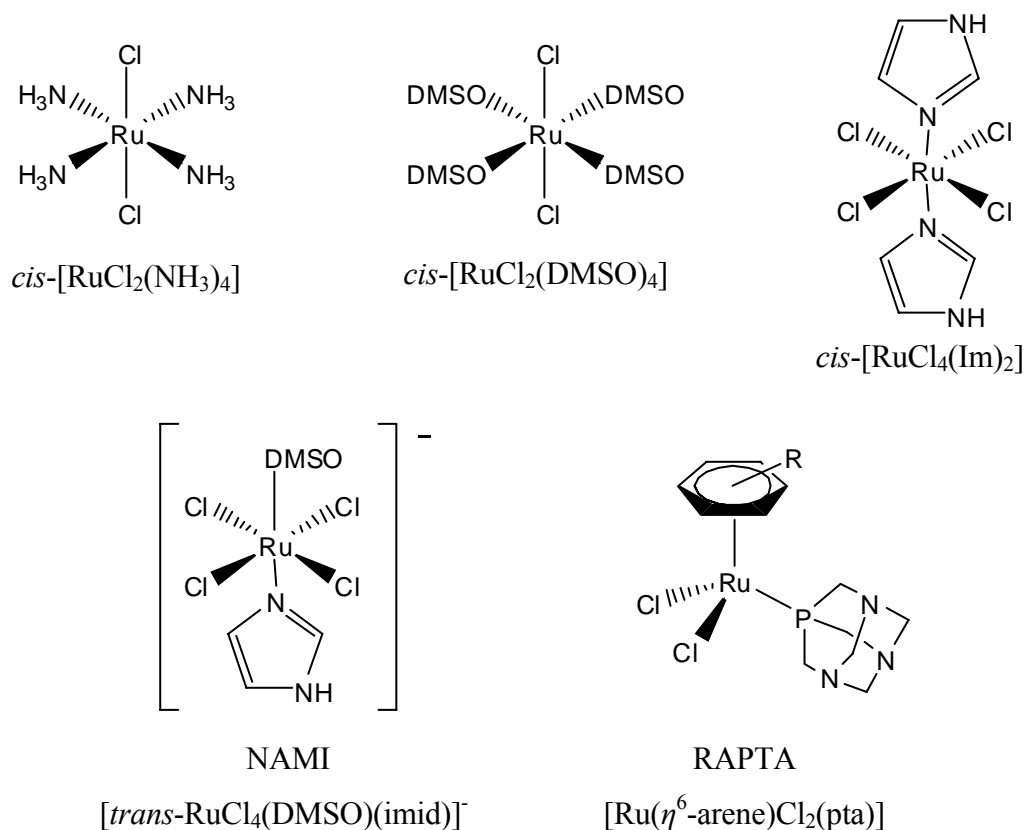


Figure 1 Examples of ruthenium anticancer complexes.

Source: Alladyce and Dyson (2001)

5. Thiazolylazo dye

Thiazolylazo dyes are organic compounds easily prepared by the diazotization of 2-aminothiazole and its derivatives. The intermediary diazotate form is highly reactive that it has to be coupled with phenolic or other aromatic substances in acidic solutions at low temperature (0 °C to -5 °C) to yield thiazolylazo dyes.

General appearances of thiazolylazo dyes are red, violet or brownish colors in their crystalline state. Most of these compounds are only partly soluble or water insoluble. Nevertheless, their solubility can be increased by the addition of organic solvent such as chloroform, methanol, ethanol, dichloromethane, dimethylformamide,

tetrahydrofuran and acetone. The general structure of thiazolylazo dye is shown in Figure 2.

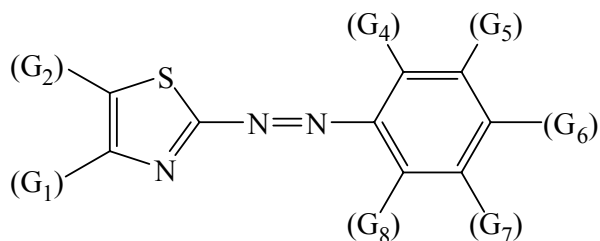


Figure 2 General structure of thiazolylazo dyes. G may be H, OH, NH₂, SO₃H, halogen atom or other groups.

Source: Lemos (2007)

Azo dyes comprise the largest group of organic reagent used in spectrophotometric analysis. They are found in a variety of industrial applications because of their color fastness. These dyes are characterized by chromophoric azo group (-N=N-) offering a wide range spectrum of colors. They also used for coloring consumer goods such as leather, clothes, food, toys, plastic and cosmetics.

Thiazolylazo dyes are sensitive chromogenic reagents in addition to being interesting complexing agents, and have been used as reagents for spectrophotometry, solid phase extraction (Saeed, 2005), and liquid chromatography (Chen, 2005). The application in spectrophotometry is based on the colored compounds resulting from their reaction with most metals, particularly some transition metals, usually stable chelate complexes are produced. They have been used in separation procedures, because of their limited solubility in aqueous solution but greater in organic solvent. Some of them have also proved to be particularly useful as indicators in complexometric titrations.

For a thiazolylazo dye which has an amino group in the *ortho* position relative to the azo group, the metal ion is bonded to the nitrogen of the amino group, the azo group and the hetero atom of the thiazole ring, forming to five-membered rings.

Thiazolylazo dye derivative, chosen in this work, is 3-(2'-thiazolylazo)-2,6-diaminopyridine (TADAP). TADAP can form complex with palladium(II) (Garcia, 1982) and platinum(IV) (Toral, 2000). Due to the platinum group metal relationship of ruthenium(III) with palladium(II) and platinum(IV), TADAP might act as a complexing agent with ruthenium(III).

For the application, calf thymus DNA solution was prepared from DNA sodium salt from calf thymus. After that, the purity of DNA was studied by A260/A280 method and then DNA binding properties with the ruthenium(III)-TADAP complex was investigated by experimental and theoretical study to optimize the structure between the complex and nucleobases.

Moreover, in this research, the chelating resin was prepared from silica gel which already modified the surface. The modified silica gel was immobilized with 3-(2'-thiazolylazo)-2,6-diaminopyridine (TADAP) for determine the adsorption ability of ruthenium(III) from aqueous solutions and selectivity of this chelating resin with other precious metals.

6. Calf thymus DNA (CT-DNA)

In general, calf thymus DNA is used for a number of purposes, such as a substrate for DNA-modifying enzymes, in DNA-binding assays, as carrier DNA and a blocking agent in hybridization solutions. Calf thymus DNA has been used in many DNA researches and laboratories probably because it is available in large quantities, stable for long time and easy to handle.

Calf thymus nuclei are extracted from calf thymus cells by chopping up calf thymus tissue in a blender with a buffer containing a mild detergent to break the plasma membrane of the cells. The resulting mixture will be centrifuged in order to separate the large dense nuclei from organelles, fragments of membranes and soluble components. The centrifugal force developed the nuclei to collect at the bottom of the tube. Next, DNA will be liberated from the proteins found in chromatin. These nucleoprotein complexes will be dissociated using a detergent (sodium dodecyl sulfate) and the DNA will be precipitated in the form of long fibers using alcohol. In the presence of alcohol, DNA molecules precipitate as long fibers, whereas contaminating RNA molecules and proteins precipitate as finer particles.

7. Chelating resin

A class of polymers which is known as specific and selective (selectivity and specificity in IUPAC) ion exchange resin has been developed and discovered since the late 1940's. These resins are the polymeric complexing and chelating compounds which are characteristic of one ionic species only. Since then, the field of chelating ion-exchange resins possessing ion-selective properties has been developed continuously (Sahni and Reedijk, 1986). There are several applications of complexing and chelating resins in transition metal as well as alkali and alkaline earth metal ions, for example, separations (Svendsen and Lund, 2000), preconcentration and recovery of trace metal ions (Ma *et al.*, 2000), catalysis (Waller, 1986), organic synthesis (Yadav and Kulkarni, 2000), water treatment, waste water treatment (Rengaraj *et al.*, 2001) and various miscellaneous applications in analytical chemistry (Landing *et al.*, 1986).

Chelating resin and chelating reagent immobilized (supported and chemically bound) supports have found widespread application for enrichment of aimed metals from a variety of matrix. Silica gel is relatively easy to immobilize chelate ligand. Various chemically bound gels have been prepared, for example, 8-hydroxyquinoline (Landing *et al.*, 1986), dithiocarbamates (Ramesh *et al.*, 2002) and dimethylglyoxime

(Purohit and Devi, 1995). Terada *et al.* developed a variety of adsorbents, which were simply prepared by impregnating chelating reagent on activated silica gel. The gel was successfully used to preconcentrate and determine trace metals. For example, 2-mercaptobenzothiazole-silica gel for gold(III), palladium(II), and platinum(IV) (Pu *et al.*, 1998), *p*-dimethylaminobenzilidenerhodanine-silica gel for gold(III), silver(I) and palladium(II) (Terada *et al.*, 1980), thionalide-silica gel for palladium(II) (Terada *et al.*, 1983), *o*-phenanthroline and 2,2'-bipyridine-silica gel for iron(II), cobalt(II), nickel(II) and copper(II) (Park *et al.*, 1993) and 1-nitroso-2-naphthol for cobalt(II) uranyl(VI) (Ghosh *et al.*, 1981).

Silica gel has been modified with chelating group in order to use in many fields of applications such as ion exchanger and liquid chromatography. These materials are frequently used as adsorbent of metal ions from dilute solutions. The preparation method of chemically modified silica gel with organic molecules containing nitrogen, sulfur and oxygen including the study of the adsorption ability of metal ions are great interesting.

Azo compounds containing hetero rings are useful as the analytical reagents because their complexation properties are often specific. In the present study, several chelating adsorbents which supported azo dyes on silica gel were prepared and attempts were made to evaluate their usefulness as a preconcentration aid for metal ions.

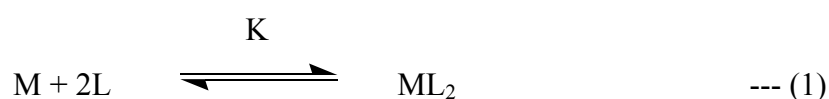
8. Complexation and stability constant

The complex formation between TADAP with ruthenium(III) are determined by using continuous variation method and conductivity measurement for studying the ratio between metal ion and TADAP of complex. To predict the molecular geometry of the complex, the quantum chemical calculation is used to calculate the energy of complex formation between ruthenium(III) and TADAP. The determination of

stability constant was performed by Benesi-Hildebrand equation (Benesi, 1949) and compared with continuous variation method (Connors, 1987).

8.1 Stability constant by Benesi-Hildebrand equation

The determination of equilibrium constant, K , the Benesi-Hildebrand equation was applied from equilibrium reaction of complex.



The equilibrium constant for the above reaction is defined by the equation

$$K = \frac{[ML_2]}{([M]-[ML_2])([L]-[ML_2])^2} \quad \text{--- (2)}$$

Where $[ML]$ is molar concentration of the complex, $[M]-[ML]$ is molar concentration of free metal ion and $[L]-[ML]$ is molar concentration of free ligand.

From Beer's law, the true molar extinction coefficient, ϵ_0 , of the complex at the wavelength of maximum absorption will then be given by the equation

$$\epsilon_0 = \frac{A}{cb} = \frac{A}{[ML_2]b}$$

$$[ML_2] = \frac{A}{\epsilon_0 b} \quad \text{--- (3)}$$

In this reaction, ligand is added in excess. Therefore, $[L]$ is much more than $[ML_2]$. The $[ML_2]$ can be eliminated and the equation (2) can be arranged and obtained as the relationship;

$$K = \frac{[ML_2]}{([M]-[ML_2])([L]-[ML_2])^2}$$

$$K = \frac{A/\epsilon b}{([M]-A/\epsilon b)(L)^2}$$

$$K = \frac{A}{\epsilon b[M][L]^2 - [L]^2 A}$$

$$A = K\epsilon b[M][L]^2 - K[L]^2 A$$

$$K\epsilon b[M][L]^2 = A + K[L]^2 A$$

$$K\epsilon b[M][L]^2 = A(1 + K[L]^2)$$

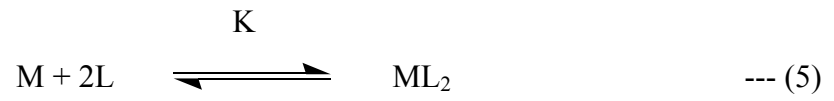
$$\frac{[M]b}{A} = \frac{1}{K\epsilon[L]^2} + \frac{1}{\epsilon} \quad \text{--- (4)}$$

The equation (4) is “Benesi-Hildebrand equation” which is in the form of the linear equation, $y = mx + c$.

For the experiment, the concentration of ruthenium(III) is fixed while the concentrations of ligand are varied. When the relationship between $[M]/A$ and $1/[L]^2$ are plotted, the equilibrium constant is obtained from the slope.

8.2 Stability constant by continuous variation method

Another method for the determination of equilibrium constant is obtained from continuous variation method by using equation (2) in the last topic, where $[M]$ and $[L]$ are initial concentration of free metal ion and free ligand, respectively. $[ML]$ is equilibrium concentration of the optimum ratio of complex solution from continuous variation method which observed from equation (3) in the last topic. The extinction coefficient can be obtained from linear calibration curve of complex solution.



$$K_f = \frac{[ML_2]}{[M][L]^2}$$

$$C_M = [M] + [ML_2]$$

$$[M] = C_M - [ML_2] = C_M - \frac{A}{A_{ex}} C_M \quad \text{when } [ML_2] = \frac{A}{A_{ex}} C_M$$

$$[L] = C_L - [ML_2] = C_L - \frac{A}{A_{ex}} C_L \quad \text{when } [ML_2] = \frac{A}{A_{ex}} C_L$$

$$[ML_2]_{ex} = C_M$$

$$A_{ex} = \epsilon b [ML_2]_{ex} = \epsilon b C_M$$

$$A = \epsilon b [ML_2]$$

$$\frac{A}{A_{ex}} = \frac{\epsilon b [ML_2]}{\epsilon b C_M}$$

$$[ML_2] = \frac{A}{A_{ex}} C_M$$

$$K_f = \frac{\frac{A}{A_{ex}} C_M}{(C_M - \frac{A}{A_{ex}} C_M)(C_L - \frac{A}{A_{ex}} C_M)}$$

So,

$$K_f = \frac{\frac{A}{A_{ex}}}{(1 - \frac{A}{A_{ex}})(C_L - \frac{A}{A_{ex}} C_M)}$$

9. Quantum chemical calculation

Computational calculation has a potential role in the molecular modeling development. Molecular structure can be created in the virtual model on computer by bonding the elements into 3-dimension structure. The thermodynamic parameters and some physical properties can be calculated.

The study of molecular structure of complex between ruthenium(III) and TADAP was investigated. Therefore, the stabilization energy of the complex was theoretically calculated to predict the possible structure by using the Density Functional Theory (DFT) at B3LYP level of theory using 6-31G* basis set for each atom other than the metal and the effective core potential (ECP) of SDD was employed on transition metal of ruthenium.

The stabilization energy of the complex when bound with nucleobases such as adenine and guanine and the optimized structure were also calculated by the same method.

OBJECTIVES

There are four main objectives of this work which are

1. To study the formation of complex between 3-(2'-thiazolylazo)-2,6-diaminopyridine (TADAP) and ruthenium(III).
2. To characterize the structure of the complex by experimental methods and quantum chemical calculation via the determination of the stabilization energy of the complex.
3. To study the possibility in binding between ruthenium(III)-TADAP complex and calf thymus DNA.
4. To use TADAP supported on silica gel (TADAP-SG) as the chelating agent for removal of ruthenium(III) in aqueous solution.

LITERATURE REVIEW

The reviews studied the previous researches on the complexation between thiazolylazo dyes and various metal ions, and the determination of ruthenium(III) by using thiazolylazo dyes as reagent for spectrophotometric method. Quantum chemical calculations of ruthenium complexes including ruthenium-DNA complex and application in recovery of ruthenium(III) by using chelating resin are reviewed.

1. The complexes between transition metal ions and thiazolylazo dyes

Jensen (1960) synthesized 1-(2'-thiazolylazo)- β -naphthol-6-sulphonic acid (TAN-6-S), 2-(2'-thiazolylazo)-*p*-cresol (TAC), 6-(2'-thiazolylazo)-resorcinol (TAR), 6-(2'-thiazolylazo)-orcinol (TAO) and 6-(2'-thiazolylazo)-1-oxy-3-dimethylamino-benzene (TAM) which could be used as complexometric metal indicator. These azo dyes were prepared by diazotization of 2-aminothiazole and then coupling with β -naphthol-6-sulphonic acid, *p*-cresol, resorcinol, orcinol and *m*-dimethylamino-phenol, respectively. The compounds were investigated for their properties as metal indicators for thorium(V), lanthanum(III), lead(II), mercury(II), copper(II), cobalt(II), nickel(II), zinc(II), cadmium(II), magnesium(II) and calcium(II).

Garcia *et al.* (1982) studied 3-(2'-thiazolylazo)-2,6-diaminopyridine that reacted with palladium(II) in strong HClO₄ media, to produce a blue 1:1 complex ($\lambda_{\max} = 665 \text{ nm}$, $\epsilon = 1.37 \times 10^4 \text{ L mol}^{-1} \text{ cm}^{-1}$), which allowed the spectrophotometric determination of 0.6-4.5 ppm palladium(II). The method was applied to the determination of palladium(II) in small sample of hydrogenation catalysts.

Gonzalez *et al.* (1986) studied the complexation equilibrium between cobalt(III) and 3-(2'-thiazolylazo)-2,6-diaminobenzene (2,6-TADAB) and 3-(2'-thiazolylazo)-2,6-diaminopyridine (2,6-TADAP) spectrophotometrically and determined the protonation constants of the complexes. 2,6-TADAB ($\epsilon_{580} = 9.5 \pm 104$, $H_0 = 1.86$) and 2,6-TADAP ($\epsilon_{595} = 1.16 \pm 104 \text{ L mol}^{-1} \text{ cm}^{-1}$, $H_0 = 0.98$) allowed the

determination of 0.024-0.47 and 0.12-2.36 ppm of cobalt(III), respectively. The method using 2,6-TADAP was applied to the determination of cobalt(III) in low alloy steels and hydrofining catalysts.

Busev *et al.* (1968) studied the methods which were given for the synthesis and purification of 5-(2-thiazolylazo)-2,6-diaminopyridine (2,6-TADAP). The maximum absorption wavelengths were given as a function of acidity (H_2SO_4 and HCl in various concentrations). Molar extinction coefficients were calculated and were given as a function of pH. 2,6-TADAP was not associated over a wide pH range.

Shraydeh *et al.* (1986) studied a sensitive method for the determination of trace amounts of mercury(II) by complexation with 3-(2-thiazolylazo)-2,6-diaminopyridine in the presence of gelatin as a solubilizing agent. Mercury(II) formed a 1:2 complex with the 3-(2-thiazolylazo)-2,6-diaminopyridine. Beer's law was obeyed over the range of 5 μg to 40 μg in the total volume of 10 ml. The molar absorptivity was $1.4 \times 10^4 \text{ L mol}^{-1} \text{ cm}^{-1}$. This method was simple and rapid and did not require any extension steps.

Perez *et al.* (1987) studied the complexation equilibrium between copper(II) and 3-(2'-thiazolylazo)-2,6-diaminopyridine (I) and 3-(4'-methyl-2'-thiazolylazo)-2,6-diaminopyridine (II) spectrophotometrically. The stability constants of the CuR^{2+} complexes ($\log \beta_{101}$) were 3.94 ± 0.03 and 3.98 ± 0.02 with I and II, respectively, and those for Cu(OH)R^+ ($\log \beta_{111}$) were 13.19 ± 0.11 and 13.14 ± 0.09 , respectively, where R = I or II. Both reagents were applied to the spectrophotometric determination of copper(II) in low-alloy steels and Al-base alloys.

Toral *et al.* (2000) studied a second derivative spectrophotometric method that had been developed for the determination of palladium(II) and platinum(IV) in mixtures. The method was based on the formation of the platinum(IV) and palladium(II) complexes with 3-(2-thiazolylazo)-2,6-diaminopyridine, (2,6-TADAP), in the presence of 1.7 M perchloric acid solution, upon heating at 90 °C for 30 min and on the subsequent direct derivative spectrophotometric measurement. The zero-

crossing approach and the graphic method were used for determination of platinum(IV) and palladium(II), respectively. Each analyte was determined in the presence of one another in the ranges of 8.9×10^{-7} M to 3.1×10^{-5} M for platinum(IV) and 4.6×10^{-7} M to 6.8×10^{-5} M, for palladium(II). The detection limits achieved (3σ) were found to be 2.7×10^{-7} M of platinum(IV) and 1.4×10^{-7} M of palladium(II). The relative standard deviations were in all instances less than 1.0 %. This work was also included a study of effect of interferences and the application of the proposed method in synthetic mixtures.

Sharov and Ivanov (2003) studied the protolytic equilibria of 3-(2'-thiazolylazo)-2,6-diaminopyridine (TADAP) in aqueous solutions and 14 organic solvents, isobestic points and absorbance maxima wavelengths were determined. The molar absorbance coefficients was calculated and the correlation between isobestic points and protonizing/deprotonizing definite acidic forms were performed. Acidic constants of all protolytic TADAP forms were calculated. Protolytic equilibria were revealed to be heavily influenced by TADAP molecules dimerization in low dielectric permeability (ϵ) environments. The dependence of acidic constants upon dielectric permeability of a solvent was found to be in the solvents under investigation and was explained.

Salazar and Toral (2004) studied the physical and chemical stability of 3-(2'-thiazolylazo)-2,6-diaminopyridine (2,6-TADAP) which had been used as chromophore reagent for determination of metals in the platinum group. A synergetic action of temperature, the reaction time and the acidity of the medium were studied as the stability parameters of 2,6-TADAP. The results showed that with the increase of temperature (15 °C to 90 °C), the 2,6-TADAP spectral band changed to the blue region. Besides, there was a significant spectral change when increased the reaction time (10 min to 80 min). In case of acidity, the band near 500 nm began to disappear when increased the acidity (pH 2.1 to -6.4) and further increased to 400 nm. Finally, according to the spectral behavior, it can be postulated that 2,6-TADAP suffers structural changes to form another new azo compound which is 3-[*N,N*-ethyl-met-azo]-2,6-diaminopyridine or 2,6-DAPEMA. This compound can be used for

quantitative determination purposes for platinum, palladium and rhodium because it formed complexes with defined spectral bands and the structures were constant under some specified conditions of acidity, temperature and reaction time.

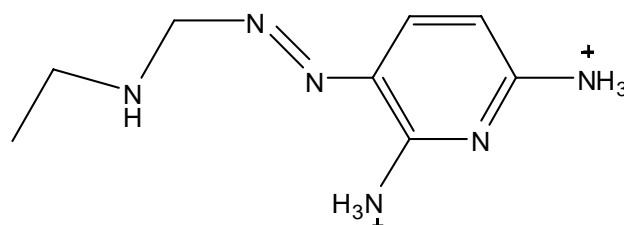


Figure 3 The structure of 3-[*N,N*-ethylmet-azo]-2,6-diaminopyridine (2,6-DAPEMA).

Velders *et al.* (2004) presented the isolation of a fourth isomer of the bidentate ligand 2-phenylazopyridine (azpy) which in theory can give five different isomeric complexes of the type $[\text{Ru}(\text{azpy})_2\text{Cl}_2]$. The isomeric structure of δ - $[\text{Ru}(\text{azpy})_2\text{Cl}_2]$ was determined by $^1\text{H-NMR}$ spectroscopy and single crystal X-ray diffraction analysis. The structures of these complexes (α -, β -, γ - and δ -) were compared and discussed with particular emphasis on 1D and 2D (NOESY) ^1H NMR spectroscopy. The bis(azpy)-ruthenium(II) isomers were of interest because of the pronounced cytotoxicity they exhibit tumor cell lines.

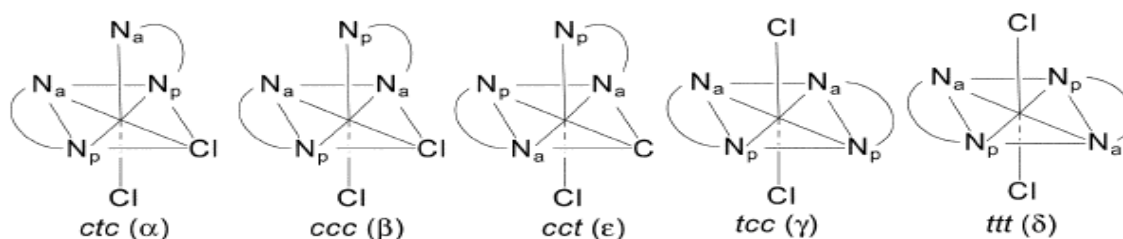


Figure 4 The five possible $[\text{Ru}(\text{azpy})_2\text{Cl}_2]$ isomers, with a systematic three-letter code indicating the *cis*(*c*), or *trans*(*t*) geometries of the chlorides (Cl), the pyridine (N_p) and the azo nitrogen (N_a), respectively.

Corral *et al.* (2005) synthesized and characterized three ruthenium polypyridyl compounds of structural formula $[\text{Ru}(\text{apy})(\text{tpy})\text{L}^{n-}](\text{ClO}_4)_{(2-n)}$ ($\text{apy} = 2,2'$ -azobispyridine; $\text{tpy} = 2,2':6',2''$ -terpyridine; $\text{L} = \text{Cl}, \text{H}_2\text{O}, \text{CH}_3\text{CN}$) (1a-c). These

complexes were fully characterized by 1D and 2D ^1H NMR spectroscopy, as well as mass spectrometry and elemental analysis. The study of their crystal structures revealed *trans* azo-nitrogen coordination similar to that reported for 2-phenylazo pyridine and π - π stacking between the pyridine ring. The $[\text{Ru}(\text{apy})(\text{tpy})\text{L}^n](\text{ClO}_4)_{(2-n)}$ complexes showed an improve water solubility. Moreover, the ligand apy was structurally related to azpy, which was reported cytotoxic ruthenium complexes.

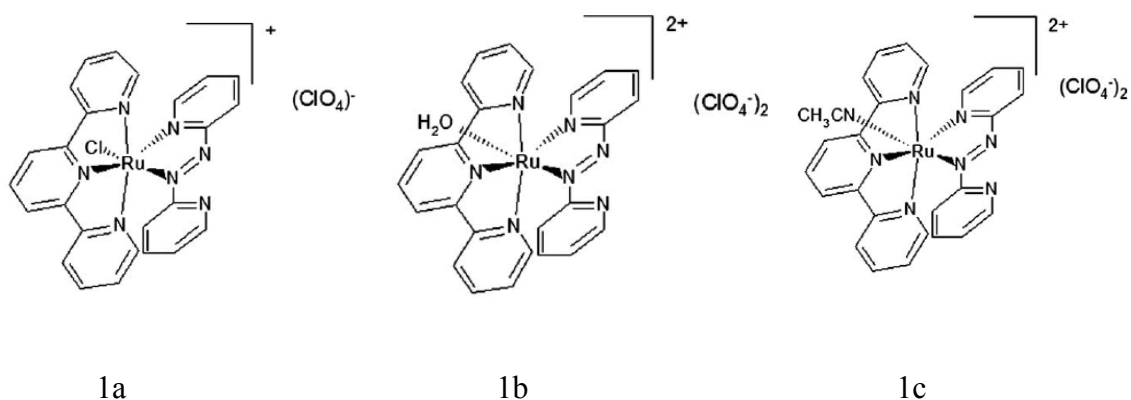


Figure 5 Three structures of $[\text{Ru}(\text{apy})(\text{tpy})\text{L}^n](\text{ClO}_4)_{(2-n)}$; $\text{L} = \text{Cl}, \text{H}_2\text{O}, \text{CH}_3\text{CN}$ (1a-1c).

Sharov and Ivanov (2005) studied the complexation of 3-(2-thiazolylazo)-2,6-diaminopyridine (TADAP) with palladium in 15 associated solvents with an ordered spatial structure and in 26 non-associated and non-structured aprotic solvents. The acid-base forms of TADAP involved in complexation were identified and shown to be different for the two groups of solvents. The optimal conditions of complexation were found. The molar absorption coefficients at the absorption maxima were determined. The stability constants for the palladium complexes with TADAP in various solvents were calculated. The dependence of the stability constants on the dielectric constant and polarizability of the solvent molecules was elucidated.

Sharov and Ivanov (2005) studied the complexation of rhodium(III) with 3-(2'-thiazolylazo)-2,6-diaminopyridine (TADAP). The optimal conditions of the complexes were found. Three rhodium(III) complexes with TADAP are formed: $[\text{Rh}(\text{H}_2\text{L}_2)]^{7+}$, $[\text{Rh}(\text{H}_2\text{L})_2]^{5+}$ and $[\text{Rh}(\text{HL})_2]^{5+}$. The stability constants for these complexes and for the mixed-ligand complexes with TADAP and chloride, bromide,

iodide, or thiocyanate ions were also calculated. Moreover, the reaction orders and rate constants were determined in order to identify the reaction mechanism.

Thaveema (2005) synthesized the ligand 3-(2'-thiazolylazo)-2,6-diaminopyridine (TADAP) by diazotization of 2-aminothiazole and coupling reaction with 2,6-diaminopyridine and complexes between TADAP and palladium(II) and between TADAP and gold(III). These products were characterized by FT-IR, ¹H NMR, mass spectroscopy and elemental analysis. TADAP formed blue complex with palladium(II) in HClO₄ solution and formed red-brown complex with gold(III). The stoichiometric ratios of both complexes were 1:1. The stability constants of the palladium(II)-TADAP complex was 4.00×10^4 under pH 1 whereas the gold(III)-TADAP complex was 6.67×10^2 under pH 4. Quantum chemical calculation at B3LYP level of theory using 6-31G* basis set for all atoms and SDD basis set with Stuttgart/Dresden electron core potential for metal atom was used to confirmed the structures of the complex. In addition, TADAP could be applied as the analytical reagent for the analysis of gold(III) by spectrophotometric method. The linear range of the method was 3.9×10^{-6} M to 5.2×10^{-5} M.

Mubarak *et al.* (2007) prepared and characterized five *bis*-[5-(4'-R-phenylazo)-8-hydroxyquinoline] ruthenium complexes [RuL_n·Cl₂·OH₂]; where L_n = 5-(4'-R-phenylazo)-8-hydroxyquinolinol, R = OCH₃ (n=1), CH₃(2), H(3), Cl(4) and NO₂(5) on the basis of elemental analyses, IR, ¹H NMR, ESR, thermal analyses and magnetic susceptibility measurements. The data show that these complexes exist in trans-isomeric solid form. Two inversion-related ligands and two Ru(III) atoms form a cage-like dimer. Both ligands of the dimer were bridged by a pair of inversion-related Ru-N (azodye) bonds. The octahedral coordination geometry of Ru(III) was made up of an N of pyridine, the deprotonated quinoline O atom, one of the azodye N-atoms, two chlorides and one water. The ligands in the dimer were stacked over one another. In the solid state of azo-8- hydroxyquinoline, the dimers had inter-and intramolecular hydrogen bonds. The azo group was involved in chelation for all the prepared complexes. The azodye derivatives were tridentate ligands, coordinating *via* N=N, C=N and OH groups. HL_n was a mononegative tridentate ligand *via* OH group

(^1H NMR and IR spectra) forming a five-membered ring. Finally, the magnetic results for all complexes indicated low-spin t_{2g}^5 Ru(III) in an octahedral environment.

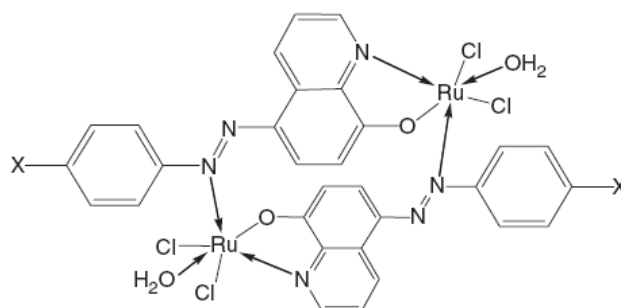


Figure 6 Structure of bis-[5-(4'-R-phenylazo)-8-hydroxyquinoline] ruthenium.

2. Quantum chemical calculation of complexes and biomolecules

Xiong *et al.* (2002) investigated the mechanism of the recognition of shared DNA $d(\text{CCGAATGAGG})_2$ by Λ - or Δ -[Ru(phen) $_2$ dppz] $^{n+}$ by calculating and comparing the potential energy of the assembly in the interaction process. They proposed a new way based on ESFF force field and SGI work station. The starting structures of the two isomers were constructed using the builder module of INSIGHT II. From calculation data, both isomers intercalate in G7A7/A8G8 with much lower potential energy of the system than into other sites. So, the intercalation in G7A7/A8G8 from minor groove was preferential than all intercalation modes from major groove. In addition, the potential energy of intercalation from minor groove is relatively lower than from major groove. This was because in the major groove, steric interference occurs when the dppz ligand was intercalated. On the contrary, in the minor groove, relatively few steric interferences occur at any selective depth. Finally, interaction between the complex and DNA was enantioselective because of the distribution of the partial charge of the intercalator. Relatively, Δ -[Ru(phen) $_2$ dppz] $^{3+}$ was preferable to the other one.

Parasuk (2003) investigated the structures of complexes of *trans*-3-(2'-thiazolylazo)-2,6-diaminopyridine (L) with some divalent metal ions by B3LYP level

of theory. The conformation of the ligand determined the chelation of the metal-ligand complex to be either mono- or bidentate. However, the bidentate chelation complexes were the more stable. For $MLCl_2$ complexes, the smaller ions i.e. magnesium(II), zinc(II), copper(II) formed tetrahedral complexes while the larger ions i.e. calcium(II), barium(II), formed square planar complexes. The stabilization energies of the complexes were in the range of 440 to 680 kcal/mol.

Han *et al.* (2004) studied the structural characterization of the interaction of metal (ruthenium and rhodium) complexes containing the ligand such as bpy, phen, dpq, dppz, tppez and phi with oligonucleotide $d(CGAATTGCG)_2$ or B-DNA. The calculation was carried out with the Amber96 in the Hyperchem 6.0 program package on 2.4G PC. The optimum binding position of each complex with B-DNA fragment was found by analyzing the potential curve of docking process. The intercalative depth (reaction coordinate) was defined as the distance from ruthenium atom to nucleobase N atom. From the observation, intercalative depth obviously increases from phen through dpq to dppz which meant that the most significant factor should be molecular shape. Meanwhile, the steric interference of two ancillary ligands (phen and bpy) limited the optimum intercalative depth of the intercalative ligand which indicated that the Van der Waals interaction between overhanging H atoms of ancillary ligands and base-pairs plays a role in selecting intercalation site.

El-Gorary and Koehler (2007) investigated the intercalation forces between the complexes of psoralen and 8-methoxy psoralen (8-MOP) with DNA base and base-pair. Psoralens were used in treatment of skin diseases. The geometry of adducts of psoralens with adenine and thymine as well as adenine-thymine base-pair were optimized in two main orientation, planar and stacked, by means of HF (Hartree-Fock) and DFT (Density Functional Theory). All computational calculations on isolated and molecular complexes were performed with Gaussian 98 package in combination with B3LYP (Lee, Yang and Parr correlation functional) and MP2 (second order Møller-Plesset perturbational method). The basis sets were used with these methods, the split valence 6-31G(d,p) and Dunning's correlation consistent double-zeta basis set (cc-pVDZ). From geometrical values, bond lengths, bond angles and dihedral angles, the

results obtained from MP2 and B3LYP levels were better than that obtained at HF level due to the effect of electron correlation. In computation at all levels showed that the co-planar complexes were much more stable than the stacked complexes. Finally, *ab initio* methods which account for the electron correlation effects were the minimum level for investigating the non-covalent interaction.

3. Transition metal complexes and biomolecules

Hao and Shen (2000) studied the use of the palladium(II) complex with 2-(2-thiazolylazo)-5-dimethylaminobenzoic acid (TAMB) for the spectrophotometric determination of nucleic acid with the detection limit at ng level. At pH 5.9, Pd(II), TAMB and nucleic acids interacted rapidly at room temperature to form a supramolecular complex, leading to absorbance decreased at 621 and 675 nm of the palladium(II)-TAMB complex. The calibration linearity at 675 nm for calf thymus DNA, fish sperm DNA and yeast RNA extended up to 3.5, 3.5 and 2.0 $\mu\text{g ml}^{-1}$, respectively. Compared to other colorimetric assays, the outstanding aspects of the method were sensitivity, simplicity and practicality.

Hotze *et al.* (2000) synthesized and characterized the ruthenium complex α -[Ru(azpy)₂(NO₃)₂] (azpy is 2-(phenylazo)pyridine, α indicates the isomer in which the coordinating pairs ONO₂, N(py) and N(azo) are *cis*, *trans* and *cis*, respectively). The solid state structure of the complex was determined by X-ray crystallography. Its structure was orthorhombic with $a = 15.423(5) \text{ \AA}$, $b = 14.034(5) \text{ \AA}$, $c = 10.970(5) \text{ \AA}$, $V = 2374(2) \text{ \AA}^3$, space group $P2_12_12_1$, $Z = 4$ and $D_{\text{calc}} = 1.655 \text{ g cm}^{-3}$. The octahedral complex showed monodentate coordination of the two nitrate ligands. The Ru-N(azo) bond distances (2.014(4) and 1.960(4) \AA) was slightly shorter than the Ru-N(py) bonds (2.031(4) and 2.059(4) \AA), which agreed well with the π -back-bonding ability of the azo groups. The binding of the DNA-model bases 9-ethylguanine (9egua) and guanosine (guo) to the complex were studied. The ligands 9egua and guo appeared to form monofunctional adducts, which could be isolated as α -[Ru(azpy)₂(9egua)Cl]PF₆, α -[Ru(azpy)₂(9egua)-(H₂O)]PF₆, α -[Ru(azpy)₂(guo)(H₂O)](PF₆)₂ and α -[Ru(azpy)₂

(guo)Cl]Cl. The orientations of 9egua and guo in these complexes were determined in detail with the use of 2D NOESY NMR spectroscopy. The guanine derivatives in the azpy complexes could have more orientations than that found for related *cis*-[Ru(bpy)₂Cl₂] species. This fluxionality was considered to be important in the binding of the α -bis(2-(phenylazo)pyridine)ruthenium(II) complex to DNA.

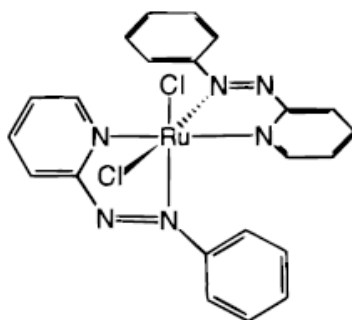


Figure 7 The schematic structure of α -[Ru(azpy)₂Cl₂].

Mura *et al.* (2004) prepared and characterized two ruthenium(III) complexes bearing thiazole ligand, namely, thiazolium (bisthiazole) tetrachlororuthenate (I, TzICR) and thiazolium (thiazole, DMSO) tetrachlororuthenate (II, TzNAMI). The crystal structures of both complexes were solved by x-ray diffraction methods and found to match those of the corresponding imidazole complexes. The behavior in aqueous solution of both TzICR and TzNAMI were analyzed spectroscopically. It was observed that replacement of imidazole with thiazole, a less basic ligand, produced a significant decrease of the ligand exchange rates in the case of NAMI-like compound. The appreciable stabilization of TzNAMI might be advantageously exploited for clinical applications. Moreover, in terms of biological aspects of these ruthenium(III) thiazole complexes, both complexes exhibited higher reactivity toward serum albumin than toward calf thymus DNA.

4. Thiazolylazo dyes as chelating reagents to determination of metal ions

Zacharaisen and Beamish (1962) described a method for the separation of ruthenium from large amounts of associated base metals in dilute hydrochloric acid solution by cation exchange resin. This method had been applied for determination of ruthenium in copper-nickel-iron assay button. The chlororuthenate solution was passed through the cation exchange resin Dowex 50 at pH 1.5. It showed that only 80 to 90 % of ruthenium was recovered in the effluent. The rest was retained by the resin. The amount of ruthenium retained on the resin when the base metal solution was salted with 5 mg of ruthenium was about 25 μg or 0.5 %. In the fire assay of copper-nickel-iron and ruthenium button, they observed that no ruthenium was detected in the distillate using thiourea as the coloring reagent.

Ueda *et al.* (1985) synthesized the chelating adsorbents, heterocyclic azo dyes supported on silica gel, and investigated their adsorption behavior toward metal ions. The 1-(2-pyridylazo)-2-naphthol (PAN-SG) and 2-(2'-thiazolylazo)-p-cresol (TAC-SG) show greater affinity for uranyl(II) and zirconyl(II) compared with other metal ions such as copper(II), cadmium(II), iron(II), iron(III) and alkaline earths. Trace uranyl(II) can be quantitatively retained on the column of gels at neutral pH region and flow rate 3 to 4 ml min^{-1} . The uranyl(II) retained was easily eluted from the column bed with a mixture of acetone and nitric acid (9:1 v/v) and determined by spectrophotometry using Arzenazo-III. Matrix components in seawater did not interfere and the spiked recovery of uranyl(II) in artificial seawater was found to be average 98.6 % with the relative standard deviation of 1.08 %. Both gels were applied to the determination of uranium in seawater with satisfactory results.

Terada and Kawamura (1991) synthesized dithiocarbamate-chitin (DTC-chitin) and used this for preconcentration of gold(III), palladium(II) and ruthenium(III) from an acidic solution. Gold(III) and palladium(II) were quantitatively retained on the polymer from 6 M hydrochloric acid even at a high flow rate (15 ml min^{-1}). In contrast, ruthenium(III) retained only 80 % in a narrow pH range 3.0 to 4.5. After passing the sample solution at flow rate of 15 ml min^{-1} , 85 % gold retained on the

polymer could be eluted with 10 ml of 1 M nitric acid containing 5 % thiourea, while palladium with 20 ml of 1.6 fold diluted inverse aqua regia. Moreover, the results showed that more than 99 % of gold and palladium was sorbed within 1 min and 30 s, respectively, while ruthenium required 5 min for the maximum retention. Finally, this present method was applied to a river sediment and a gold ore sample.

Lee *et al.* (1997) investigated the chromatographic sorption behavior of a chelating resin containing 4-(2-thiazolylazo)resorcinol (TAR) functional groups by a breakthrough experiment, and evaluated its analytical applicability to the preconcentration and separation of several metal ions including uranium(VI) in the trace concentration range. On the mini-column filled with 100 mg of the chelating resin, U(VI) and La(III) were preconcentrated with a concentration factor of 200 and then determined quantitatively by neutron activation analysis. From uranium waste solutions containing large amounts of Mg(II), Ca(II), Na(I) and carbonate ion, trace amounts of U(VI) were quantitatively sorbed on the resin column in the pH range 4.3~4.5, where formation of U(VI)-carbonate complexes is negligible, and easily recovered by eluting with 10 ml of 0.5 M HNO₃. In addition, the chelating resin was successfully applied to the separation of Cu(II), Ni(II), Cd(II), Co(II), Zn(II), Pb(II), Al(III), Mn(II) and several rare earth metal ions from U(VI) by using 1 mM EDTA as an eluent.

Lemos *et al.* (2000) used polyurethane foamed modified by 2-(2'-benzothiazolylazo)-2-p-cresol (B-TAC) as an adsorbent for determination of cadmium(II) trace levels. It was found that pH had effect on the adsorption of cadmium(II) on B-TAC. The adsorption of cadmium(II) by B-TAC was investigated within the pH range of 6.50 to 9.25. It was found that the maximum adsorption of cadmium(II) was achieved at pH 9 in the ammonium buffer solution. Cadmium(II) was eluted from the column by using hydrochloric acid at various concentrations as eluents. The results showed that 0.1 M hydrochloric acid was the most suitable eluent for desorption of cadmium(II) from B-TAC.

Lee *et al.* (2001) synthesized a new polystyrene-divinylbenzene resin (XAD-16) containing 1-(2-thiazolylazo)-2-naphthol (TAN) functional group and investigated its sorption behavior for 19 metal ions including Zr(IV), Hf(IV) and U(VI) by batch and column experiment. The chelating resin was stable in acidic and alkaline solution below 5 M and can be reused more than five times. The chelating resin (XAD-16-TAN) showed a high sorption affinity for Zr(IV) and Hf(IV) at pH 2. The overall capacities of Zr(IV) and Hf(IV) that were higher than those of the other metal ions were 0.92 and 0.87 mmol/g, respectively. The elution order of metal ions at pH 4 was evaluated as: Zr(IV) > Hf(IV) > Th(IV) > V(V) > Nb(V) > Cu(II) > U(VI) > Ta(V) > Mo(VI) > Cr(III) > Sn(IV) > W(IV). Quantitative recovery of most metal ion except Zr(IV) was achieved using 2 M nitric acid. Desorption and recovery of Zr(IV) was successfully performed with 2 M perchloric acid and 2 M hydrochloric acid.

Toral *et al.* (2002) proposed a new method for the simultaneous determination of iron and ruthenium at ultra-trace level. Moreover, this method was used inexpensive instrumentation and yields accurate and reproducible results. This method was on the basis of formation of the iron and ruthenium complexes with 2,4,6-tri-(2-pyridil)-1,3,5-triazine (TPTZ) in the presence of hydroxylamine hydrochloride and buffer CH₂ClCOOH/CH₂ClCOONa (pH 3.0). The formation of the complexes and their retention on a cationic resin SP-Sephadex C25 were integrated in one step at 90 °C while stirring for 90 min. A high preconcentration level was achieved for both analytes. The complexes retained on the solid phase were evaluated by second derivative spectrophotometry. The results indicated that the selected analytical wavelengths were 539.7 and 553.3 nm for the determination of ruthenium and iron, respectively. The detection and quantification limits were 0.54 ng ml⁻¹ and 1.79 ng ml⁻¹ for ruthenium and 0.41 ng ml⁻¹ and 1.38 ng ml⁻¹ for iron. The recovery for iron and ruthenium were 101.4 and 99.5 %, respectively. Finally, this proposed method was applied for the determination on synthetic mixtures and real industrial liquid waste samples.

Veerachalee (2007) synthesized and characterized ligand 3-(2'-thiazolylazo)-2,6-diaminopyridine (TADAP) and the complex between TADAP and cobalt(II) in

various pH by FT-IR, ^1H NMR and elemental analyzer. It was found that the stoichiometry of the complex was 1:2 (Co(II):TADAP) and the stability constant of the complex was 1.86×10^{10} under pH 10. TADAP was used in application as analytical reagent for the analysis of cobalt(II) by spectrophotometric method. The linear range was 2.0×10^{-6} M to 1.2×10^{-5} M. In addition, the chelating resin Si-TADAP was prepared and the adsorption capacity of cobalt(II) by Si-TADAP was analyzed by batch equilibrium experiment. The capacity of Si-TADAP was 0.021 mmol/g and cobalt(II) was eluted by 0.3 M K_2HPO_4 .

MATERIALS AND METHODS

Materials

1. Apparatus

Absorbance measurements were carried out on a Perkin Elmer Lambda 35 UV-Vis spectrophotometer. Conductivity of the complex was measured by ORION model 120 microprocessor conductivity measure. Melting Point of TADAP and the complex were measured by melting point SMP10 Stuart Scientific. Infrared spectra ($4000\text{-}370\text{ cm}^{-1}$) were obtained by a Perkin Elmer system 2000 Fourier transform infrared spectrometer. All absorptions were reported in wavenumber (cm^{-1}). Nuclear magnetic resonance spectra were recorded on an INNOVA VARION NMR spectrometer 400 MHz. An elemental analyzer was performed with a LECO CHNS-932 and VTF-900. Mass spectrum of TADAP was obtained from Mass Spectrometer (Agilent 1100). The pH values were measured by using an inolab level 1-pH meter. The adsorption capacity of TADAP supported silica gel to ruthenium(III) and other metal ions was determined by Perkin Elmer Analyst 800 Atomic absorption spectrophotometer under air-acetylene flame. Quantum chemical calculations were performed using Guassian 03 program on a Linux PC 2.4 GHz. and a windows XP (home edition) operating system laptop 1.73 GHz.

2. Reagents

- 2-aminothiazole ($\text{C}_7\text{H}_6\text{N}_2\text{S}$, Lab. grade, Fluka, Buchs, Switzerland)
- Sodium nitrite (NaNO_2 , Lab. grade, Merck, Darmstadt, Germany)
- 2,6-diaminopyridine ($\text{C}_5\text{H}_7\text{N}_3$, Lab grade, Acros organics, New Jersey, U.S.A.)
- Sodium acetate trihydrate ($\text{CH}_3\text{COONa}\cdot 3\text{H}_2\text{O}$, Lab. grade, BDH, Poole, England)
- Ruthenium standard for atomic absorption 1000 mg/l (RuCl_3 in 1 molar hydrochloric acid, AR. grade, Fluka, Buchs, Switzerland)

- Iron standard for atomic absorption 1 mg/ml ($\text{FeCl}_3 \cdot 6\text{H}_2\text{O}$ in diluted hydrochloric acid, AR. grade, Carlo Erba Reagenti, Milan, Italy)
- Copper standard for atomic absorption 1 mg/ml ($\text{CuCl}_2 \cdot 2\text{H}_2\text{O}$ in diluted hydrochloric acid, AR. grade, Carlo Erba Reagenti, Milan, Italy)
- Gold standard for atomic absorption 1 mg/ml ($\text{HAuCl}_4 \cdot 3\text{H}_2\text{O}$ in diluted hydrochloric acid, AR. grade, Carlo Erba Reagenti, Milan, Italy)
- Palladium standard for atomic absorption 1 mg/ml (Pd in 10% hydrochloric acid, AR. grade, Acros Organics, New Jersey, USA)
- Ruthenium trichloride hydrate ($\text{RuCl}_3 \cdot x\text{H}_2\text{O}$ 35 – 40 % Lab. grade, Acros organics, New Jersey, U.S.A.)
- Deoxyribonucleic acid sodium salt from calf thymus lyoph. (AR. grade, Fluka, Steinheim, Germany)
- (3-chloropropyl)trimethoxysilane ($\text{C}_6\text{H}_{15}\text{ClO}_3\text{Si}$, AR. Grade, Buchs, Switzerland)
- Thiourea (H_2NCSNH_2 , AR. grade, Merck, Damstadt, Germany)
- Potassium Bromide (KBr, spectroscopy (IR) grade, Carlo Erba, Rodano, Italy)
- Sodium chloride (NaCl , AR. Grade, BDH, Poole, England)
- Sodium dihydrogen phosphate (NaH_2PO_4 , AR. grade, Merck, Darmstadt, Germany)
- Sodium hydrogen phosphate (Na_2HPO_4 , AR. grade, Merck, Darmstadt, Germany)
- Sodium phosphate (Na_3PO_4 , AR. grade, J.T. Baker Chemicals, Deventer, Holland)
- Sodium acetate anhydrous (CH_3COONa , AR. grade, Merck, Damstadt, Germany)
- tris(hydroxymethyl)aminomethane ($\text{C}_4\text{H}_{11}\text{NO}_3$, Lab. grade, Fluka, Buchs, Switzerland)
- Nitric acid (HNO_3 , Lab. grade, Carlo Erba, Rodano, Italy)
- Acetic acid (glacial) 100 % (CH_3COOH , Lab. grade, Lab Scan, Bangkok, Thailand)
- Perchloric acid (HClO_4 , Lab. grade, Lab Scan, Bangkok, Thailand)

- Hydrochloric acid (HCl, Lab. grade, Lab Scan, Bangkok, Thailand)
- Sodium hydroxide (NaOH, Lab. grade, Carlo Erba, Rodano, Milan, Italy)
- Dimethylsulfoxide, D-6 (C_2D_3OS , AR. grade, Merck, Darmstadt, Germany)
- Ethyl alcohol (CH_3CH_2OH , AR. grade, Mallinckrodt, St. Louis, Missouri, U.S.A.)
- Methyl alcohol (CH_3OH , AR. grade, Merck, Darmstadt, Germany)
- Tetrahydrofuran (C_4H_8O , AR. grade, Lab Scan, Bangkok, Thailand)
- Dichloromethane (CH_2Cl_2 , AR. grade, Fisher Scientific, Leicestershire, UK)
- Acetone (C_3H_6O , Lab. grade, Lab Scan, Bangkok, Thailand)
- Silica gel 60 0.063-0.200 mm (AR. Grade, Merck, Damstadt, Germany)
- Double distilled water

Methods

1. Synthesis of 3-(2'-thiazolylazo)-2,6-diaminopyridine (TADAP)

A gram of 2-aminothiazole was dissolved in 16 ml of 6 M hydrochloric acid and cooled in an ice-bath. Sodium nitrite (0.70 g) was dissolved in a small amount of water. After crushed ice was added to both solutions, the nitrite solution was slowly poured into the 2-aminothiazole solution while stirring with a glass rod under low temperature (-5 °C to 0 °C). The solution of diazonium salt was slowly poured while stirring into a well cooled solution of 2,6-diaminopyridine (1.0 g) in 40 ml of 4 M hydrochloric acid. The mixture was stirred in the ice-bath for 1 hour and then 0.001 M sodium hydroxide solution was added into the mixture until pH 6.0 was reached. The pH was determined by a universal paper. A red precipitate began to settle immediately. The solution was filtered and the precipitated was washed with water and air-dried to give 3-(2'-thiazolylazo)-2,6-diaminopyridine (TADAP). The crude product was purified by recrystallization with a mixture of ethanol-water (3:1) to give red needles-shaped crystals with melting point of 226-227 °C. The resultant product was characterized by FT-IR (KBr), ¹H NMR, mass spectroscopy and elemental analysis as shown in Figure 9, Figure 10, Figure 11 and Table 3, respectively.

2. Preparation of solutions

2.1 Preparation of buffer solutions

Buffer solutions used in this work were prepared by mixing various reagents as stated in Table 2.

2.2 Preparation of 4.0×10^{-3} M TADAP

For the preparation of 4.0×10^{-3} M, 0.022 g of TADAP was dissolved and made up to 25 ml by 0.1 M HClO₄ and double distilled water in a volumetric flask.

2.3 Preparation of 4.0×10^{-3} ruthenium(III) solutions

For the preparation of 4.0×10^{-3} M ruthenium(III), 0.0207 g of RuCl₃·xH₂O was dissolved and made up to 25 ml by double distilled water in a volumetric flask.

Table 2 The buffer solutions which were prepared and used in this work.

pH	Buffer system
3.0	0.1 M KHP and 0.1 M HCl
4.0	0.1 M KHP and 0.1 M NaOH
5.0	0.1 M KH ₂ PO ₄ and 0.1 M NaOH
6.0	0.1 M KH ₂ PO ₄ and 0.1 M NaOH
7.0	0.1 M tris(hydroxymethyl)aminomethane and 0.1 M HCl
	0.1 M KH ₂ PO ₄ and 0.1 M NaOH

3. Complex formation between 3-(2'-thiazolylazo)-2,6-diaminopyridine (TADAP) and ruthenium(III)

The reactions of TADAP with ruthenium(III) at various pH were investigated in order to determine the appropriate pH for studying on the formation of complex between ruthenium(III) and TADAP. The following procedure for formation of complex was used in this work. Pipetted 0.75 ml of 4.0×10^{-3} M TADAP into 25 ml volumetric flasks followed by 0.75 ml of 4.0×10^{-3} M ruthenium(III) solution in buffer solution (pH range 3.0 to 7.0) was pipetted into the previous volumetric flasks. Then,

complex solutions were diluted to the mark with buffer solutions. The formation of complex between ruthenium(III) and TADAP was studied by spectrophotometric method. The results are shown in Figure 13 to Figure 17.

4. Stoichiometric determination of complex between 3-(2'-thiazolylazo)-2,6-diaminopyridine (TADAP) and ruthenium(III)

4.1 Continuous variation method

From the studying on the complex formation in the previous section, the appropriate pH for studying on the stoichiometric determination of ruthenium(III) complex was at pH 7.0.

Firstly, pipetted 0.00, 0.10, 0.20, 0.30, 0.40, 0.50, 0.60, 0.70, 0.80, 0.90 and 1.00 ml of 4.0×10^{-3} M TADAP into each of eleven 25 ml volumetric flasks. Secondly, 1.00, 0.90, 0.80, 0.70, 0.60, 0.50, 0.40, 0.30, 0.20 and 0.10 ml of 4.0×10^{-3} M ruthenium(III) was pipetted into each volumetric flasks, respectively. Then, the solutions were diluted to the mark with phosphate buffer at pH 7.0. Finally, the absorbances of the solutions were measured by UV-Vis spectrophotometer at 480 nm for pH 7.0. The results are shown in Figure 20.

4.2 Conductivity measurement

To confirm the stoichiometry of the complex, conductivity of mixture solution between 1000 ppm ruthenium(III) and TADAP was measured at various mole ratios of ruthenium(III):TADAP; 1:1, 1:2, 1:3, 1:4, 1:5, 1:6 and 1:7. Conductances of all complexes are reported in Table 5. The plot between conductance and the mole ratio of the complex is shown in Figure 21.

5. Structural determination of complex between 3-(2'-thiazolylazo)-2,6-diaminopyridine (TADAP) and ruthenium(III)

This complex was synthesized according to the following procedure. 0.03 g (0.144 mmol) of $\text{RuCl}_3 \cdot x\text{H}_2\text{O}$ was added to a solution of 0.0058 g (0.1 mmol) of NaCl in 2.5 ml tetrahydrofuran (THF) and also five drops of methanol. Then, 0.1056 g (0.048 mmol) of the ligand TADAP was dissolved in 2.5 ml tetrahydrofuran. Next, TADAP solution was added to the ruthenium solution in 50 ml round bottom flask. The system was kept under reflux for eight hours. The precipitate was collected after evaporation. Finally, the precipitate of complex was dried at room temperature under low pressure and studied by FT-IR (KBr) (Figure 23 and Table 8), ^1H NMR (Figure 24 and Table 9), and melting point measurement.

6. Calculation for the stabilization energy of complex formation between 3-(2'-thiazolylazo)-2,6-diaminopyridine (TADAP) and ruthenium(III)

All quantum chemical calculations of various ruthenium complex structures were performed with the Gaussian 03 suite of programs on a Linux PC 2.4 GHz. and a windows XP (home edition) operating system laptop 1.73 GHz. Density functional theory (DFT) using the three parameter compound functions of B3LYP (Becke, Lee-Yang-Parr correlation functional) with the 6-31G* basis set for all atoms except ruthenium atom and electron core potential of SDD for metal was used to calculate the energies of complexes between ruthenium(III) and TADAP.

The geometries of ruthenium(III)-TADAP complex was fully optimized by using the 6-31G* and SDD basis sets at B3LYP level of theory until the individual gradients were less than 10^{-7} hartree bohr $^{-1}$.

For the calculation of stabilization energy of complex between ruthenium(III) and TADAP, $[\text{Ru}(\text{TADAP})_2]^{3+}$, the reaction of complex formation should be



The stabilization energy, E , of the complex $[\text{Ru}(\text{TADAP})_2]^{3+}$ was calculated as followed:

$$E = (E_{\text{product}}) - (E_{\text{reactant}})$$

$$E = [(E_{\text{complex}})] - [(E_{\text{Ru(III)}}) + 2(E_{\text{TADAP}})]$$

The optimized structures of the complexes used in calculation are shown Figure 22 and the optimized structures are show in Figure 25 to Figure 31. Selected parameters and stabilization energies of the complexes are shown in Table 10 to Table 15. The stabilization energy and output data of all complexes are shown in Appendix C.

7. Stability of complex between 3-(2'-thiazolylazo)-2,6-diaminopyridine (TADAP) and ruthenium(III)

The stability of complex between TADAP and ruthenium(III) was determined by measuring the absorbance at wavelength 480 nm of ruthenium(III)-TADAP complex in phosphate buffer pH 7.0 for every five minutes over a period of 2 hours. The results are shown in Figure 32.

8. Determination for stability constant of complex between 3-(2'-thiazolylazo) - 2,6-diaminopyridine (TADAP) and ruthenium(III)

8.1 Equilibrium constant by continuous variation methods

The stability constant of the complex can be determined by using data form the continuous variation method (Job's plot) by assume that only single complex

is present (Likussar, 1971). The complex between ruthenium(III) and TADAP in KH_2PO_4 buffer solution of pH 7.0 was studied by UV-Vis spectrophotometer at 480 nm. The calculation of stability constant of complex between ruthenium(III) and TADAP is shown in Appendix A.

8.2 Equilibrium constant by Benesi-Hildebrand's Equation

The ruthenium(III)-TADAP complex solution was prepared by mixing variable amounts of ruthenium(III) solution into a constant volume of TADAP solution. The concentrations of ruthenium(III) ranged between 1.0×10^{-5} M and 1.0×10^{-4} M while the concentrations of TADAP remained constant at 4.0×10^{-5} M. The series of complex solution were prepared in phosphate buffer at pH 7.0. The absorbances of the complex solution was measured by using UV-VIS spectrophotometer at the wavelength 480 nm. The calculation of stability constant is shown in Appendix B.

9. Calf thymus DNA solution

9.1 Preparation of calf thymus DNA

A hundred milligram of deoxyribonucleic acid sodium salt from calf thymus (CT-DNA) was dissolved in 50 mM 100 ml tris-HCl(trishydroxymethyl-aminomethane hydrochloride) buffer and 5 mM NaCl pH 7.4 which prepared in boiled double distilled water. In addition, a vial which used to keep CT-DNA should be cleaned by ethyl alcohol before using. Finally, CT-DNA was stored at low temperature (4°C).

9.2 Purity assessment by using A260/A280 ratios

Calf thymus DNA should be test to confirm that it has a little contamination of any protein by measuring the absorbance at wavelengths 280 and 260 nm. Absorbance at 260 nm (A260) is frequently used to measure DNA/RNA concentration and Absorbance at 280 nm (A280) is used to measure protein concentration. A ratio of $A_{260}/A_{280} > 1.8$ suggests little protein contamination in a DNA/RNA sample (Glasel, 1995). This method is fully explained in Appendix D.

To determine the absorbance ratio, 100 ppm of calf thymus DNA was prepared from standard 1000 ppm DNA solution. Then, the sample was measured by spectrophotometer at wavelengths 260 and 280 nm. Finally, the ratio of absorbance at A260 and A280 was calculated.

10. Investigation of binding between ruthenium(III)-TADAP complex and calf thymus DNA

To determine the binding between the complex and calf thymus DNA, the solutions were prepared by mixing a constant volume of ruthenium(III)-TADAP complex solution into the presence and the absence of calf thymus DNA solution. The concentrations of calf thymus DNA ranged between 5 ppm and 100 ppm while the concentrations of TADAP remained constant at 4.0×10^{-5} M. The absorption spectra of calf thymus DNA in various concentrations is shown in Figure 33 and the absorption spectra of ruthenium(III)-complex and DNA is shown in Figure 34.

11. Calculation for the stabilization energy between ruthenium(III)-TADAP complex and nucleobases

The optimized ruthenium(III)-TADAP complex which has the lowest formation energy was used as the main structure for calculations. Structures of

nucleobases, adenine and guanine, were fully optimized by using B3LYP correlation functional and 6-31G* basis set in Gaussian03 program on Linux PC 2.4 GHz. After that, the ruthenium complex and the nucleobase were combined and rearranged the structure. Finally, SDD basis set was added to the function to calculate the energy of ruthenium atom and then optimized the formation energies of the compounds. The five coordinated intermediate complexes are shown in Figure 35 to 37. The selected donor atoms of an adenine and a guanine base are shown in Figure 38 and 39, respectively. The optimized structures of all adducts are shown in Figure 40 to 45. The stabilization energy and the activation energy of all adducts are shown in Table 16 and Figure 46, respectively.

12. Preparation of 3-(2'-thiazolylazo)-2,6-diaminopyridine resin (TADAP-SG) (Veerachalee, 2007)

12.1 Surface modification of silica gel

Fifty grams of silica gel which was suspended in 200 ml of dried toluene was refluxed and mechanically stirred under nitrogen atmosphere for 2 hours. Then to this suspension, 20 ml of (3-chloropropyl)trimethoxysilane was added dropwise and then further refluxed for 24 hours. After that, the solid was filtered and washed with ethanol. This immobilized silica gel was dried under vacuum at room temperature.

12.2 Immobilization of 3-(2'-thiazolylazo)-2,6-diaminopyridine (TADAP) on modified silica gel

Seven and half grams of the modified silica gel were suspended in 100 ml of dried toluene, under reflux while being mechanically stirred with 1 g of TADAP for 12 hours. The solid, name TADAP-SG, was dried at room temperature at low pressure condition. The synthesis pathway of TADAP-SG is shown Figure 47.

13. Determination of adsorption capacity for ruthenium(III) by TADAP-SG

The adsorption of ruthenium(III) was studied under static condition. To determine the capacity of TADAP-SG, the influence of two parameters which are pH, and shaking time were optimized under static by using batch equilibrium experiment.

13.1 Effect of pH

Capacity of TADAP-SG was determined in the range from 3.0 to 7.0. The pH of the solution in each experiment was adjusted by acetate buffer solutions. Fifty milligrams of TADAP-SG was equilibrated with 10.00 ml of 20 ppm of ruthenium(III) solution, which were prepared in the acetate buffer solution at pH 3.0, 4.0, 5.0, 6.0 and 7.0. Then, the mixtures were shaken for 4 hours. After the mixtures were filtered, the filtrates were then determined for ruthenium(III) by atomic absorption spectrophotometer. The results are shown in Figure 48.

13.2 Effect of shaking time

Fifty milligrams of TADAP-SG was equilibrated with 10.00 ml of 20 ppm of ruthenium(III) solutions in acetate buffer pH 7.0. Then, the mixtures were shaken for 0.5, 1.0, 2.0, 3.0, 4.0 and 5.0 hours, respectively. After the mixtures were filtered, the filtrates were then determined for ruthenium(III) by atomic absorption spectrophotometer. The results are shown in Figure 49.

14. Desorption of ruthenium(III) on TADAP-SG

Fifty milligrams of TADAP-SG loaded with 25.00 ml of 20 ppm of ruthenium(III) solution was mechanically shaken for 4 hours. Then, the loaded resin was filtered off, washed with double distilled water. The loaded resin was shaken

individually in 10.00 ml of 8 eluents which were 0.5 M, 1.0 M, 2.0 M, 3.0 M, 4.0 M hydrochloric acid, 0.1 M, 0.5 M and 1.0 M thiourea. After the shaking period for 4 hours, the mixtures were filtered and the filtrates were analyzed for ruthenium(III) by atomic absorption spectrophotometer. The results are shown in Figure 50.

15. Adsorption Efficiency of reused TADAP-SG for ruthenium(III)

Fifty milligrams of TADAP-SG loaded with 10.00 ml of 20 ppm of ruthenium(III) in acetate buffer pH 7.0 solution was mechanically shaken for 4 hours. Then, the loaded resin was filtered off, washed with distilled water and air-dried. The ruthenium(III) on the TADAP-SG was desorbed by using 0.1 M thiourea as eluent at the shaking time of 4 hours. Then, the desorbed TADAP-SG was reused for the adsorption of ruthenium(III). The efficiency for adsorption of ruthenium(III) was determined by atomic absorption spectrophotometer. The results are shown in Figure 51.

16. Adsorption capacity of TADAP-SG for other metal ions

Fifty milligrams of TADAP-SG was mechanically shaken with 10.00 ml of 20 ppm of iron(III), gold(III), palladium(II), and copper(II) ions in acetate buffer solution pH 7.0. After shaking for 4 hours at room temperature, the mixtures were filtered and the filtrates were analyzed for each metal ion by atomic absorption spectrophotometer. The results are shown in Figure 52.

RESULTS AND DISCUSSIONS

1. Synthesis of 3-(2'-thiazolylazo)-2,6-diaminopyridine (TADAP)

Figure 8 shows the synthesis pathway of 3-(2'-thiazolylazo)-2,6-diaminopyridine (TADAP) which was synthesized by diazotization of 2-aminothiazole in hydrochloric acid at $-5\text{ }^{\circ}\text{C}$ to $0\text{ }^{\circ}\text{C}$, then coupling with 2,6-diaminopyridine in hydrochloric acid at the same temperature. Finally, TADAP was precipitated with $1.0 \times 10^{-3}\text{ M}$ sodium hydroxide solution. The crude product was purified by recrystallization from ethanol-water (3:1) solution, which gave TADAP as red needle crystal with the melting point of $226\text{--}227\text{ }^{\circ}\text{C}$ and 51.10 % yield.

The red needle shaped crystalline of TADAP was characterized by FT-IR, ^1H NMR, mass spectrometry and elemental analysis as shown in Figures 9, 10, 11, and Table 3, respectively. TADAP in phosphate buffer pH 7.0 gave red color solution with the maximum absorption at 480 nm.

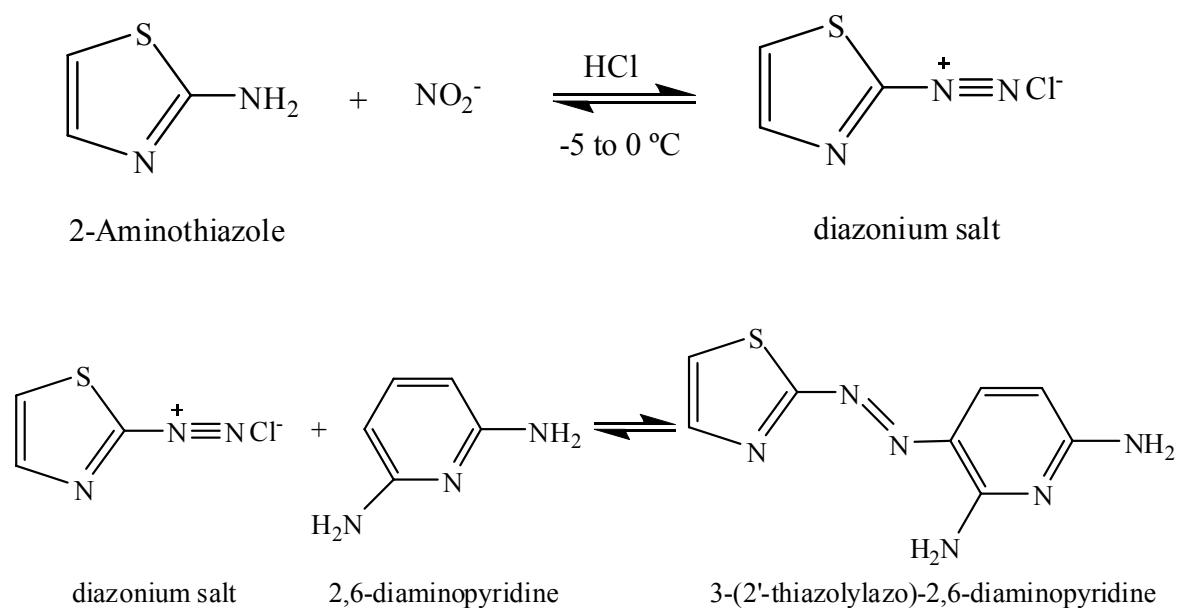
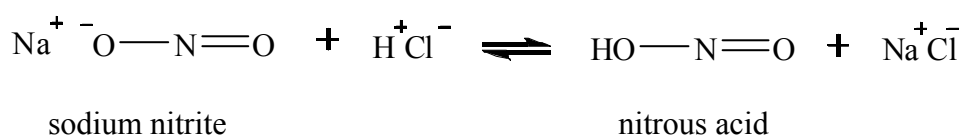


Figure 8 Synthesis pathway of 3-(2'-thiazolylazo)-2,6-diaminopyridine (TADAP).

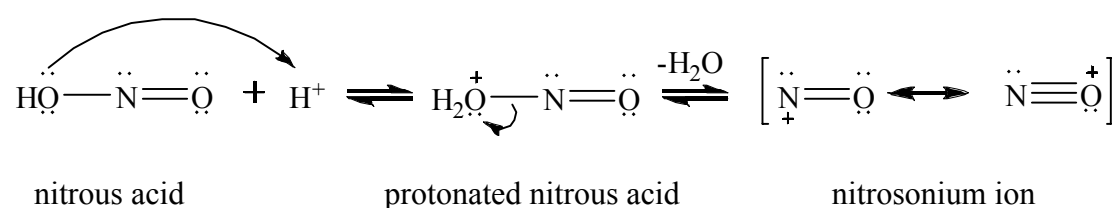
1.1 Mechanism of the reaction (Wade, 1999)

Elementary steps of reaction mechanism for the synthesis of TADAP are as followed:

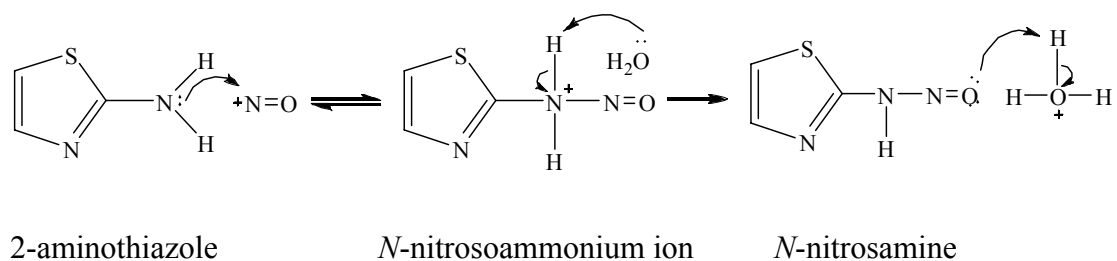
1. The unstable nitrous acid is generated in situ by mixing sodium nitrite with cold and dilute hydrochloric acid.



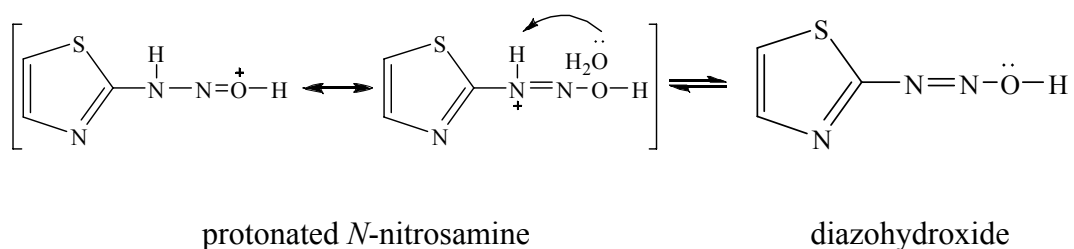
2. In an acidic solution, nitrous acid is protonated and lost water to give the reactive intermediate, nitrosonium ion.



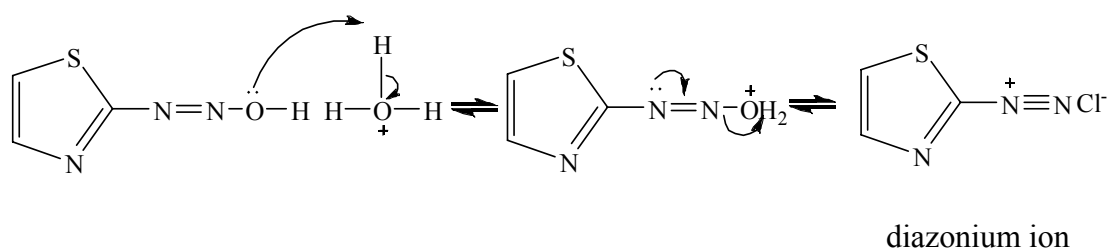
3. A nucleophilic attack on nitrosonium ion from primary amine (2-aminothiazole) forms an unstable *N*-nitrosoammonium ion as an intermediate. This intermediate then loses a proton to form an *N*-nitrosamine.



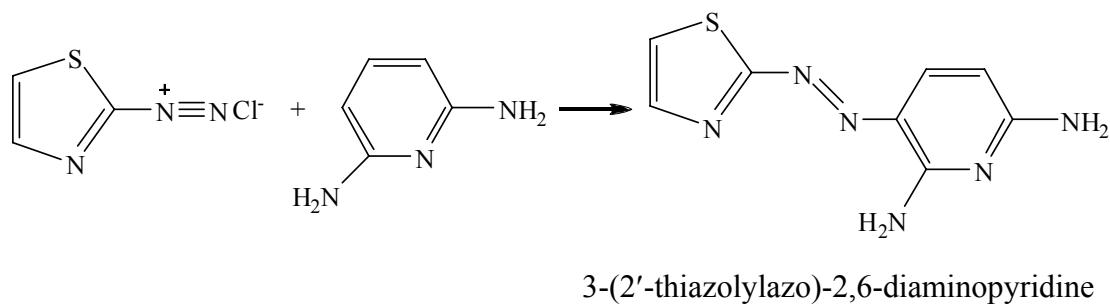
4. *N*-nitrosamine then tautomerizes to a diazohydroxide.



5. In the presence of acid, the diazohydroxide loses water to form the diazonium ion.



6. Finally, diazonium ion reacts with aromatic compounds to give a thiazolylo-azo dye.



2. Characterization of 3-(2'-thiazolylazo)-2,6-diaminopyridine

2.1 Infrared spectrum

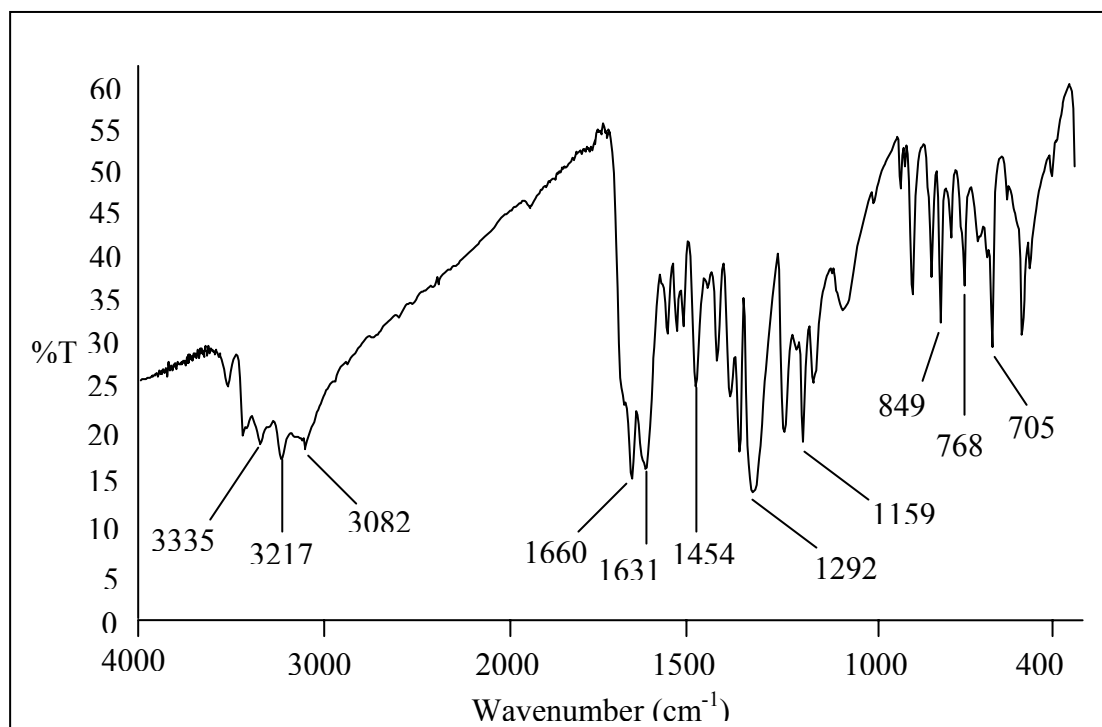


Figure 9 IR spectrum (KBr) of 3-(2'-thiazolylazo)-2,6-diaminopyridine (TADAP).

The infrared spectrum of 3-(2'-thiazolylazo)-2,6-diaminopyridine (TADAP) showed absorptions bands at 3335 cm^{-1} , 3217 cm^{-1} (w, N-H stretch), 3082 cm^{-1} (w, C-H stretch aromatic), 1660 cm^{-1} (s, C=N stretch), 1631 cm^{-1} (s, N-H bend aromatic) 1454 cm^{-1} (m, N=N stretch), 1292 cm^{-1} (s, C-N stretch) and 1159 cm^{-1} (m, C-S stretch) (Pavia, 1996).

In addition, the out-of-plane C-H bending vibrations, which appear between 900 cm^{-1} and 690 cm^{-1} , can be used to assign the positions of substituents on the aromatic ring (Pavia, 1996). In this case, IR absorption peak at 705(s), 768(m) and 849(s) cm^{-1} are consistent with *meta*-disubstituted ring (two amino groups in 2,6-diaminopyridine) of TADAP.

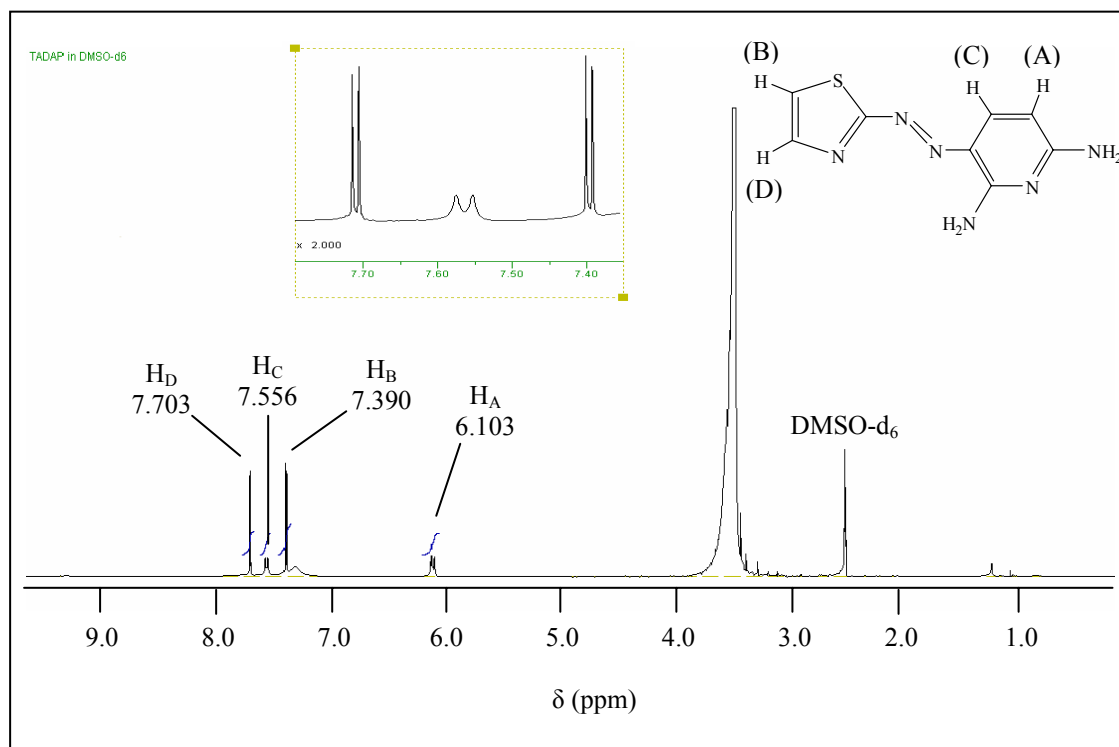
2.2 ^1H NMR spectrum

Figure 10 400 MHz. ^1H NMR spectrum of 3-(2'-thiazolylazo)-2,6-diaminopyridine (TADAP).

The ^1H NMR spectrum (DMSO-d_6 , 400 MHz) of 3-(2'-thiazolylazo)-2,6-diaminopyridine (TADAP) showed chemical shifts at δ 6.100 (1H, d, H_a , $J = 9.03$ Hz.), 7.390 (1H, d, H_b , $J = 3.67$ Hz.), 7.556 (1H, d, H_c , $J = 8.89$ Hz.) and 7.703 (1H, d, H_d , $J = 3.65$ Hz.).

The signal of the four protons on the two amino groups of TADAP were not observed in ^1H NMR spectrum of TADAP because they were acidic hydrogen atoms, which could exchange with deuterium atoms of solvent (Pavia, 1996).

2.3 ESI-Mass spectrum

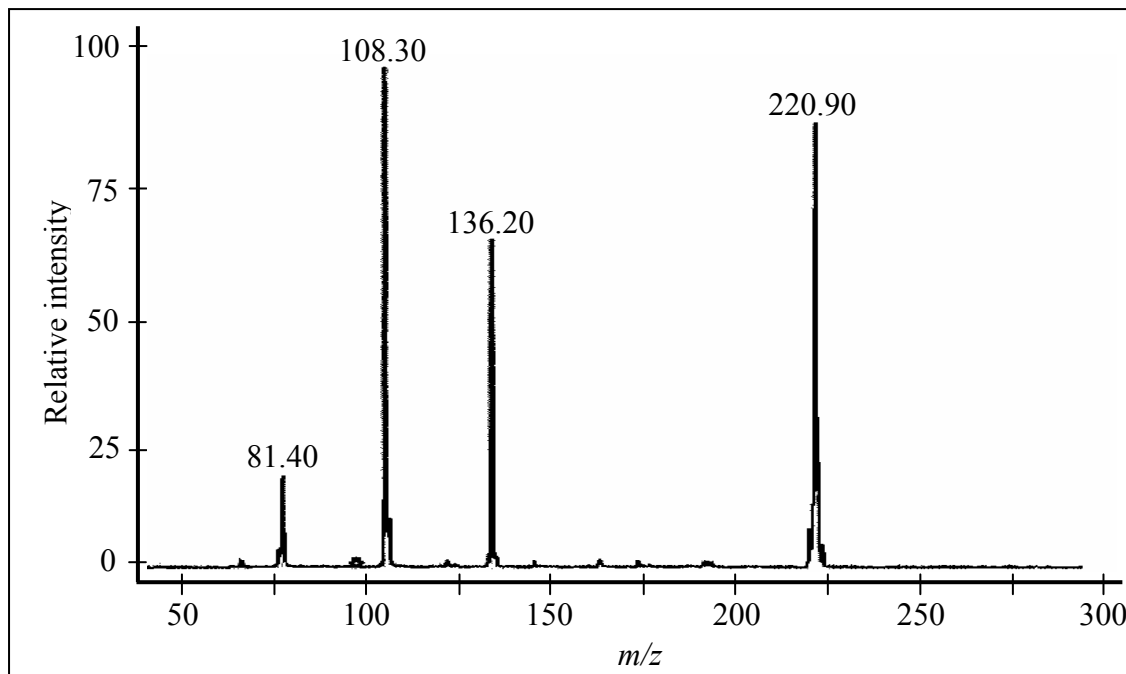


Figure 11 ESI-Mass spectrum of 3-(2'-thiazolylazo)-2,6-diaminopyridine (TADAP).

The ESI-Mass spectrum showed the m/z (relative intensity) at 220.90 (88.48), 136.20 (70.67), 108.30 (100.00) and 81.40 (21.30). The expected pathway of the fragmentation of 3-(2'-thiazolylazo)-2,6-diaminopyridine is shown in Figure 12.

Table 3 The elemental analysis of 3-(2'-thiazolylazo)-2,6-diaminopyridine (TADAP).

Element	Theoretical value (%)	Experimental value (%)	Error (%)
C	43.64	43.80	0.367
H	3.66	3.79	3.578
N	38.16	38.45	0.760
S	14.56	14.78	1.511

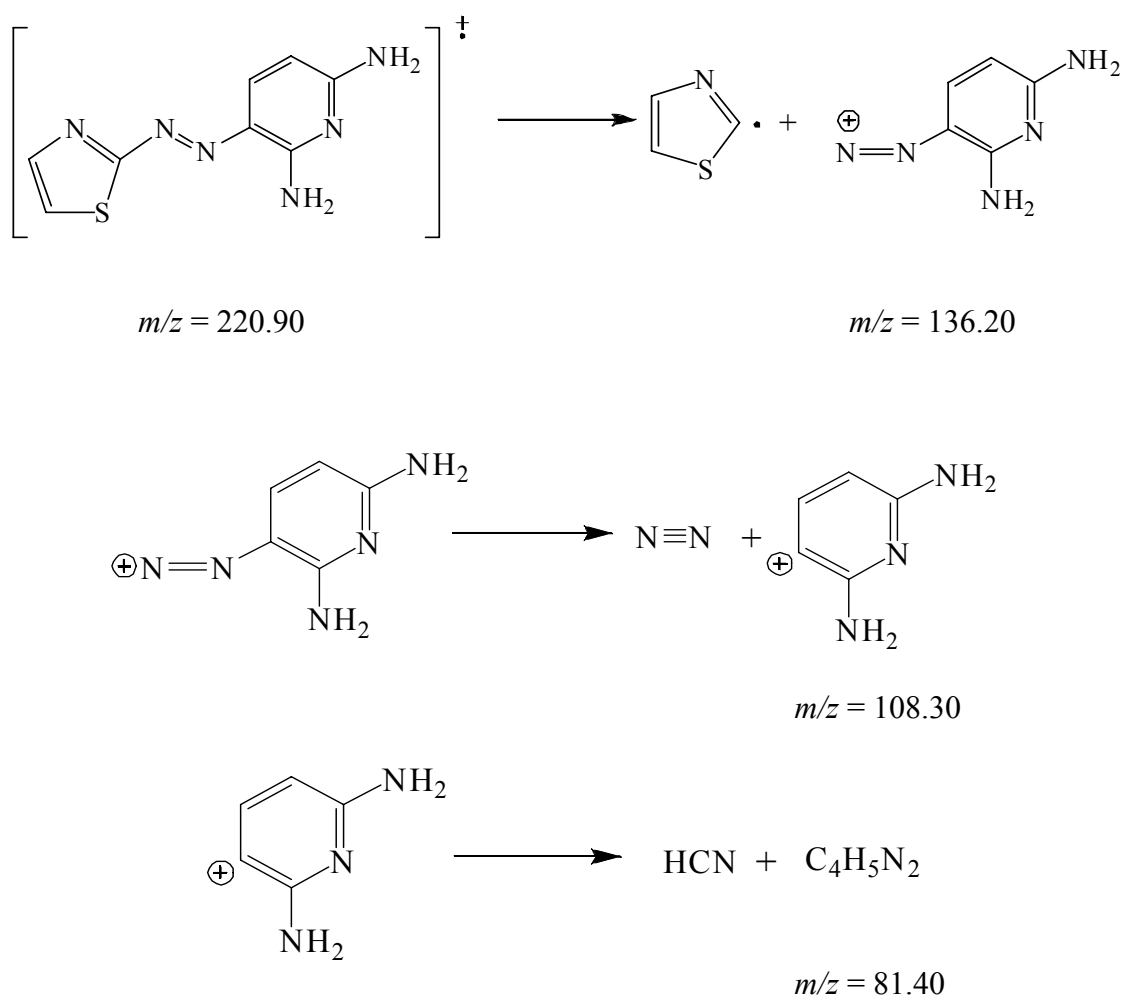


Figure 12 Pathway of the fragmentation of 3-(2'-thiazolylazo)-2,6-diaminopyridine (TADAP).

FT-IR, ^1H NMR, Mass spectroscopy and elemental analysis were used to identify the structure of TADAP. IR peaks of functional groups of TADAP such as $\text{N}=\text{N}$, $\text{N}-\text{H}$, $\text{C}-\text{S}$ and $\text{C}-\text{N}$ were identified as described in Figure 9 including the *meta*-substituent peaks of 2,6-diaminopyridine. ^1H NMR spectrum showed chemical shifts of protons in the prepared product which corresponded to the structure of the TADAP. Mass spectrum gave the molecular base peak at m/z 220.90 of TADAP and its fragmentation peaks consistent with its successive fragments as shown in Figure 11 and Figure 12. In addition, the percentage of theoretical and experimental values from C, H, N, S analysis in TADAP were also insignificantly different as seen in Table 3.

From the results, therefore, it can be concluded that the synthesized product was TADAP.

3. Complex formation between TADAP and ruthenium(III)

The absorption of TADAP was studied in aqueous buffer solution in the visible region. The azo compound displays mainly a broad band in the visible region which was assigned as $n \rightarrow \pi^*$ transition within the azo linkage influenced by intramolecular charge transfer. The formation of complex between TADAP and ruthenium(III) at various pH showed that TADAP could form complexes with ruthenium(III) at pH 3.0, 4.0, 5.0, 6.0 and 7.0. However, pH 7.0 seems to be the most suitable pH for the formation of complex between ruthenium(III) and TADAP because of the highest difference between the absorption bands of the complex and TADAP (Figure 17). The ruthenium(III) complex gave a deep-brown color at pH 3.0, 4.0, 5.0, 6.0 and 7.0. The results are shown in Figure 13 to Figure 17, and Table 4.

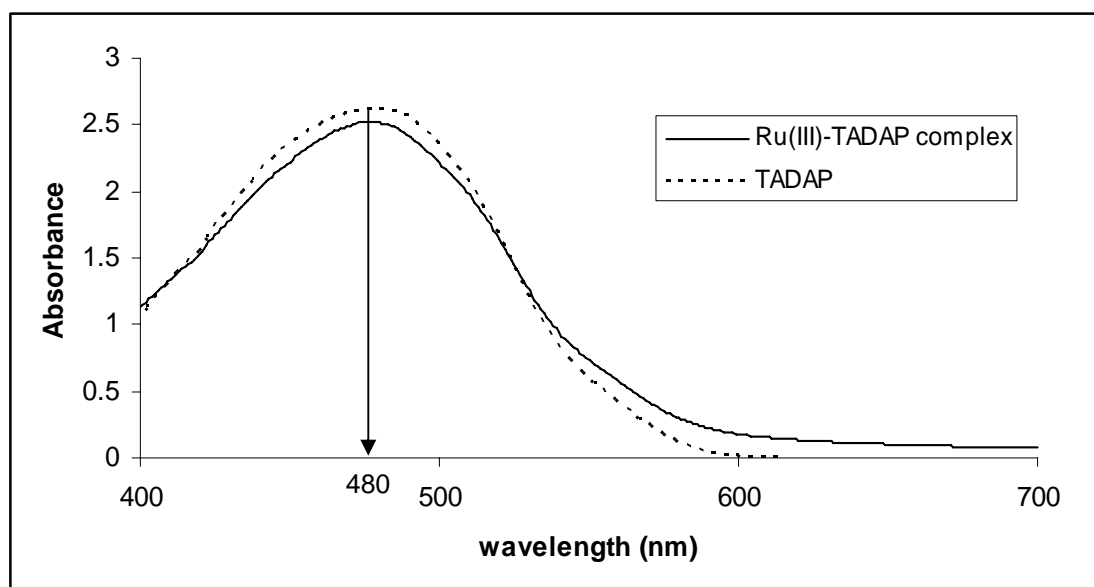


Figure 13 Absorption spectra of TADAP and Ru(III)-TADAP complex at pH 3.0.

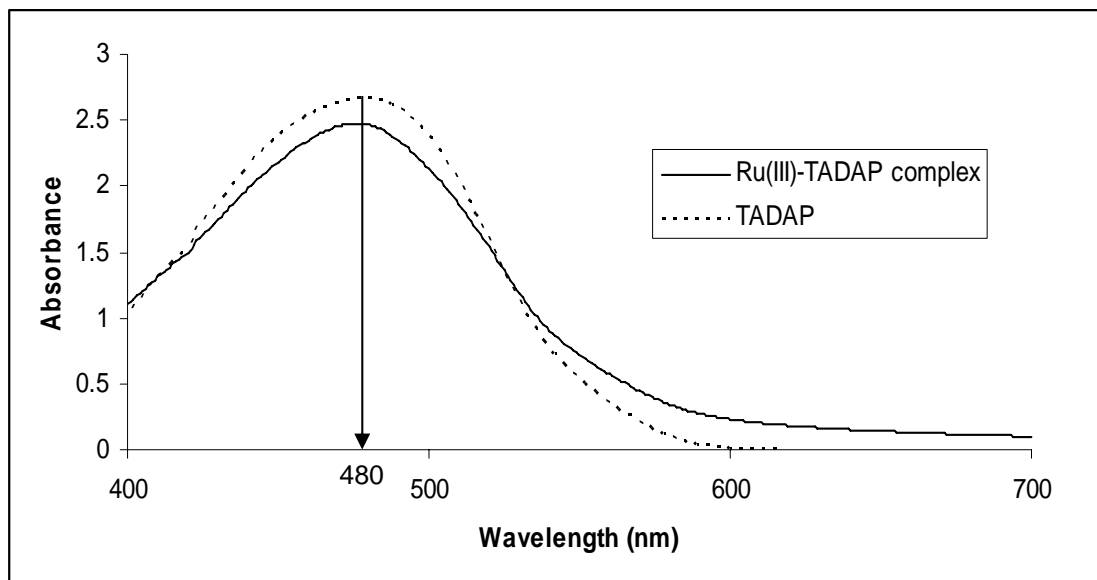


Figure 14 Absorption spectra of TADAP and Ru(III)-TADAP complex at pH 4.0.

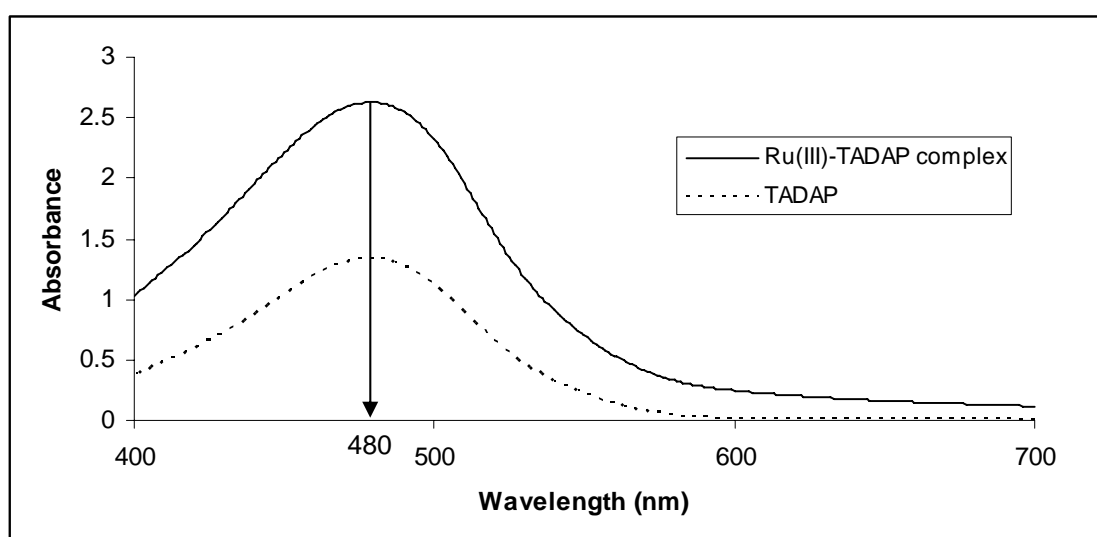


Figure 15 Absorption spectra of TADAP and Ru(III)-TADAP complex at pH 5.0.

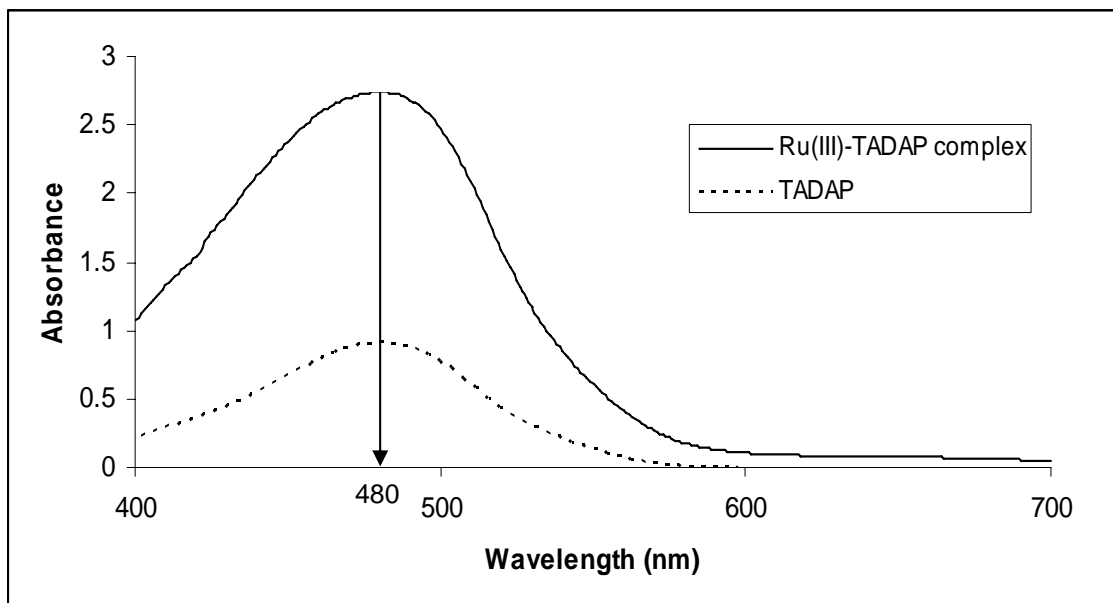


Figure 16 Absorption spectra of TADAP and Ru(III)-TADAP complex at pH 6.0.

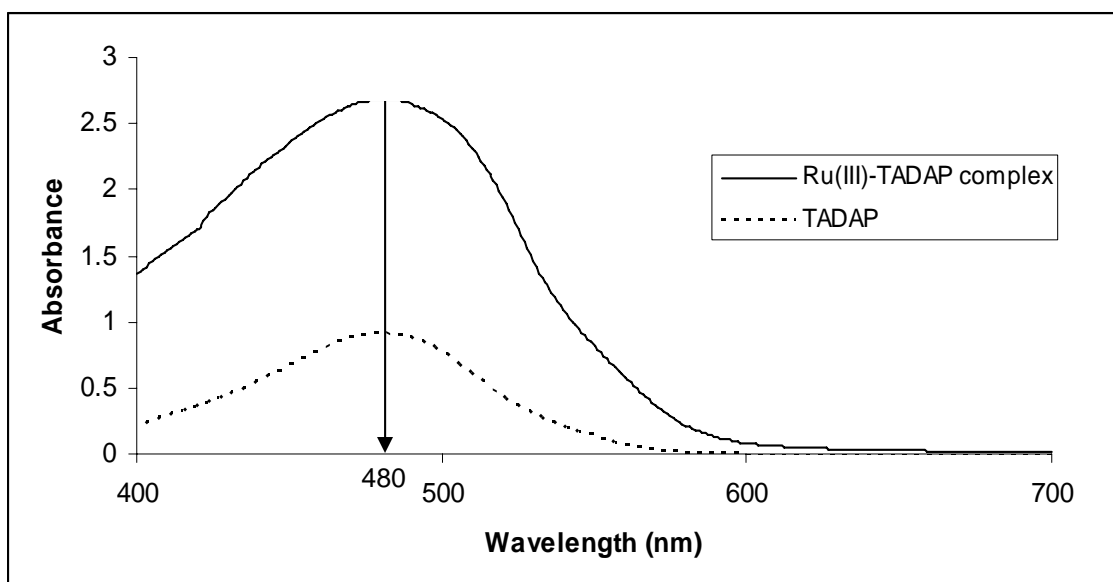
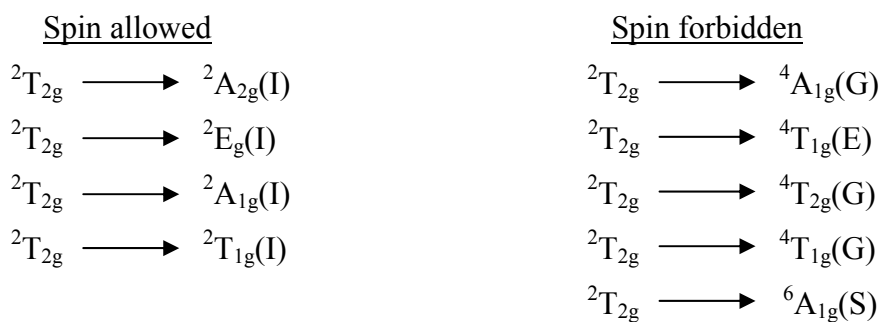


Figure 17 Absorption spectra of TADAP and Ru(III)-TADAP complex at pH 7.0.

Table 4 Complex formation between ruthenium(III) and TADAP at pH 3.0-7.0.

pH	Color of TADAP solution	Color of ruthenium(III)-TADAP complex solution	Wavelength (nm)
3.0	Orange-red	Deep-brown	480
4.0	Orange-red	Deep-brown	480
5.0	Orange-red	Deep-brown	480
6.0	Orange-red	Deep-brown	480
7.0	Orange-red	Deep-brown	480

To indicate the electronic transitions of the ruthenium(III)-TADAP complex, the Tanabe-Sugano diagram for d^5 configuration of low spin complex as shown in Figure 18 was considered. There are four spin-allowed transitions and five spin-forbidden transitions according to the spin selection rules (Miessler, 1999).



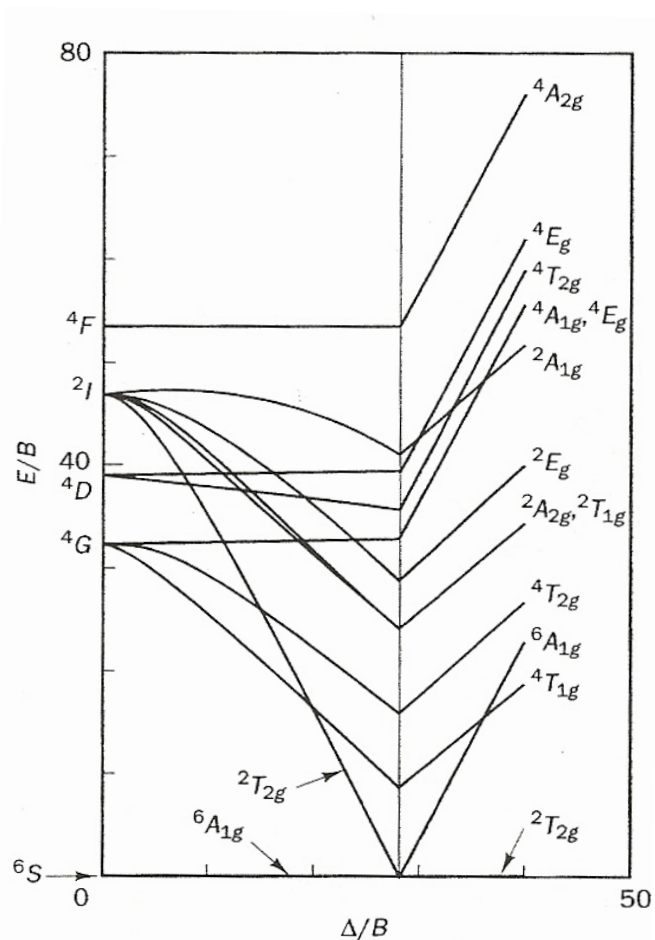


Figure 18 Tanabe-Sugano diagram of d^5 electron configuration (Kettle, 1998).

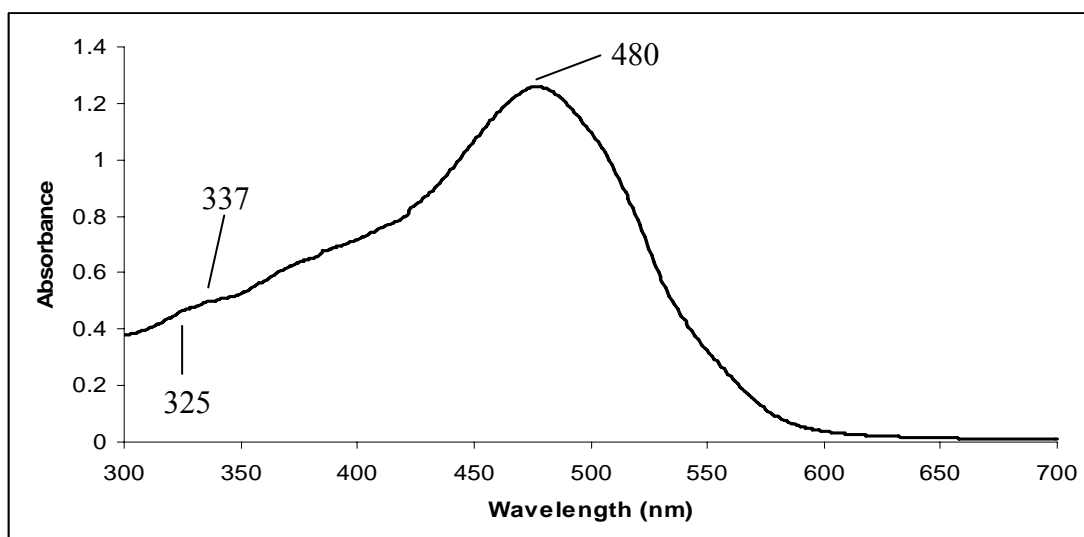


Figure 19 Absorption spectrum of 4.0×10^{-5} M ruthenium(III)-TADAP complex at pH 7.0 ($\epsilon_{480} = 3.14 \times 10^4$ L mol $^{-1}$ cm $^{-1}$).

According to the Tanabe-Sugano diagram for low-spin d^5 complex, the absorption spectrum for spin allowed d-d transition should show four bands. However, the experimental absorption spectrum of the ruthenium(III)-TADAP complex, as shown in Figure 19, showed only one broad peak at 480 nm and a shoulder between 300 nm to 350 nm. Comparing to the spectrochemical series, TADAP should be classified as a strong-field ligand with nitrogen donor atoms and N=N azo group which has a π -acceptor ability. Besides, ruthenium(III) is a member of the second transition series, therefore, the crystal field splitting energy (Δ) of the ruthenium(III)-TADAP complex should be very high. This might caused the transition energy of the complex occurred at ultraviolet and near ultraviolet region and the transition bands observed from the experiment did not resemble with that expected from the theory. So, the broad peak observed at 480 nm can be assigned as the transition from ${}^2T_{2g}$ to ${}^2A_{2g}$. In addition, high value for the molar extinction coefficient ($\sim 10^4$) indicates that this absorption band may has the charge-transfer origin, thus assigned to $t_2(\text{Ru}) \rightarrow \pi^*(\text{L})$ transition (MLCT) (Velders *et al.*, 2004).

4. Stoichiometric determination of complex between 3-(2'-thiazolylazo)-2,6-diaminopyridine (TADAP) and ruthenium(III)

From the previous sections, TADAP can form complex with ruthenium(III) at pH 7.0. Stoichiometric determination of complex between ruthenium(III) and TADAP was performed by continuous variation method (Job's method) and conductivity measurement of the mixture between ruthenium(III) and TADAP at various mole ratios.

4.1 Continuous variation method

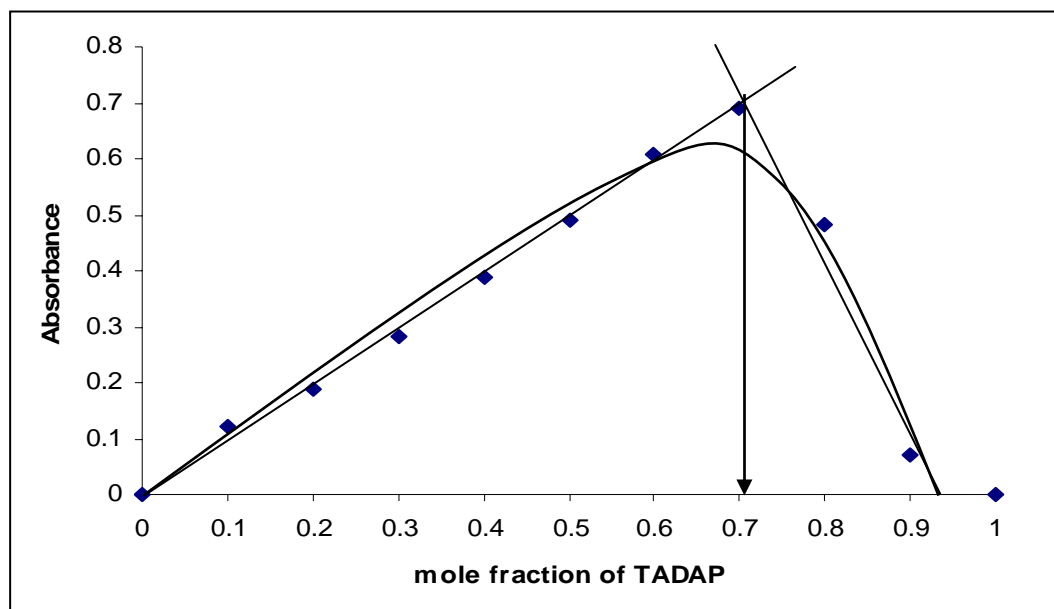


Figure 20 Continuous variation plot of complex between ruthenium(III) and TADAP in phosphate buffer at pH 7.0.

4.2 Conductivity Measurement

Table 5 Conductance of mixture solution of 1000 ppm ruthenium(III) and TADAP at various mole ratios.

Mole ratios between ruthenium(III) and TADAP (Ru(III):TADAP)	Conductance (mS)
1:0	0.393
1:1	0.259
1:2	0.200
1:3	0.169
1:4	0.146
1:5	0.133
1:6	0.123
1:7	0.114

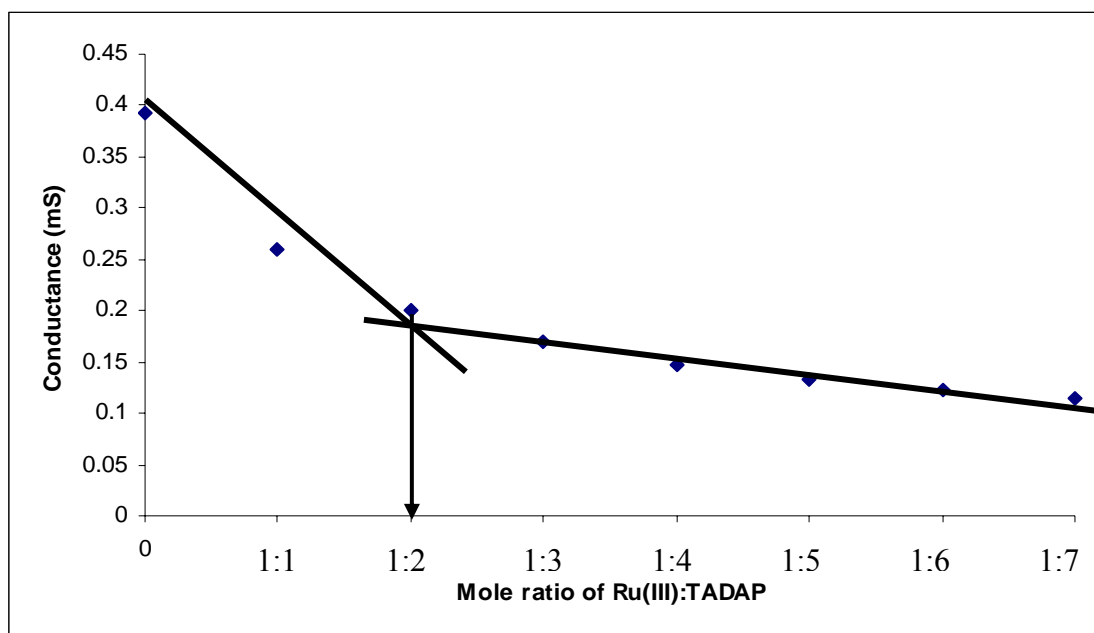


Figure 21 The plot between conductances of mixture solution of 1000 ppm ruthenium(III) and TADAP at various mole ratios.

For the stoichiometric ratio of the complex between TADAP and ruthenium(III), the plot between absorbance and mole fraction of TADAP is shown in Figure 20. It was found that the stoichiometric ratio between ruthenium(III) and TADAP was 1:2.

The conductance of ruthenium(III) was measured at room temperature while adding TADAP at various mole ratios from 1:1 to 1:7 (Ru(III):TADAP). The conductance of ruthenium(III) and ruthenium(III)-TADAP complexes are shown in Table 5 and the plots between conductance and mole ratio of ruthenium(III):TADAP are shown in Figure 21. The intercept of two theoretical straight lines in Figure 21 confirmed that this complex had 1:2 ratio (ruthenium(III):TADAP).

The result from continuous variation method seems to agree well with the result from conductivity measurement, which suggested that the stoichiometry of ruthenium(III)-TADAP complex was 1:2 (ruthenium(III):TADAP).

5. Structural determination of complex between (TADAP) and ruthenium(III)

Thiazolylazo dyes are polydentate ligand which can act as bidentate ligand which used nitrogen atoms of pyridine ring and azo group as donor atoms (Hozte *et al.*, 2000) or tridentate ligand which used nitrogen atoms of pyridine ring, azo group and amino group as donor atoms (Thaveema, 2005). According to hard and soft acids and bases as shown in Table 6 and 7. TADAP is a polydentate ligand which forms complex with metal ions via either nitrogen atom classified as borderline base or sulfur atom classified as soft base. Ruthenium(III) is a transition metal with the characteristic of the borderline acid, therefore, it is predicted that ruthenium(III) should formed bond with TADAP via the nitrogen atom in the azo group, the thiazole ring or an amino group giving octahedral geometry complex.

In addition, the source of ruthenium(III) was RuCl_3 and a small amount of NaCl was added into the solution during the complex preparation. Therefore, chloride ions might act as another ligand in the complex. Moreover, the complex was synthesized in the aqueous solution, then, it was expected that H_2O might also act as ligand of the complex. Consequently, there should be three possible structures of the complex between ruthenium(III) and TADAP as shown in Figure 22.

Table 6 Hard and soft bases.

Hard bases	Borderline bases	Soft bases
		H ⁻
F ⁻ , Cl ⁻	Br ⁻	I ⁻
H ₂ O, OH ⁻ , O ²⁻		H ₂ S, HS ⁻ , S ²⁻
ROH, RO ⁻ , CH ₃ COO ⁻		RSH, RS ⁻ , R ₂ S
NO ₃ ⁻ , ClO ₄ ⁻	NO ₂ ⁻ , N ₃ ⁻	SCN ⁻ , CN ⁻ , RNC, CO
CO ₃ ²⁻ , SO ₄ ²⁻ , PO ₄ ³⁻	SO ₃ ²⁻	S ₂ O ₃ ²⁻
NH ₃ , RNH ₂ , N ₂ H ₄	C ₆ H ₅ NH ₂ , C ₅ H ₅ N, N ₂	R ₃ P, (RO) ₃ P, C ₂ H ₄ , C ₆ H ₆

Source: Miessler (1999)

Table 7 Hard and soft acids.

Hard acids	Borderline acids	Soft acids
H ⁺ , Li ⁺ , Na ⁺ , K ⁺		
Be ²⁺ , Mg ²⁺ , Ca ²⁺ , Sr ²⁺		
BF ₃ , BCl ₃ , B(OR) ₃	B(CH ₃) ₃	BH ₃ , Tl ⁺ , Tl(CH ₃) ₃
Al ³⁺ , Al(CH ₃) ₃ , AlCl ₃		
Cr ³⁺ , Mn ²⁺ , Fe ³⁺ , Co ³⁺	Fe ²⁺ , Co ²⁺ , Ni ²⁺ , Cu ²⁺ , Zn ²⁺ , Rh ³⁺ , Ir ³⁺ , Ru ³⁺ , Os ²⁺	Cu ⁺ , Ag ⁺ , Au ⁺ , Cd ²⁺ , Hg ₂ ²⁺ , Hg ²⁺ , CH ₃ Hg ⁺ , Pd ²⁺ , Pt ²⁺ , Pt ⁴⁺

Source: Miessler (1999)

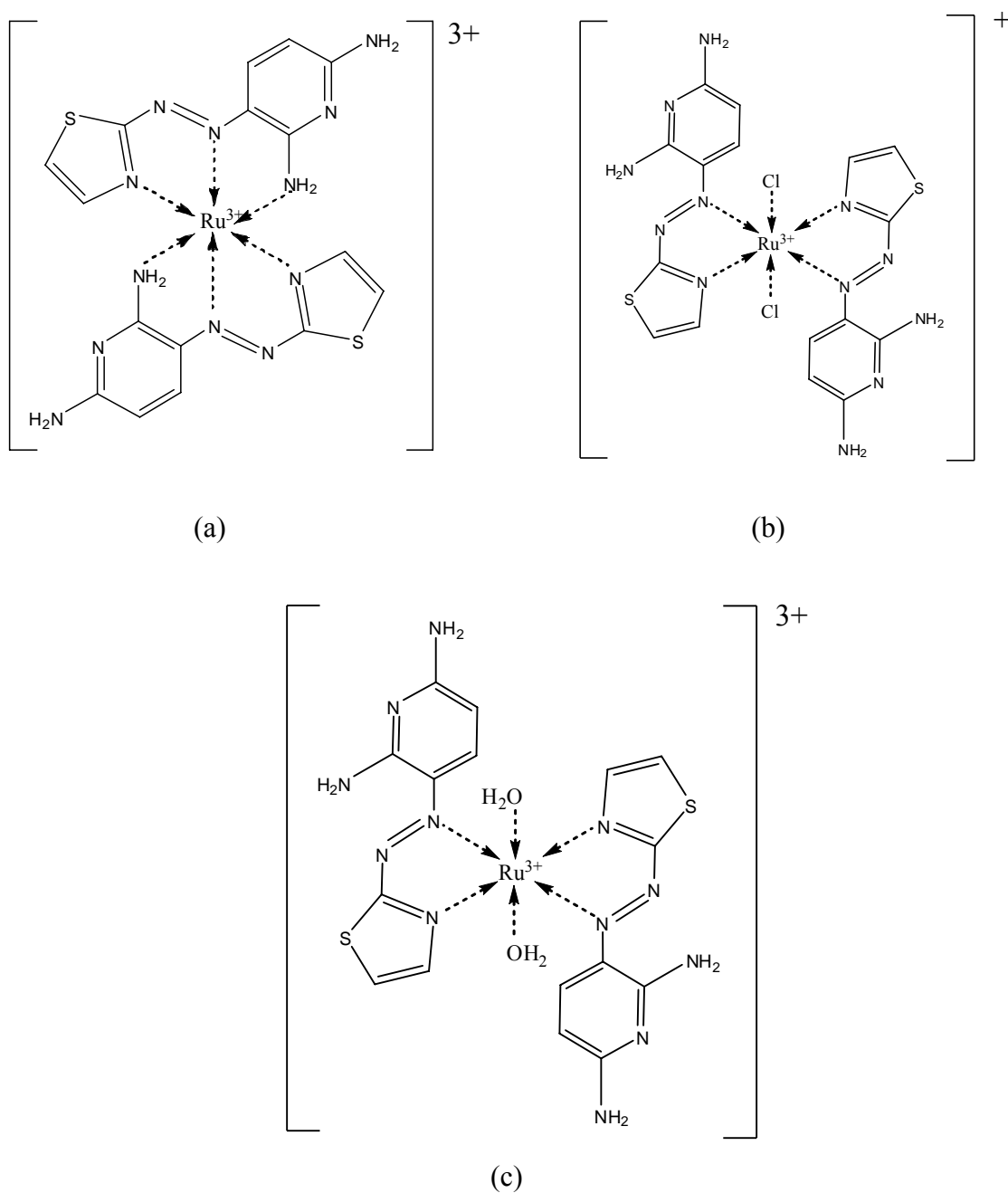


Figure 22 Postulated structures of complexes between ruthenium(III) and TADAP.

- (a) octahedral structure with six nitrogen atoms as donor atom
- (b) octahedral structure with four nitrogen atoms and two chloride ions as donor atoms
- (c) octahedral structure with four nitrogen atoms and two oxygen atoms of two water molecules as donor atoms

IR spectroscopy is a method that can be used to identify the donor atoms in the molecule of TADAP in a complex, observed by the red shift of the spectrum due to the decreasing of the bond order of the donor atom. The IR spectra of TADAP and ruthenium(III)-TADAP complex and assigned peaks of the spectra are shown in Figure 23 and Table 8, respectively. The peak assigned for N-H stretching at 3335 cm^{-1} and 3218 cm^{-1} were shifted to 3303 cm^{-1} , N=N stretching was shifted from 1454 cm^{-1} to 1443 cm^{-1} , C=N stretching was shifted from 1660 cm^{-1} to 1627 cm^{-1} , and C-S stretching was shifted from 1159 cm^{-1} to 1138 cm^{-1} . Therefore, TADAP might acted as a tridentate ligand by using nitrogen atom of $-\text{NH}_2$, nitrogen atom of N=N and nitrogen or sulfur atom in thiazolylazo ring as donor atoms. From the difference in the shift (red shift) of wavenumber of C=N and C-S bonds in the complex, the nitrogen atom in the thiazole ring should acted as the donor atom in the complexation.

Finally, peaks assigned for out-of-plane C-H bending vibrations of meta-substituents in 2,6-diaminopyridine ring were shifted to the lower energy (red shift). This also confirmed that nitrogen atom of amino group of TADAP was used to formed coordinated covalent bond with ruthenium(III).

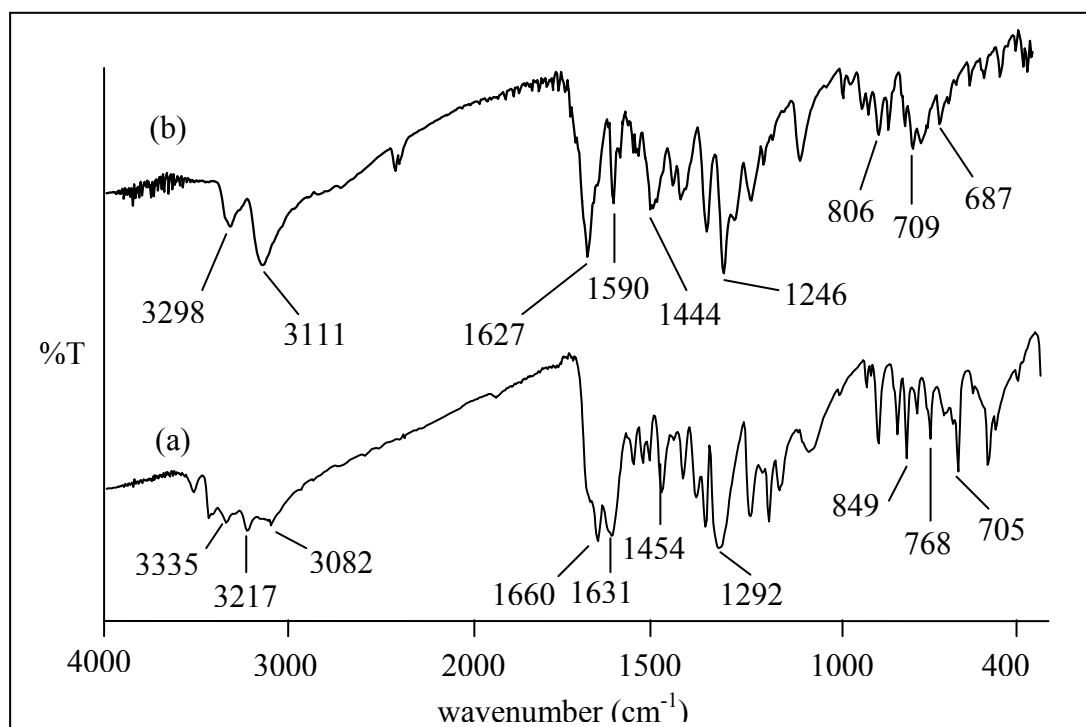


Figure 23 Infrared spectra of (a) TADAP and (b) ruthenium(III)-TADAP complex.

Table 8 Data from the IR spectra of TADAP and ruthenium(III)-TADAP complex.

TADAP		Ru(III)-TADAP complex	
Wavenumber (cm^{-1})	Functional group	Wavenumber (cm^{-1})	Functional group
3335 and 3217	N-H stretch	3298	N-H stretch
3082	C-H Stretch aromatic	3111	C-H Stretch aromatic
1660	C=N stretch	1627	C=N stretch
1631	N-H bend aromatic	1590	N-H bend aromatic
1454	N=N stretch	1444	N=N stretch
1292	C-N stretch	1246	C-N stretch
1159	C-S stretch	1138	C-S stretch
849	out-of-plane C-H	806	out-of-plane C-H
768	bending of <i>meta</i> - disubstituents	709	bending of <i>meta</i> - disubstituents
705		687	

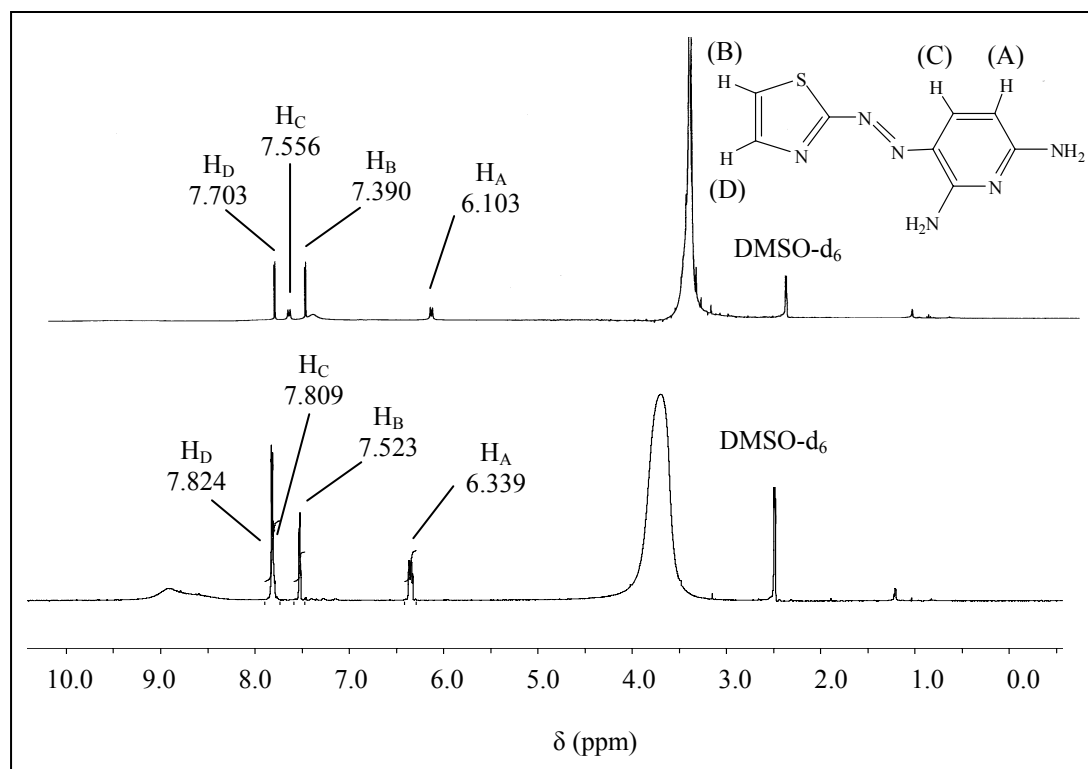


Figure 24 400 MHz. ¹H NMR spectra (DMSO-d₆) of TADAP and ruthenium(III)-TADAP complex.

Table 9 Data from the ¹H NMR spectra of TADAP and ruthenium(III)-TADAP complex.

TADAP		Ru(III)-TADAP complex	
Chemical shift (ppm)	Proton	Chemical shift (ppm)	Proton
6.103	H _A	6.339	H _A
7.390	H _B	7.523	H _B
7.556	H _C	7.809	H _C
7.703	H _D	7.824	H _D

^1H NMR spectrum can also use to indicate the donor atom of ligand for bonding with metal ions. Generally, the chemical shift of the proton closed to the donor atom shifts to lower field due to the decreasing of electron density (deshielded) of that proton. The ^1H NMR spectra of TADAP and ruthenium(III)-TADAP complex and assigned chemical shift of the spectra are shown in Figure 24 and Table 9, respectively. The peak assigned for H_A atom at 6.103 ppm was shifted to 6.339 ppm, H_B atom was shifted from 7.390 ppm to 7.523 ppm, the peak assigned for H_C atom was shifted from 7.556 ppm to 7.809 ppm and the peak assigned for H_D atom was shifted from 7.703 ppm to 7.824 ppm. It was found that chemical shifts of all protons were shifted to downfield because electrons in TADAP molecule were donated to ruthenium(III).

In addition, the data in Table 9 showed that the difference of chemical shift of H_B and H_D (both protons are in thiazole ring) between TADAP and the complex was smaller than the difference of chemical shift of H_A and H_C (both protons are in 2,6-diaminopyridine ring). This is because electrons in 2,6-diaminopyridine ring are delocalized π -electrons due to the aromaticity of the ring unlike electrons in thiazole ring. Therefore, the electron donation from any atoms in 2,6-diaminopyridine have greater affects on the change in electron density of protons in the ring, which causes the change in the chemical shift to deshielded, than the affects that might occur from the electron donation of the thiazole ring. So, ^1H NMR data indicated that either nitrogen atom or sulfur atom in the thiazole ring probably acted as donor atoms including nitrogen atoms of amino groups in 2,6-diaminopyridine ring.

From IR and ^1H NMR spectra, it can be concluded that donor atoms of TADAP to ruthenium(III) probably be the nitrogen atom of thiazole ring, the nitrogen atom of the azo group and the nitrogen atom of the amino group in 2,6-diaminopyridine ring.

The formation of complex between ruthenium(III) and TADAP when RuCl_3 was used as the ruthenium(III) source should be as followed:



As already mentioned in the previous section that Cl^- and H_2O are also two potential ligands in the complex formation, therefore, three possible complex structures as shown in Figure 22 were calculated for stabilization energies by Gaussian03 program. These are (i) six coordinate covalent bonds from two molecules of TADAP of which molecular planes are perpendicular to each other, (ii) four coordinate covalent bonds from two molecules of TADAP and two coordinate covalent bonds from two chloride ions, and (iii) four coordinate covalent bonds from two molecules of TADAP and two coordinate covalent bonds from two oxygen atoms of water. The optimized structures of TADAP and ruthenium(III)-TADAP complexes are shown in Figure 25 to Figure 28.

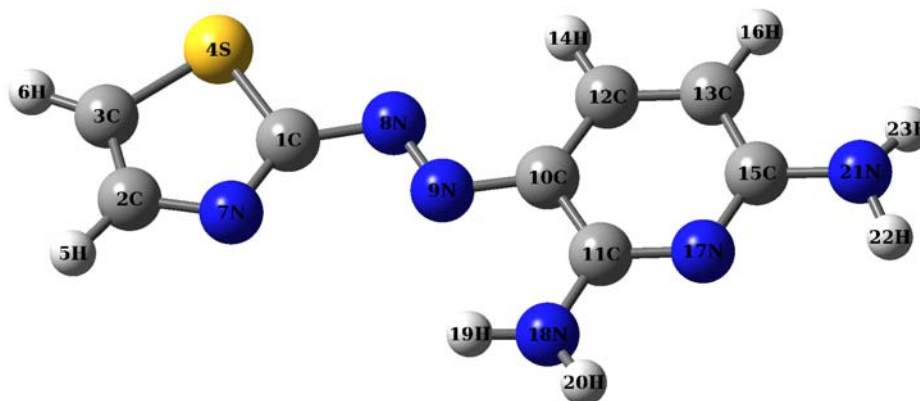


Figure 25 The optimized structure of TADAP (GaussView 3.09).

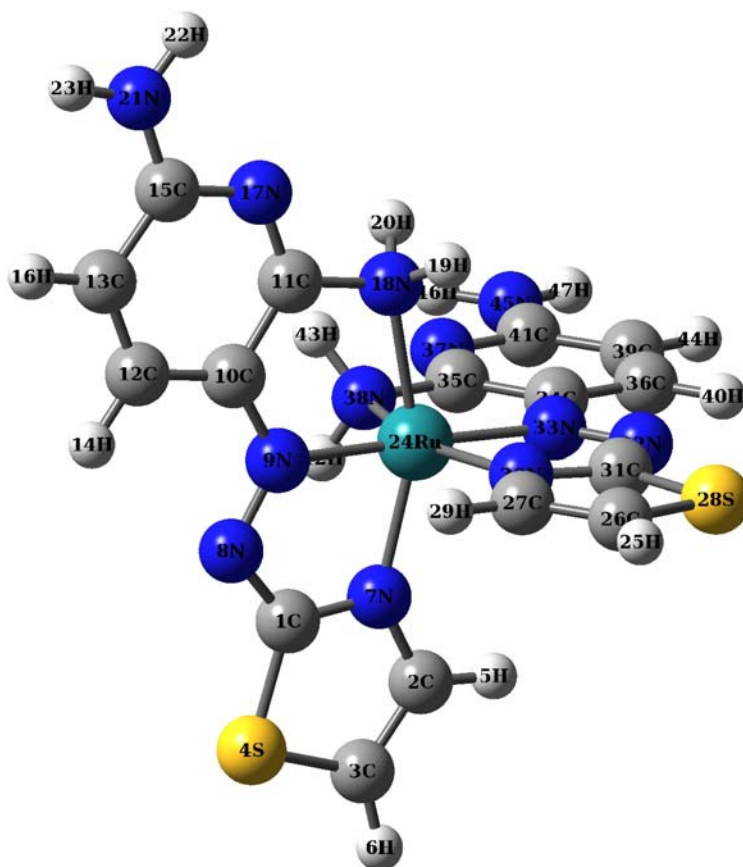


Figure 26 The optimized structure of $[\text{Ru}(\text{TADAP})_2]^{3+}$ (GaussView 3.09).

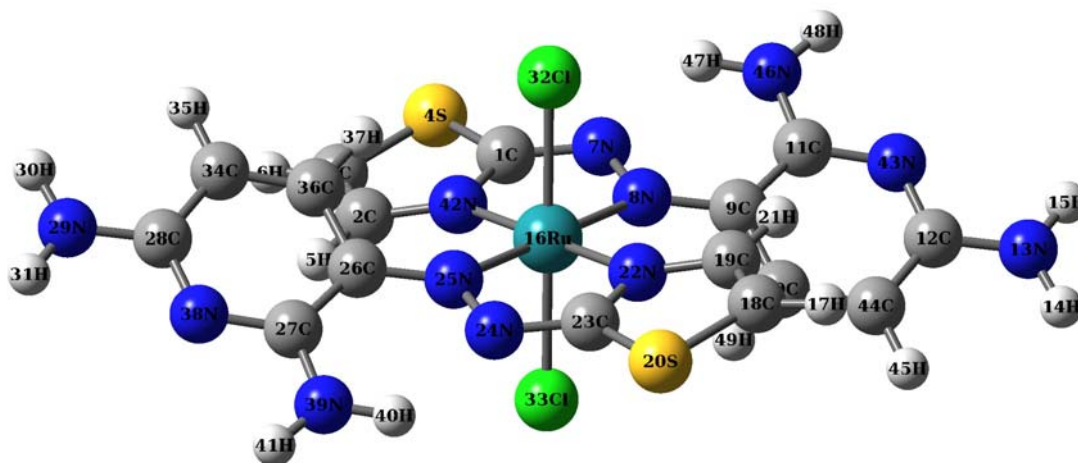


Figure 27 The optimized structure of $[\text{Ru}(\text{TADAP})_2\text{Cl}_2]^+$ (GaussView 3.09).

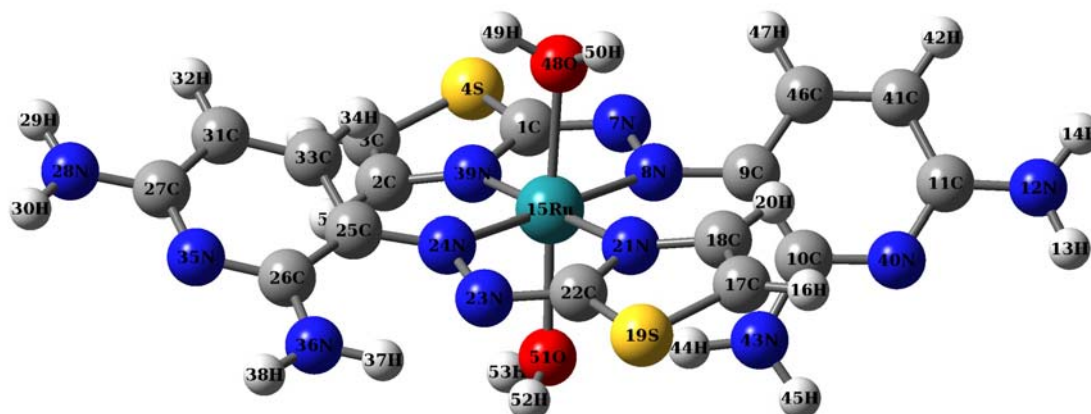


Figure 28 The optimized structure of $[\text{Ru}(\text{TADAP})_2(\text{H}_2\text{O})_2]^{3+}$ (GaussView 3.09).

Table 10 Selected bond lengths of TADAP and TADAP in $[\text{Ru}(\text{TADAP})_2]^{3+}$, $[\text{Ru}(\text{TADAP})_2\text{Cl}_2]^+$ and $[\text{Ru}(\text{TADAP})_2(\text{H}_2\text{O})_2]^{3+}$.

TADAP		$[\text{Ru}(\text{TADAP})_2]^{3+}$		$[\text{Ru}(\text{TADAP})_2\text{Cl}_2]^+$		$[\text{Ru}(\text{TADAP})_2(\text{H}_2\text{O})_2]^{3+}$	
bond	distance (Å)	bond	distance (Å)	bond	distance (Å)	bond	distance (Å)
7N-1C	1.3107	7N-1C	1.3698	42N-1C	1.3347	39N-1C	1.3563
7N-2C	1.3672	7N-2C	1.3684	42N-2C	1.3754	39N-2C	1.3691
8N-1C	1.3878	8N-1C	1.3515	7N-1C	1.3510	7N-1C	1.3407
8N-9N	1.2787	8N-9N	1.3034	7N-8N	1.3103	7N-8N	1.3099
9N-10C	1.3745	9N-10C	1.3720	8N-9C	1.3678	8N-9C	1.3906
18N-19H	1.0106	18N-19H	1.0264	46N-47H	1.0106	43N-44H	1.0122
18N-20H	1.0078	18N-20H	1.0262	46N-48H	1.0113	43N-45H	1.0152
18N-11C	1.3521	18N-11C	1.4797	46N-11C	1.3402	43N-10C	1.3386
17N-11C	1.3422	17N-11C	1.3000	43N-11C	1.3390	40N-10C	1.3281
17N-15C	1.3373	17N-15C	1.3703	43N-12C	1.3351	40N-11C	1.3400
21N-15C	1.3686	21N-15C	1.3288	13N-12C	1.3480	12N-11C	1.3302
21N-22H	1.0106	21N-22H	1.0161	13N-14H	1.0085	12N-13H	1.0165
21N-23H	1.0089	21N-23H	1.0150	13N-15H	1.0108	12N-14H	1.0142
4S-1C	1.7675	4S-1C	1.7298	4S-1C	1.7355	4S-1C	1.7374
4S-3C	1.7300	4S-3C	1.7243	4S-3C	1.7382	4S-3C	1.7174

Table 11 Selected bond angles between ruthenium atom and donor atoms in $[\text{Ru}(\text{TADAP})_2]^{3+}$, $[\text{Ru}(\text{TADAP})_2\text{Cl}_2]^+$ and $[\text{Ru}(\text{TADAP})_2(\text{H}_2\text{O})_2]^{3+}$.

$[\text{Ru}(\text{TADAP})_2]^{3+}$		$[\text{Ru}(\text{TADAP})_2\text{Cl}_2]^+$		$[\text{Ru}(\text{TADAP})_2(\text{H}_2\text{O})_2]^{3+}$	
Bond angle	degree	Bond angle	degree	Bond angle	degree
7N-24Ru-9N	76.90	8N-16Ru-22N	104.90	8N-15Ru-21N	102.64
7N-24Ru-18N	156.12	8N-16Ru-25N	180.00	8N-15Ru-24N	178.05
7N-24Ru-30N	94.14	8N-16Ru-32Cl	87.19	8N-15Ru-48O	83.98
7N-24Ru-33N	101.90	8N-16Ru-33Cl	92.80	8N-15Ru-51O	94.01
7N-24Ru-38N	91.57	8N-16Ru-42N	75.09	8N-15Ru-39N	75.33
9N-24Ru-18N	79.23	22N-16Ru-25N	75.09	21N-15Ru-24N	75.73
9N-24Ru-30N	101.89	22N-16Ru-32Cl	89.72	21N-15Ru-48O	90.13
9N-24Ru-33N	178.28	22N-16Ru-33Cl	90.28	21N-15Ru-51O	88.59
9N-24Ru-38N	101.97	22N-16Ru-42N	180.00	21N-15Ru-39N	177.80
18N-24Ru-30N	91.58	25N-16Ru-32Cl	92.80	24N-15Ru-48O	94.89
18N-24Ru-33N	101.9	25N-16Ru-33Cl	87.19	24N-15Ru-51O	87.05
18N-24Ru-38N	92.50	25N-16Ru-42N	104.90	24N-15Ru-39N	106.29
30N-24Ru-33N	76.90	32Cl-16Ru-33Cl	179.99	51O-15Ru-48O	177.33
30N-24Ru-38N	156.12	32Cl-16Ru-42N	89.71	51O-15Ru-39N	90.68
33N-24Ru-38N	79.23	33Cl-16Ru-42N	89.72	48O-15Ru-39N	90.50

Table 12 Selected bond lengths of a ruthenium atom and a donor atom in $[\text{Ru}(\text{TADAP})_2]^{3+}$, $[\text{Ru}(\text{TADAP})_2\text{Cl}_2]^+$ and $[\text{Ru}(\text{TADAP})_2(\text{H}_2\text{O})_2]^{3+}$.

$[\text{Ru}(\text{TADAP})_2]^{3+}$		$[\text{Ru}(\text{TADAP})_2\text{Cl}_2]^+$		$[\text{Ru}(\text{TADAP})_2(\text{H}_2\text{O})_2]^{3+}$	
Bond	Distance (Å)	Bond	Distance (Å)	Bond	Distance (Å)
24Ru-7N	2.0625	16Ru-25N	2.1514	15Ru-21N	2.0836
24Ru-9N	2.0301	16Ru-22N	2.0908	15Ru-24N	2.1897
24Ru-18N	2.1954	16Ru-42N	2.0908	15Ru-8N	2.1505
24Ru-30N	2.0625	16Ru-8N	2.1513	15Ru-39N	2.1085
24Ru-33N	2.0301	16Ru-32Cl	2.3593	15Ru-48O	2.1469
24Ru-38N	2.1954	16Ru-33Cl	2.3594	15Ru-51O	2.1744

Table 13 Selected torsion angles of TADAP in $[\text{Ru}(\text{TADAP})_2]^{3+}$, $[\text{Ru}(\text{TADAP})_2\text{Cl}_2]^+$ and $[\text{Ru}(\text{TADAP})_2(\text{H}_2\text{O})_2]^{3+}$.

$[\text{Ru}(\text{TADAP})_2]^{3+}$		$[\text{Ru}(\text{TADAP})_2\text{Cl}_2]^+$		$[\text{Ru}(\text{TADAP})_2(\text{H}_2\text{O})_2]^{3+}$	
Torsion angle	degree	Torsion angle	degree	Torsion angle	degree
31C-32N-33N-34C	178.87	23C-24N-25N-26C	-168.09	22C-23N-24N-25C	-165.47
30N-31C-32N-33N	-1.14	22N-23C-24N-25N	-4.16	21N-22C-23N-24N	-6.13
1C-8N-9N-10C	178.87	1C-7N-8N-9C	168.09	1C-7N-8N-9C	175.22
9N-8N-1C-7N	-1.14	8N-7N-1C-42N	4.16	8N-7N-1C-39N	3.15
32N-33N-34C-35C	-178.67	24N-25N-26C-27C	-19.02	23N-24N-25C-26C	-9.28
28S-31C-32N-33N	178.94	20S-23C-24N-25N	166.73	19S-22C-23N-24N	166.77
8N-9N-10C-11C	-178.66	7N-8N-9C-11C	19.04	7N-8N-9C-10C	-140.40
4S-1C-8N-9N	178.94	4S-1C-7N-8N	-166.73	4S-1C-7N-8N	-166.58

The data in Table 10 to Table 13 showed the selected parameters of three possible complexes which use to describe the orientation of atoms in each complex. The data in Table 10 confirmed the results from the experiment that donor atoms of TADAP were the nitrogen atom of thiazole ring, i.e. 7N-10C of TADAP, azo group, i.e. 8N-9N, and amino group, i.e. 18N-19H due to the bond lengths of these positions were longer. In addition, the sulfur atom of the thiazole ring should not be consider as

the donor atom because the bond lengths of these position were shorter as concluded in Table 14.

Besides, bond distances between ruthenium atom and all six donor atoms of all complexes as shown in Table 12 were very similar which supported that these complexes have octahedral geometry. In addition, bond angles and torsion angles (Torsion angle is the angle between the plane containing atoms ABC and the plane containing atoms BCD in a nonlinear chain of atoms A–B–C–D.) of the complex as shown in Table 11 and 13, respectively, are the useful information to explain the planarity of TADAP and the orientation of octahedral structure in each complex. It was found that two TADAP molecules of $[\text{Ru}(\text{TADAP})_2]^{3+}$ had planar geometry as seen in Table 13 which torsion angles of TADAP were nearly 180° . This may be due to their tridentate character, less steric repulsion between each TADAP molecule and the π -conjugated system of TADAP molecule. In contrast, all TADAP molecules in $[\text{Ru}(\text{TADAP})_2\text{Cl}_2]^+$ and $[\text{Ru}(\text{TADAP})_2(\text{H}_2\text{O})_2]^{3+}$ had distorted planar geometry as shown in Table 13 which torsion angles in TADAP were in the range of 140° to 170° . This may be because of their bidentate character of TADAP, and steric repulsion between TADAP and Cl^- , and TADAP and H_2O in $[\text{Ru}(\text{TADAP})_2\text{Cl}_2]^+$ and $[\text{Ru}(\text{TADAP})_2(\text{H}_2\text{O})_2]^{3+}$, respectively.

Nevertheless, the bond angles between donor atoms and ruthenium atom (Table 11) indicated that $[\text{Ru}(\text{TADAP})_2\text{Cl}_2]^+$ and $[\text{Ru}(\text{TADAP})_2(\text{H}_2\text{O})_2]^{3+}$ had octahedral geometry but $[\text{Ru}(\text{TADAP})_2]^{3+}$ had a distorted octahedral geometry. This probably due to TADAP in $[\text{Ru}(\text{TADAP})_2]^{3+}$ acted as tridentate ligand, so it had more steric hindrance and more rigidity. On the other hand, bidentate character of TADAP in $[\text{Ru}(\text{TADAP})_2\text{Cl}_2]^+$ and $[\text{Ru}(\text{TADAP})_2(\text{H}_2\text{O})_2]^{3+}$ made this structure more flexible. The geometries of donor atoms around the ruthenium atom in these three complexes are shown in Figure 29.

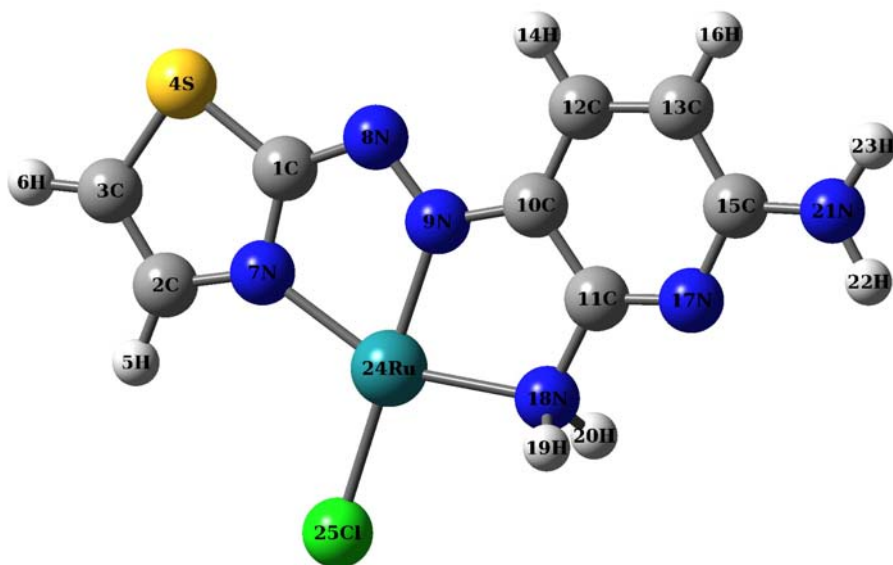


Figure 30 The optimized structure of [Ru(TADAP)Cl]²⁺ (GaussView 3.09).

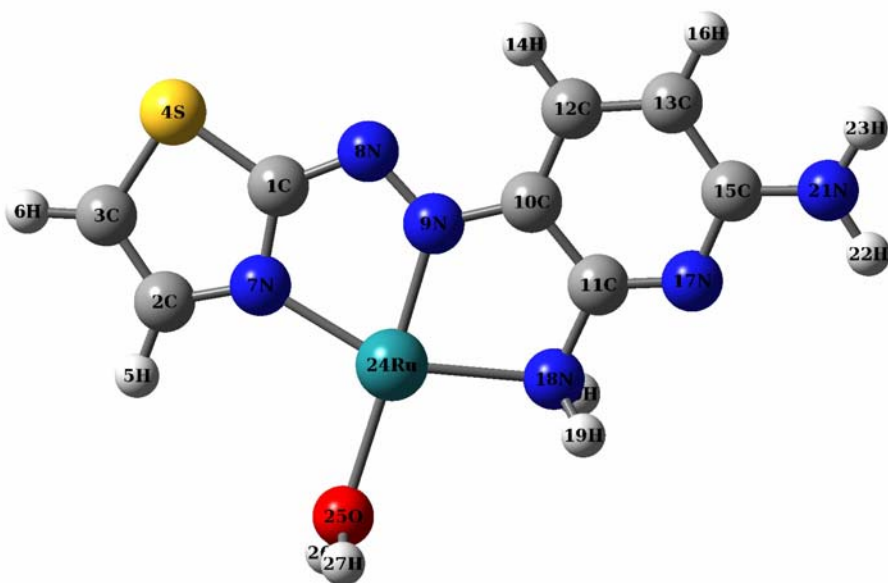


Figure 31 The optimized structure of [Ru(TADAP)H₂O]³⁺ (GaussView 3.09).

Table 15 Energies of atoms, molecules and possible structures of ruthenium(III)-TADAP complexes and stabilization energies of possible structures of ruthenium(III)-TADAP complexes obtained by the calculation on Gaussian03 at B3LYP level of theory using 6-31G* and SDD basis sets.

Atoms, molecules and complexes	Energies (a.u.)	Formation Energies (a.u.)	Stabilization Energies (kcal/mol)
Ru(III)	-92.8518159	-	-
Cl ⁻	-460.2522333	-	-
H ₂ O	-76.4089533	-	-
TADAP	-1036.331068	-	-
[Ru(TADAP)] ³⁺	-1130.150934	-0.9680503	-607.46
[Ru(TADAP)Cl] ²⁺	-1590.903888	-1.4687707	-921.66
[Ru(TADAP)H ₂ O] ³⁺	-1206.644499	-1.0526624	-660.55
[Ru(TADAP) ₂] ³⁺	-2166.760432	-1.2464812	-782.17
[Ru(TADAP) ₂ Cl ₂] ⁺	-3087.927796	-1.9093784	-1198.15
[Ru(TADAP) ₂ (H ₂ O) ₂] ³⁺	-2319.602927	-1.2710696	-797.61

Due to the solution of ruthenium(III) complex contained various potential ligand species such as Cl⁻ and H₂O. Moreover, the 1:1 complexes were also calculated to compare the stabilization energies with 1:2 complexes and to confirm the experimental results. Therefore, the more 1:1 possible structures were predicted from molecules and ions in solution. The optimized structures are shown in Figure 30 and Figure 31. Table 15 shows stabilization energies of all possible complexes. The results indicated that stabilization energies of 1:2 (Ru(III):TADAP) complexes were larger than 1:1 complexes. Due to the size and electronic configuration of ruthenium(III), it prefers an octahedral structure and stable with six coordinated bonds. It was found that [Ru(TADAP)₂Cl₂]⁺ should be the possible structure because its stabilization energy was larger than the others. The stabilization energy of this complex (-1198.15 kcal/mol) was the lowest because its structure was less rigid than the others. In addition, these results were consistent with the results from continuous variation method and conductivity measurement.

6. Stability constant of complex between 3-(2'-thiazolylazo)-2,6-diamino pyridine (TADAP) and ruthenium(III)

The stability of complex between ruthenium(III) and TADAP at pH 7.0 was studied. From Figure 32, the result shows that TADAP simultaneously formed complex with ruthenium(III) and absorbance remained constant up to 2 hours.

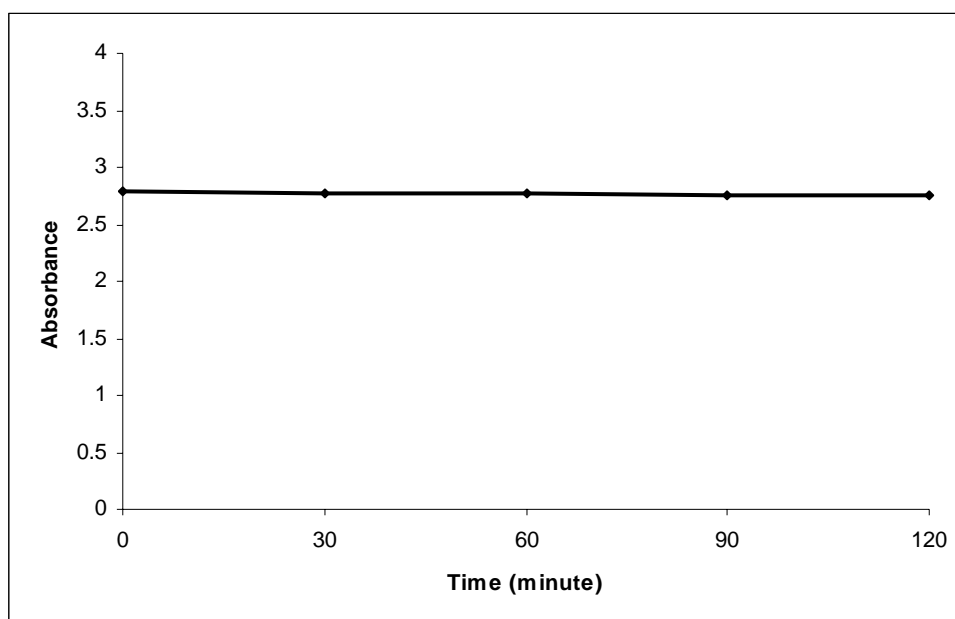


Figure 32 Relationship between absorbance of ruthenium(III)-TADAP complex and time.

The stability constant of complex between ruthenium(III) and TADAP was studied at pH 7.0 by continuous variation method (Job's method) and Benesi-Hildebrand's equation. In case of continuous variation method, the stability constant was 7.48×10^{10} whereas the stability constant from Benesi-Hildebrand's equation was 3.33×10^8 .

The stability constants of ruthenium-TADAP complex from both methods had different value due to the different process in calculation which describes in Appendix A for continuous variation method and Appendix B for Benesi-Hildebrand's Equation. It was found that the stability constants of this complex from both methods are higher than palladium(II)-TADAP (1.33×10^3) and gold(III)-TADAP (2.5×10^3) complexes in

recent research (Taveema, 2005). This may be because of the higher ratio between ruthenium(III)-TADAP complex (1:2) than palladium(II)-TADAP complex (1:1) and gold(III)-TADAP complex (1:1).

7. Investigation of binding between ruthenium(III)-TADAP complex and calf thymus DNA

7.1 Purity assessment by using A260/A280 ratios

The absorbance of a hundred ppm of calf thymus DNA was measured at 260 and 280 nm. A260 nm is frequently used to measure DNA/RNA concentration and A280 is used to measure protein concentration. It was found that A260 and A280 were 0.5813 and 0.3270, respectively. The A260/A280 ratio which approximately 1.8 indicated that there is a small amount of protein contamination in calf thymus DNA sample. The solution for A260/A280 ratio is fully explained in Appendix D.

7.2 The binding between calf thymus DNA and ruthenium(III)-TADAP

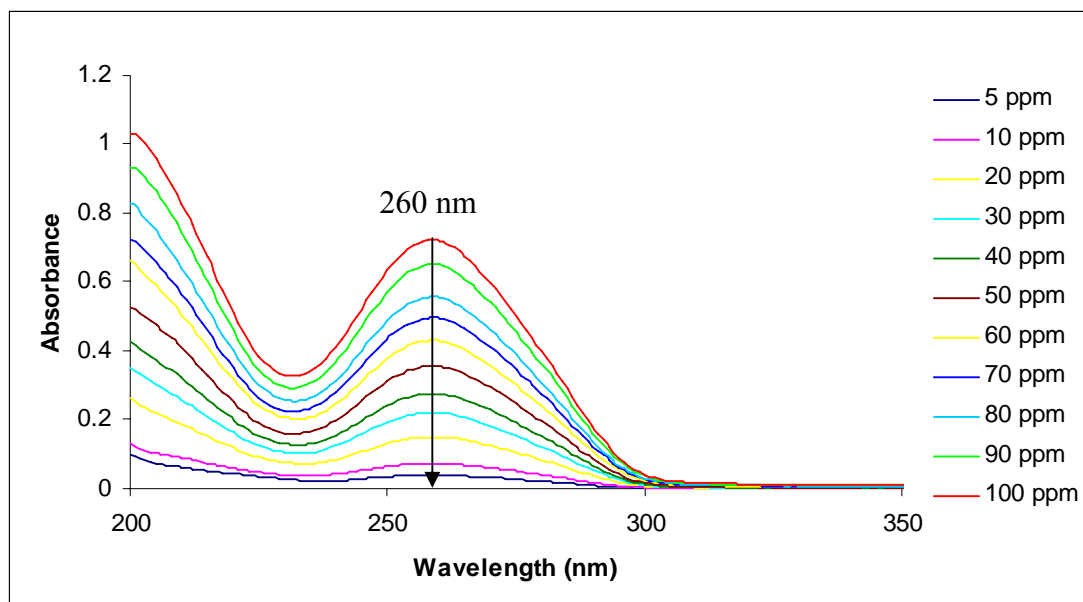


Figure 33 Absorption spectra of calf thymus DNA at various concentrations.

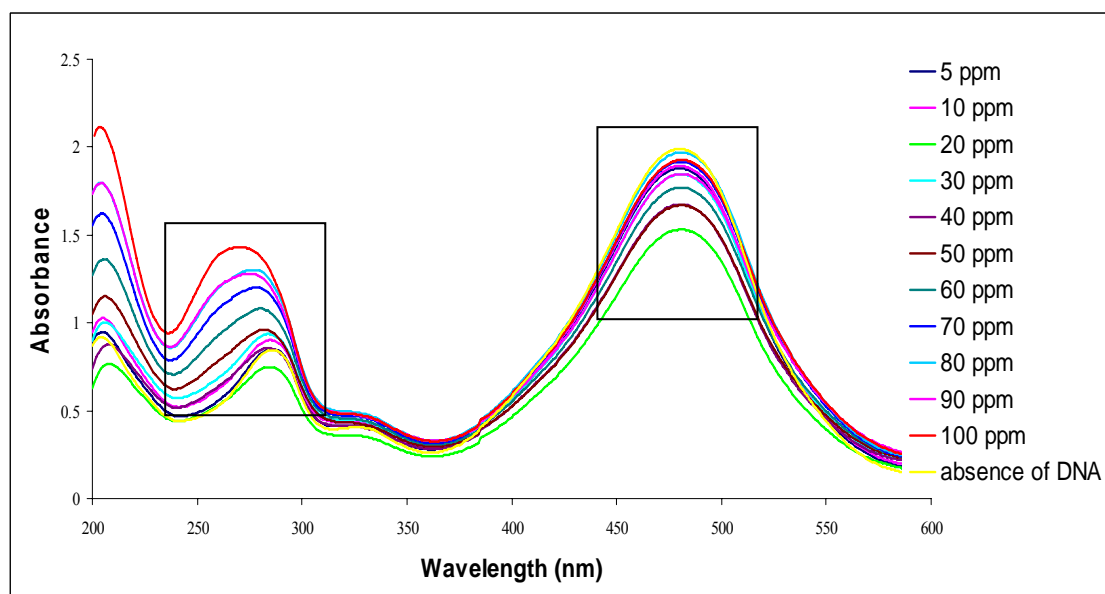


Figure 34 Absorption spectra of 4×10^{-5} M ruthenium(III)-TADAP complex in various concentrations of calf thymus DNA.

Figure 33 shows the maximum absorption of calf thymus DNA at 260 nm. Besides, the absorbances were consistent with the concentrations of calf thymus DNA.

For DNA binding study with ruthenium(III)-TADAP complex, 4.0×10^{-5} M of the complex was mixed with calf thymus DNA solution at various concentrations. The absorption spectra of the mixture solutions are shown in Figure 34. The spectra showed that the absorbance of complex was significantly changed to lower wavelength (blue shift) between 250 nm and 300 nm while increasing the DNA concentration. However, there was no change in the absorbance of the complex at 480 nm. In addition, it was found that there were some precipitates occurred after the mixing of the complex with DNA. So, there might be an interaction between the complex and DNA. To determine the binding character between calf thymus DNA and the complex, the more appropriate condition should be investigated.

7.3 Calculation for the stabilization energy between ruthenium(III)-TADAP complex and nucleobases

The bonding between ruthenium(III)-TADAP complex and nucleobase was studied by quantum chemical calculation via the Gaussian03 program. The geometries of $[\text{Ru}(\text{TADAP})_2]^{3+}$, $[\text{Ru}(\text{TADAP})_2\text{Cl}]^{2+}$ and $[\text{Ru}(\text{TADAP})_2(\text{H}_2\text{O})]^{3+}$ bound with adenine base and guanine base were optimized. In order to form bond with DNA base, one of the donor atom of the complexes have to dissociate from ruthenium atom to give five coordinated intermediate complexes. Therefore, the stabilization energy of five coordinated complexes of $[\text{Ru}(\text{TADAP})_2]^{3+}$, $[\text{Ru}(\text{TADAP})_2\text{Cl}]^{2+}$ and $[\text{Ru}(\text{TADAP})_2(\text{H}_2\text{O})]^{3+}$ were calculated. For the five coordinated complex of $[\text{Ru}(\text{TADAP})_2]^{3+}$, due to the weakest bond strength between Ru(III) and N atom from amino group, this bond was expected to break whereas the C–N bond between N azo and 2,6-diaminopyridine was expected to rotate by 180° (Figure 35) before the bonding with DNA base. Whereas one Cl^- was removed from $[\text{Ru}(\text{TADAP})_2\text{Cl}]^{2+}$ (Figure 36), and H_2O molecule was removed from $[\text{Ru}(\text{TADAP})_2(\text{H}_2\text{O})]^{3+}$ (Figure 37). Then, adenine and guanine were inserted to the available site of each complex. The donor atoms of adenine and guanine were chosen

from the free nitrogen of A–T and C–G base pairs as shown in Figure 38 and Figure 39, respectively. For adenine, the other two nitrogen atoms in six membered ring form double hydrogen bonds with thymine base (Wade, 1999). The other nitrogen atom in five membered ring is screened by deoxyribose sugar and phosphate group. For guanine, an oxygen and two nitrogen atoms in six membered ring form triple hydrogen bonds with cytosine base (Wade, 1999). The other nitrogen atom is also screened by the deoxyribose sugar and the phosphate group. The six optimized structures of complexes bound with DNA bases are shown in Figure 41 to Figure 45. The stabilization energy of all compounds is shown in Table 16.

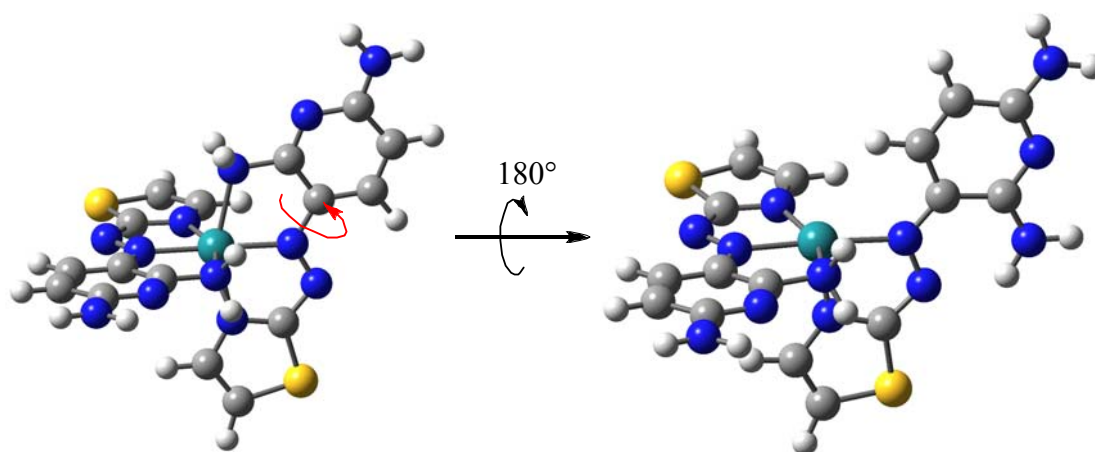


Figure 35 The five coordinated complex of $[\text{Ru}(\text{TADAP})_2]^{3+}$ by rotating the C–N bond.

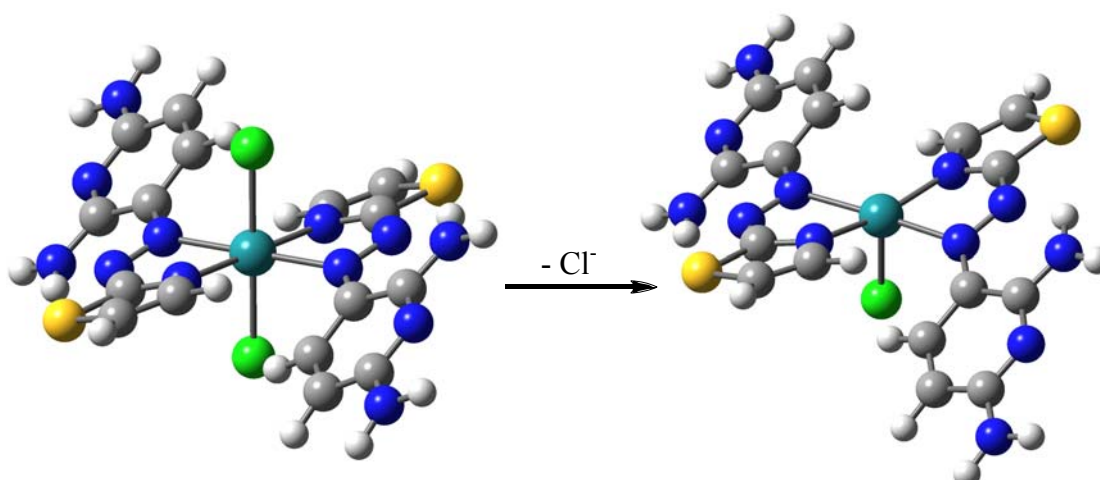


Figure 36 The five coordinated complex of $[\text{Ru}(\text{TADAP})_2\text{Cl}_2]^+$ by removing Cl^- ion.

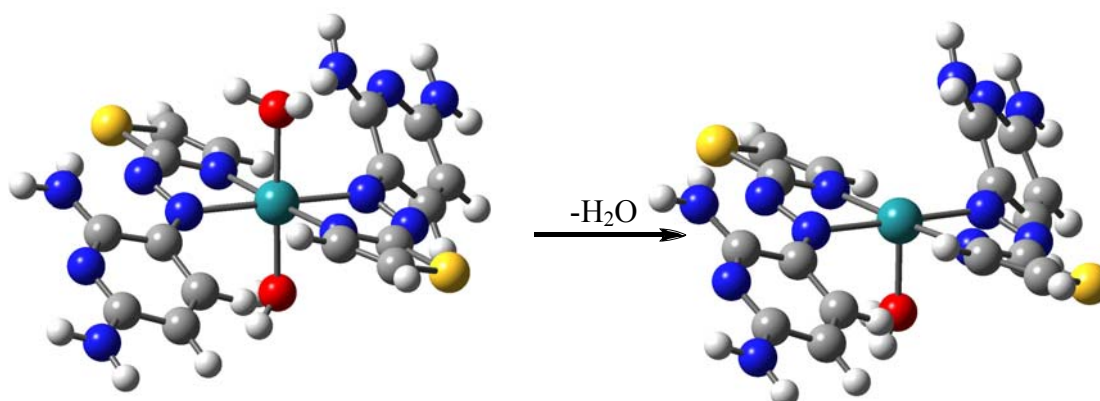


Figure 37 The five coordinated complex of $[\text{Ru}(\text{TADAP})_2(\text{H}_2\text{O})_2]^{3+}$ by removing H_2O molecule.

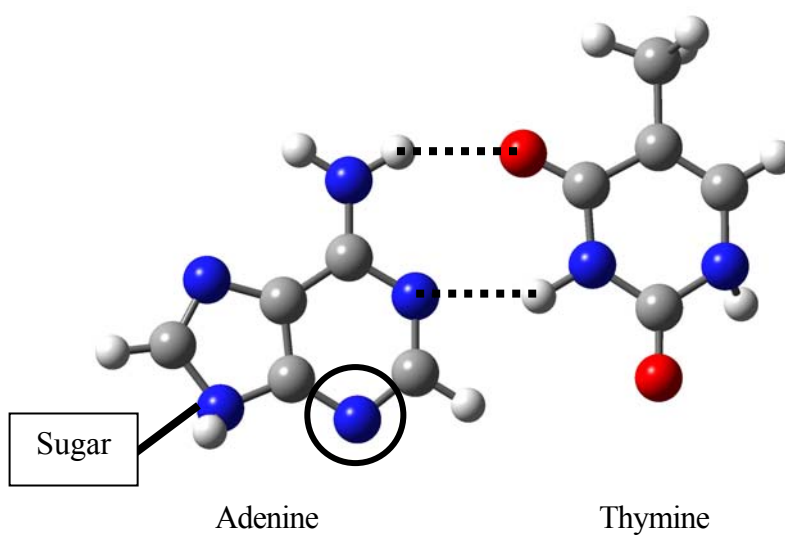


Figure 38 The available donor atom of adenine base (the nitrogen atom in a circle).

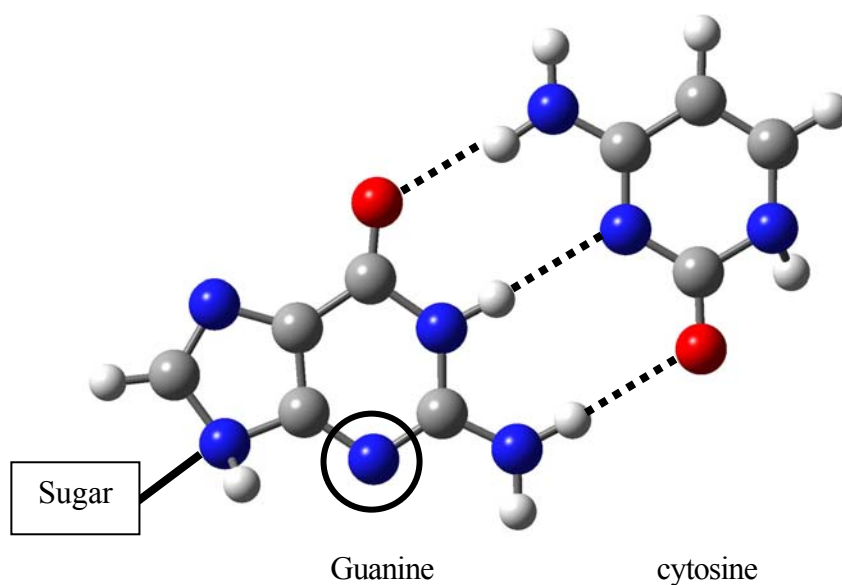


Figure 39 The available donor atom of guanine base (the nitrogen atom in a circle).

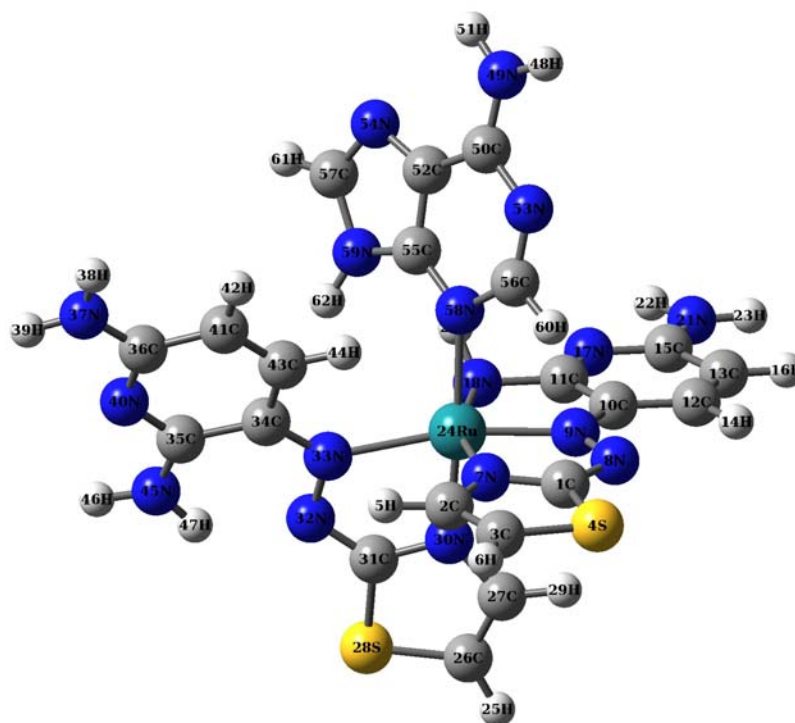


Figure 40 The optimized structure of $[\text{Ru}(\text{TADAP})_2]^{3+}$ bonding with adenine base.

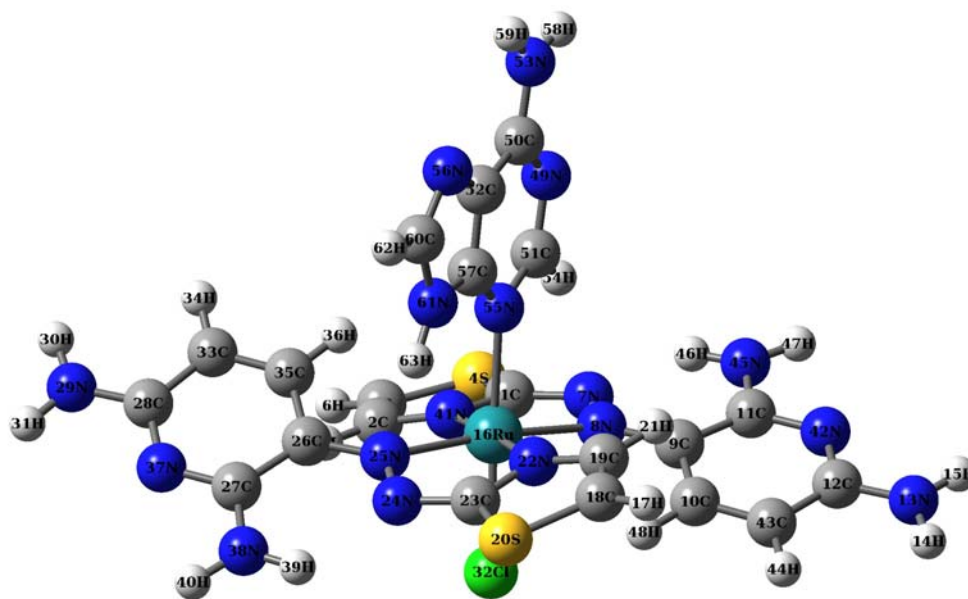


Figure 41 The optimized structure of $[\text{Ru}(\text{TADAP})_2\text{Cl}]^{2+}$ bonding with adenine base.

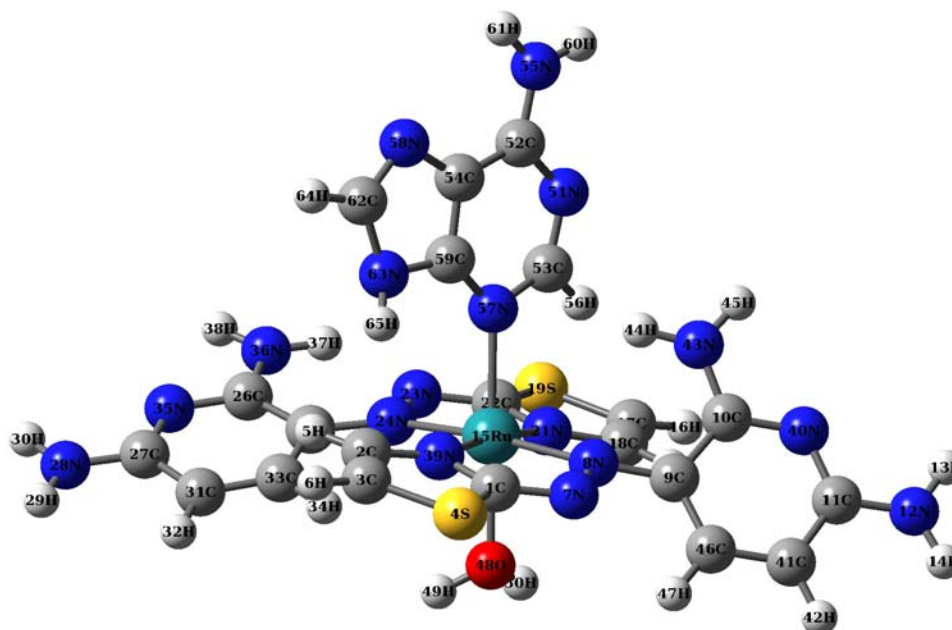


Figure 42 The optimized structure of $[\text{Ru}(\text{TADAP})_2\text{H}_2\text{O}]^{3+}$ bonding with adenine base.

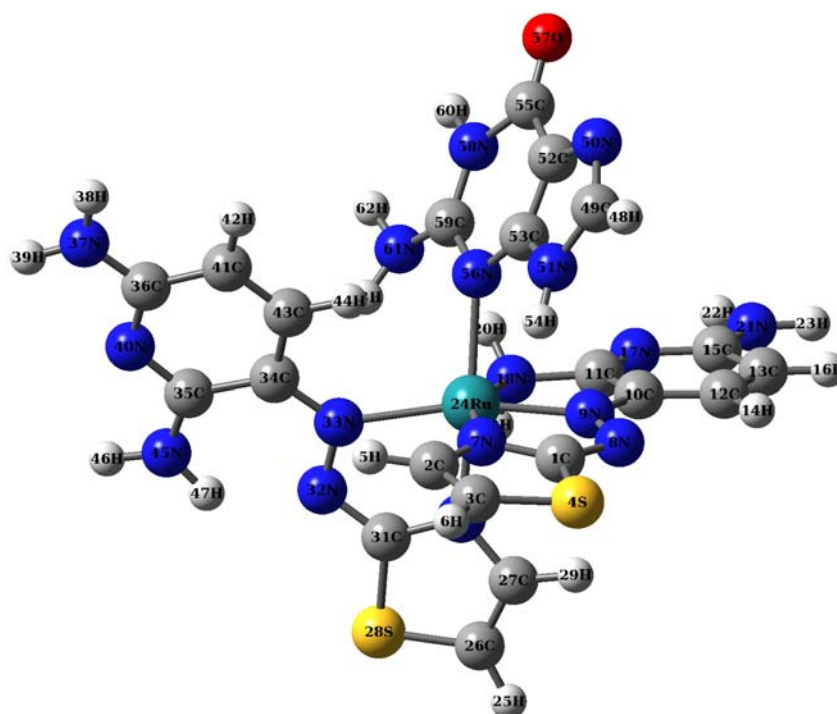


Figure 43 The optimized structure of $[\text{Ru}(\text{TADAP})_2]^{3+}$ bonding with guanine base.

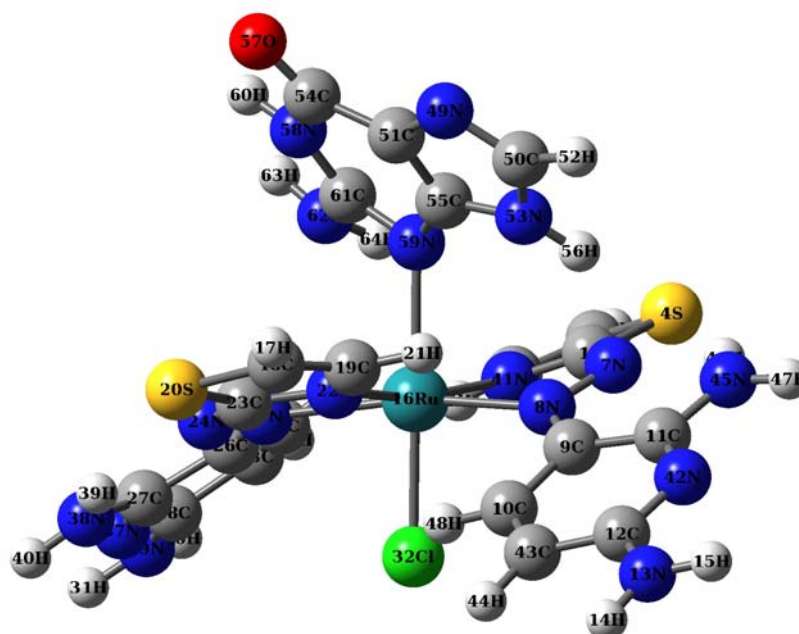


Figure 44 The optimized structure of $[\text{Ru}(\text{TADAP})_2\text{Cl}]^{2+}$ bonding with guanine base.

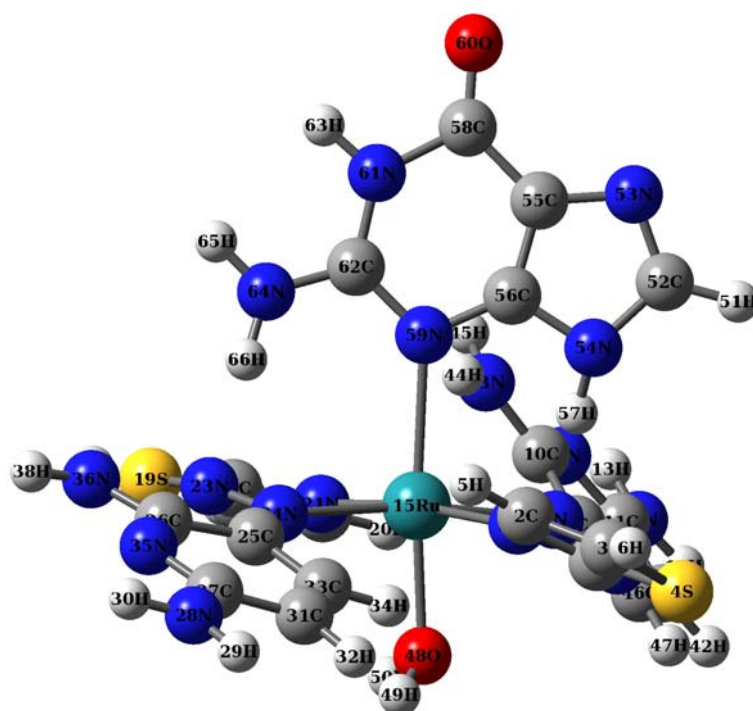


Figure 45 The optimized structure of $[\text{Ru}(\text{TADAP})_2\text{H}_2\text{O}]^{3+}$ bonding with guanine base.

Table 16 Energies of atoms, molecules, adenine base, guanine base, and compounds of $[\text{Ru}(\text{TADAP})_2]^{3+}$, $[\text{Ru}(\text{TADAP})_2\text{Cl}]^{2+}$ $[\text{Ru}(\text{TADAP})_2(\text{H}_2\text{O})]^{3+}$ with adenine and guanine base obtained by the calculation on Gaussian03 at B3LYP level of theory using 6-31G* and SDD basis sets.

Atoms, molecules and complexes	Energies (a.u.)	Stabilization Energies (a.u.)	Stabilization Energies (kcal/mol)
Ru(III)	-92.85181600	-	-
Cl ⁻	-460.2522333	-	-
TADAP	-1036.331068	-	-
$[\text{Ru}(\text{TADAP})_2]^{3+}$	-2166.760432	-1.2464812	-782.17
$[\text{Ru}(\text{TADAP})_2]^{3+}$ (5coor)	-2166.740517	-1.2265656	-769.68
$[\text{Ru}(\text{TADAP})_2\text{Cl}_2]^+$	-3087.927796	-1.9093784	-1198.15
$[\text{Ru}(\text{TADAP})_2\text{Cl}]^{2+}$	-2627.359160	-1.5929755	-999.61
$[\text{Ru}(\text{TADAP})_2(\text{H}_2\text{O})_2]^{3+}$	-2319.602927	-1.2710696	-797.61
$[\text{Ru}(\text{TADAP})_2(\text{H}_2\text{O})]^{3+}$	-2243.125825	-1.2029208	-754.84
Adenine base	-467.2901688	-	-
Guanine base	-542.5046641	-	-
$[\text{Ru}(\text{TADAP})_2]^{3+} - \text{A}^*$	-2634.133996	-1.3298765	-834.51
$[\text{Ru}(\text{TADAP})_2\text{Cl}]^{2+} - \text{A}^*$	-3094.737588	-1.6812344	-1054.99
$[\text{Ru}(\text{TADAP})_2]^{3+} - \text{G}^{**}$	-2709.329439	-1.3108240	-822.55
$[\text{Ru}(\text{TADAP})_2\text{Cl}]^{2+} - \text{G}^{**}$	-3169.934955	-1.6641065	-1044.24
$[\text{Ru}(\text{TADAP})_2(\text{H}_2\text{O})]^{3+} - \text{A}^*$	-2710.506496	-1.29342275	-811.64
$[\text{Ru}(\text{TADAP})_2(\text{H}_2\text{O})]^{3+} - \text{G}^{**}$	-2785.672866	-1.24529719	-781.44

* A = Adenine base

** G = Guanine base

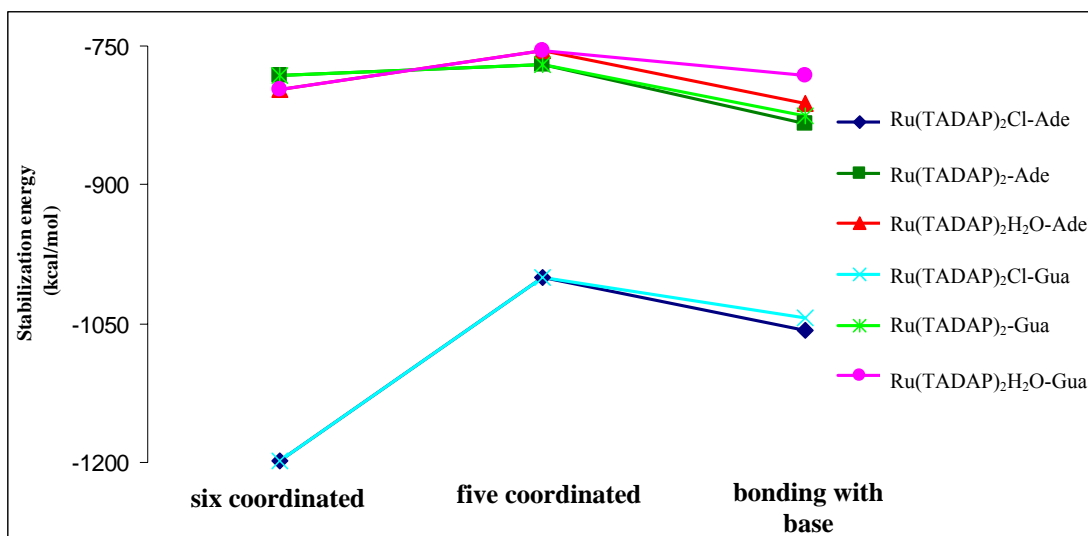


Figure 46 Stabilization energy of six, five coordinated complexes and the complexes with nucleobase adenine and guanine.

From Figure 46, the activation energy used to form five coordinated complex of $[\text{Ru}(\text{TADAP})_2\text{Cl}]^{2+}$ (198.54 kcal/mol) is higher than $[\text{Ru}(\text{TADAP})_2]^{3+}$ (12.50 kcal/mol) and $[\text{Ru}(\text{TADAP})_2(\text{H}_2\text{O})]^{3+}$ (42.76 kcal/mol). This may be due to the high stability of the complex $[\text{Ru}(\text{TADAP})_2\text{Cl}_2]^+$. In addition, the activation energy of $[\text{Ru}(\text{TADAP})_2]^{3+}$ to form the five coordinated intermediate was the lowest. This may be because the six coordinated complex has the highest energy which is related to the high rigidity of the molecule.

In nucleobase binding study, the data in Table 16 indicated that $[\text{Ru}(\text{TADAP})_2\text{Cl}]^{2+}$ -Adenine was the most stable complex with the stabilization energy of -1054.99 kcal/mol. According to the structure of the five coordinated complex, $[\text{Ru}(\text{TADAP})_2\text{Cl}]^{2+}$ has the most available space for the nucleobase because of the bidentate character and the orientation of TADAP as described in the previous section. However, it was found that $[\text{Ru}(\text{TADAP})_2]^{3+}$ -Adenine, $[\text{Ru}(\text{TADAP})_2]^{3+}$ -Guanine and $[\text{Ru}(\text{TADAP})_2(\text{H}_2\text{O})]^{3+}$ -Adenine have stabilization energies larger than their six coordinated complexes. In contrast, the energy of the adduct of $[\text{Ru}(\text{TADAP})_2\text{Cl}]^{2+}$ was higher than its parent six coordinated complex. Besides, the data showed that the stabilization energies of all adenine complexes were larger than

guanine complexes. This probably due to the structure of the nucleobase. An adenine base has three nitrogen atoms in the pyrimidine ring (six membered ring) and two nitrogen atoms in the imidazole ring (five membered ring). Similarly, a guanine base has two nitrogen atoms in the imidazole ring and three nitrogen atoms in the pyrimidine ring with one extra oxygen atom. As the nitrogen donor atom is in the six membered ring as shown in Figure 38 and 39, consequently, the electron density in the pyrimidine ring of the guanine is lower than the adenine due to the electron withdrawing character of the oxygen atom. Therefore, the chemical bond between an adenine and the complex is stronger than the bond between a guanine and the complex. Another reason may be because the structure of adenine in both complexes is perpendicular to the plane which unlikely to occur in guanine. So, the structure of adenine complex has less steric than guanine base.

According to the experimental study which described in the previous section and the results of the stabilization and the activation energy from the quantum chemical calculation, the precipitation of the mixture between the ruthenium(III)-TADAP complex and calf thymus DNA was probably from the interaction between $[\text{Ru}(\text{TADAP})_2]^{3+}$ or $[\text{Ru}(\text{TADAP})_2(\text{H}_2\text{O})]^{3+}$ with the DNA due to the excess amount of TADAP and H_2O in the experimental condition, and the low activation energy. Although adducts between $[\text{Ru}(\text{TADAP})_2\text{Cl}]^{2+}$ and the DNA bases were the most stable, but either the small amount of Cl^- in the solution or the highest activation energy made these adducts difficult to form. Therefore, the energy data indicated that the further DNA binding experiment should be performed in the water free condition to induce and investigate the formation of the adduct between $[\text{Ru}(\text{TADAP})_2]^{3+}$ and DNA bases.

8. Preparation of 3-(2'-thiazolylazo)-2,6-diaminopyridine resin (TADAP-SG)

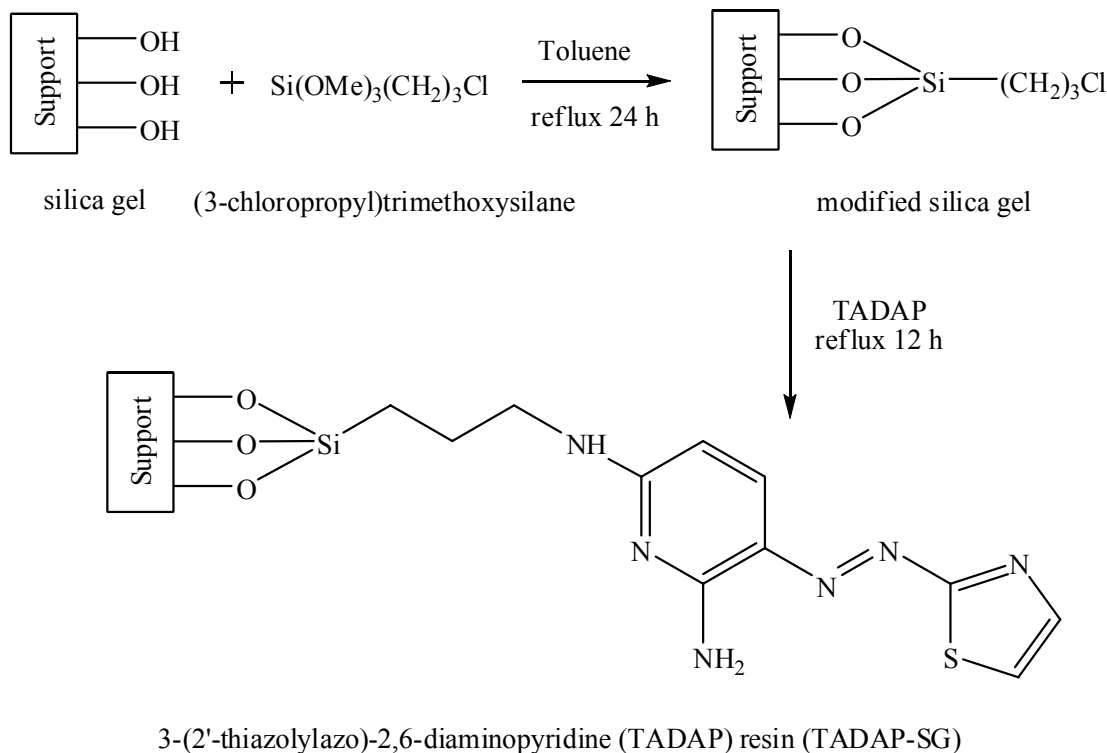


Figure 47 Synthesis pathway of 3-(2'-thiazolylazo)-2,6-diaminopyridine resin (TADAP-SG).

3-(2'-thiazolylazo)-2,6-diaminopyridine resin (TADAP-SG) was prepared in two steps. The first step was modification of silica gel surface. The polarity of hydroxyl groups on the surface of silica gel were reduced by a reaction with (3-chloropropyl)trimethylsilane under nitrogen atmosphere. Besides, the modified silica gel has a chlorine atom which acted as the very good leaving group. The final step was immobilization of TADAP on the modified silica gel by refluxing for 12 hours. A nitrogen atom of the amino group of TADAP formed a new bond to methylene carbon and released chloride ion. The synthesized product was used to recover ruthenium(III) from aqueous solution.

9. Determination of capacity for the adsorption of ruthenium(III) by TADAP-SG

To determine the adsorption capacity of TADAP-SG, pH and shaking time are the influent parameters. These parameters were optimized by using batch equilibrium experiment.

9.1 Effect of pH

The capacity of TADAP-SG at pH 3.0, 4.0, 5.0, 6.0, and 7.0 were 0.7999, 0.9998, 2.7092, 2.8900, and 2.9409 mmol/g, respectively, as shown in Figure 48. This figure illustrated that the highest capacity of TADAP-SG for ruthenium(III) was obtained at pH 7.0.

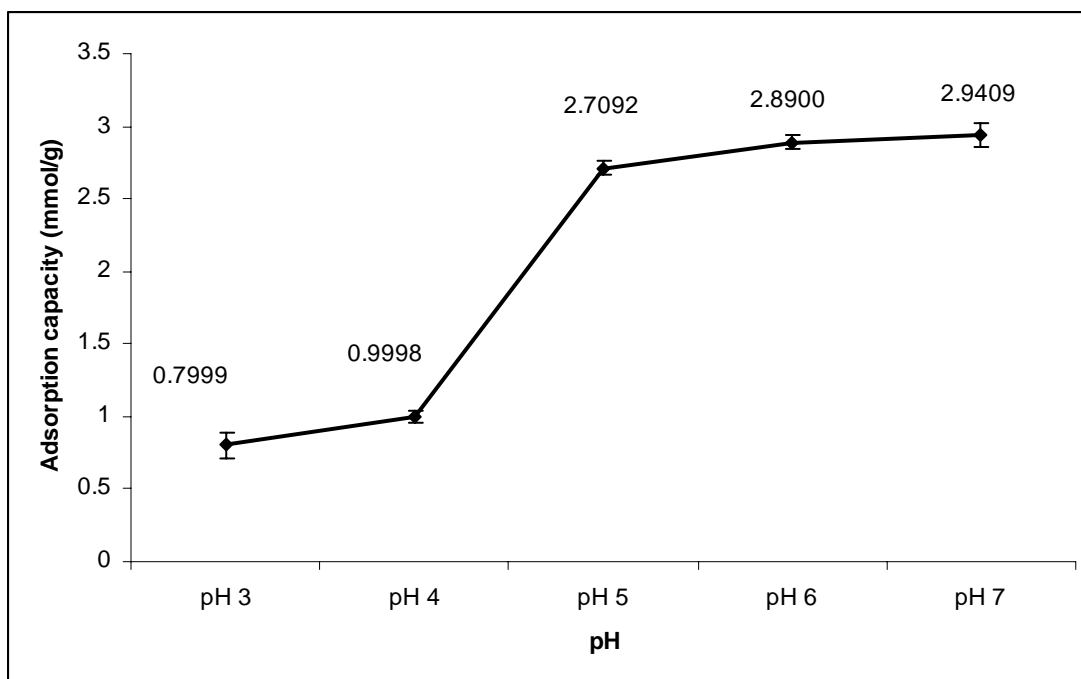


Figure 48 Effect of pH on the adsorption of ruthenium(III) by TADAP-SG.

As seen in Figure 48, the adsorption capacity decreased when pH was decreased due to the protonation of donor atoms in the structure of TADAP. These protons reduced the ability of donor atoms to donate electron pairs to metal ions.

9.2 Effect of shaking time

The capacity of TADAP-SG for the adsorption of ruthenium(III) as a function of time is shown in Figure 49. This figure indicated that the adsorption capacity of ruthenium(III) on TADAP-SG began stable since 0.5 h and constant up to 5 hours.

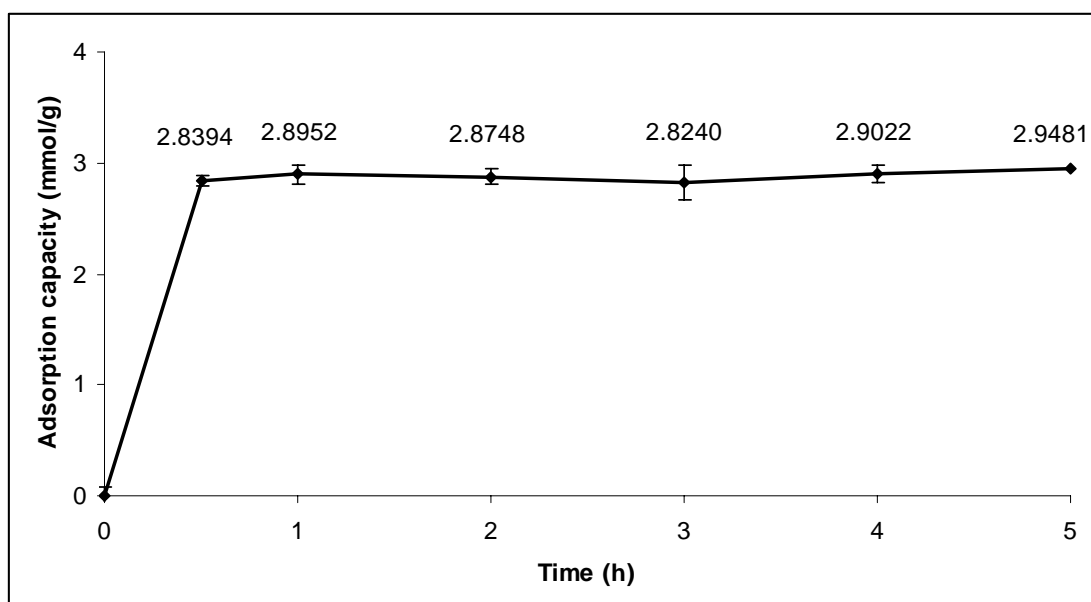


Figure 49 Effect of shaking time on the adsorption of ruthenium(III) by TADAP-SG.

The result indicated that the adsorption capacity of ruthenium(III) by TADAP-SG reached the equilibrium at 30 minutes of shaking time. This result is coherent with the high stability constant of ruthenium(III)-TADAP complex which is 3.33×10^8 .

The adsorption capacity of TADAP-SG of ruthenium(III) at the optimum condition (pH 7.0, 4 hours shaking time and 20 ppm of initial ruthenium(III) concentration) was 2.9022 mmol/g.

10. Desorption of ruthenium(III) on TADAP-SG

In batch equilibrium experiment, the desorption of ruthenium(III) from TADAP-SG by various eluents were examined. The results are shown in Figure 50. It was found that 0.1 M thiourea can be used as the eluent for the desorption of ruthenium(III) from TADAP-SG because it has the highest percentage in desorption and thiourea has two nitrogen atoms which may act as chelating ligand. Nevertheless, other eluents should be investigated for higher percentage in desorption of ruthenium(III).

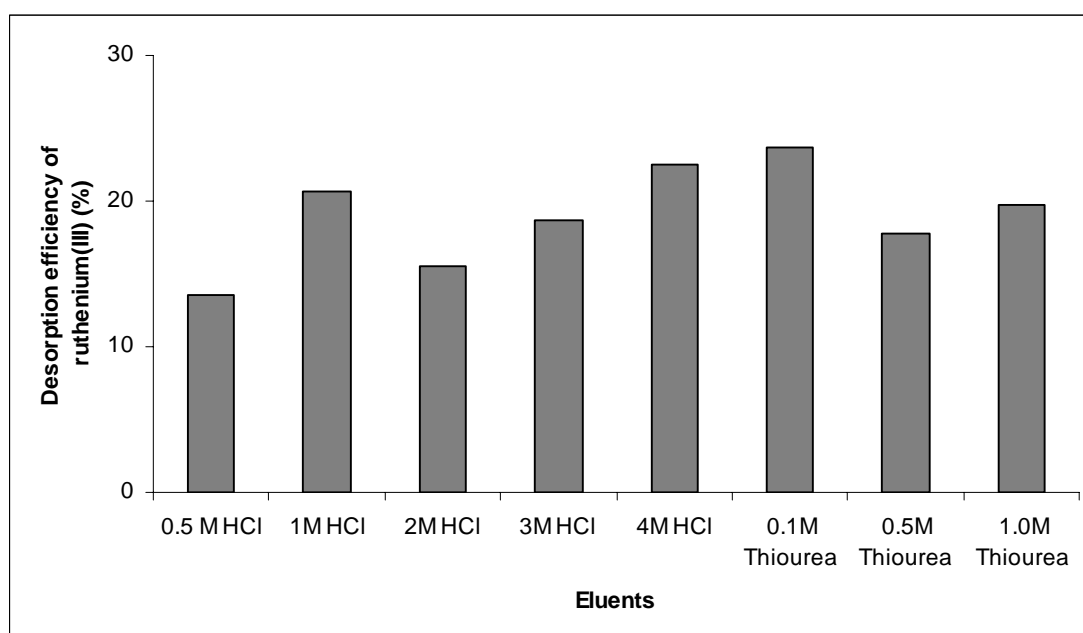


Figure 50 Desorption efficiency of ruthenium(III) from TADAP-SG by 8 eluents.

11. Adsorption efficiency of reused TADAP-SG for ruthenium(III)

The efficiency of TADAP-SG for the adsorption of ruthenium(III) was determined by batch equilibrium experiment. The result is shown in Figure 51 which indicated that TADAP-SG that had been used up to three times can still be reused as adsorbent for ruthenium(III).

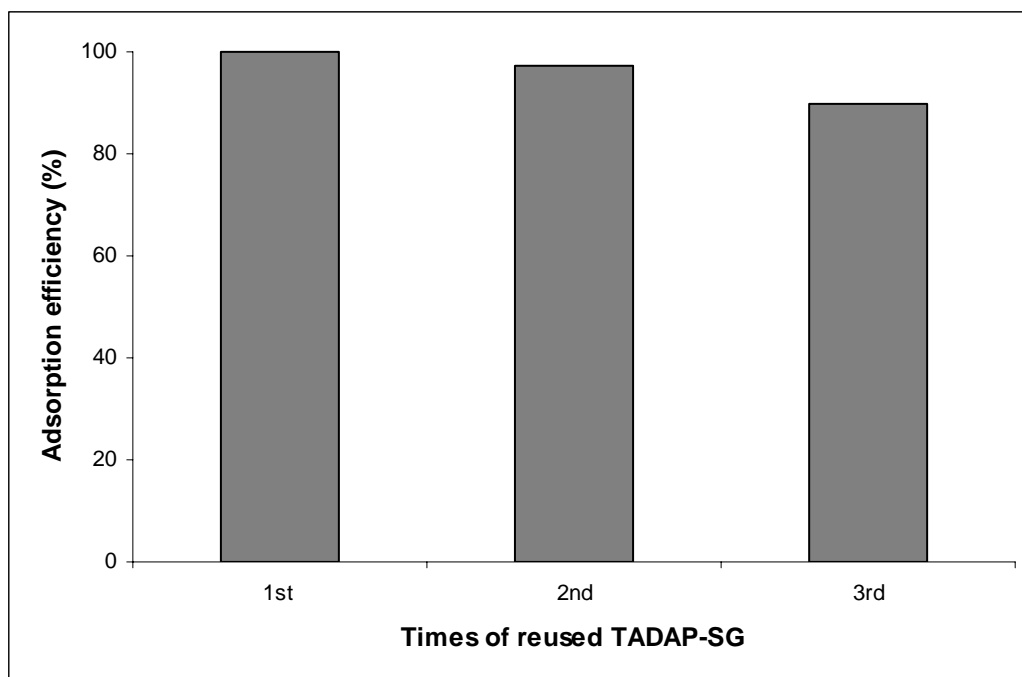


Figure 51 Adsorption efficiency (%) for ruthenium(III) of TADAP-SG that had been used 1 to 3 times.

12. Adsorption capacity of TADAP-SG for other metal ions

TADAP-SG was used to adsorb four selected metal ions namely, iron(III), copper(II), palladium(II) and gold(III), and compare its adsorption capacity of each metal ion. Copper and iron are the represents of the first row transition metal and iron is the element in the same group (VIII B) as ruthenium. Palladium and gold are members of the platinum group metals as ruthenium. In addition, palladium and gold are the represents of the second and the third row of the transition metal, respectively. Figure 48 showed the adsorption capacity of TADAP-SG when initial concentrations of each metal ion were 20 ppm in acetate buffer pH 7.0.

The data indicated that TADAP-SG has greater affinity for ruthenium(III) than other metal ions. This may be because ruthenium(III) which classify as the borderline

acid was favored with the borderline base, TADAP, by hard and soft acids and bases (HSAB) rules.

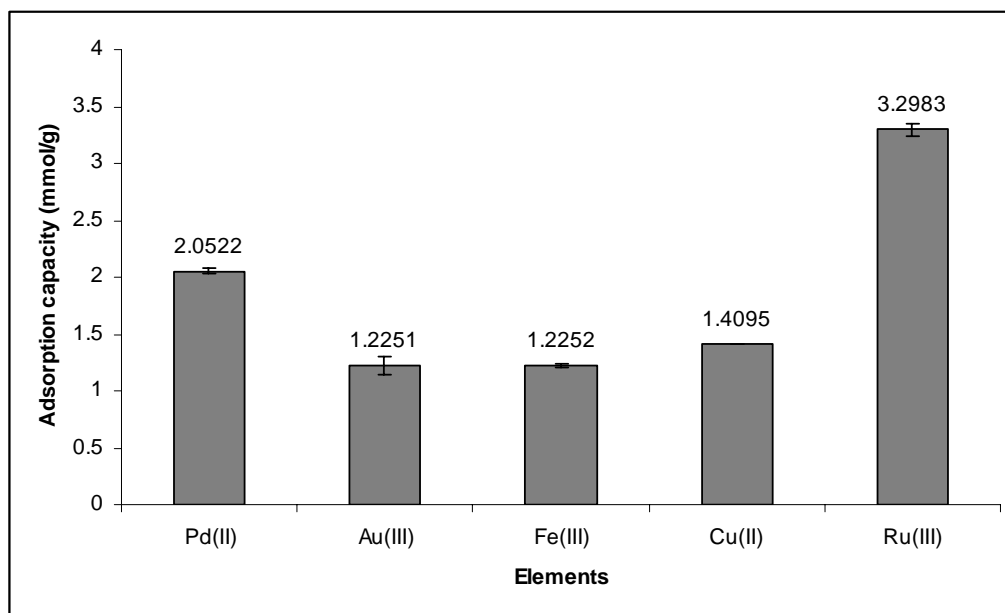


Figure 52 Adsorption capacity of TADAP-SG of 20 ppm of each metal ion at pH 7.0.

CONCLUSION

The thiazolylazo dye 3-(2'-thiazolylazo)-2,6-diaminopyridine was synthesized and its structure was characterized by FT-IR, ^1H NMR, mass spectroscopy and elemental analysis. The complex between TADAP and ruthenium(III) was studied. The complex in phosphate buffer at pH 7.0 gave the red-brown solution with a maximum absorption at 480 nm. The stoichiometric ratio of this complex verified by continuous variation and conductivity measurement was 1:2 (Ru(III):TADAP). The structure of the complex was determined by experimental (FT-IR and ^1H NMR) study and confirmed by theoretical calculation optimized by using the 6-31G* and SDD basis sets at B3LYP level of theory. According to Benesi-Hildebrand's equation and continuous variation method, the stability constants of the complex were 3.33×10^8 and 7.48×10^{10} , respectively.

In addition, according to the experiment and the quantum chemical calculation of DNA binding study, ruthenium(III)-TADAP complex can be interacted with calf thymus DNA in Tris-HCl buffer pH 7.4. The precipitate of the mixture between the the complex and calf thymus DNA was probably from the interaction between $[\text{Ru}(\text{TADAP})_2]^{3+}$ or $[\text{Ru}(\text{TADAP})_2(\text{H}_2\text{O})]^{3+}$ with the DNA. The adducts between the complexes and the adenine base showed the higher stability than the adducts between the complexes and the guanine base. However, further work need to be done.

Finally, TADAP was immobilized on silica gel surface to produce a chelating resin (TADAP-SG), which had the adsorption ability of ruthenium(III). The adsorption capacity of ruthenium(III) by TADAP-SG at pH 7.0, 4 hours and 20 ppm of ruthenium(III) initial concentration was 2.9022 mmol/g. 0.1 M thiourea could be used as the eluent for desorption of ruthenium(III) from TADAP-SG and it could be reused for adsorption of ruthenium(III) up to 3 times. The adsorption efficiency of ruthenium(III) by TADAP-SG was considerable higher than gold(III), palladium(II), iron(III) and copper(II).

LITERATURE CITED

- Allardyce, C.S. and P.J. Dyson. 2001. Ruthenium in Medicine: Current Clinical Uses and Future Prospects. **Platinum Met. Rev.** 45(2): 62-69.
- Allen, A.D. and F. Bottomley. 1968. Inorganic Nitrogen Fixation. Nitrogen Compounds of the Transition Metal. **Acc. Chem. Res.** 1(12): 360-365.
- Aynsley, E.E., R.D. Peacock P.L. Robinson. 1952. The preparation and properties of selenium tetrafluoride and oxyfluoride. **J. Chem. Soc.** 1231-1234.
- Banks C.V. and J.W. O'Laughlin. 1957. Spectrophotometric Determination of Ruthenium with 1,10-phenanthroline. **Anal. Chem.** 29(10): 1412-1417.
- Benesi, H.A. and J.H. Hildebrand. 1949. A spectrophotometric investigation of the interaction of iodine with aromatic hydrocarbons. **J. Am. Chem. Soc.** 70: 2703-2707.
- Brabec, V. and O. Nováková. 2006. DNA binding mode of ruthenium complexes and relationship to tumor cell toxicity. **Drug Resist. Update.** 9(3): 111-122.
- Busev, A.I., V.M. Ivanov and E.D. Usama. 1968. Spectrophotometric investigation of 5-(2-thiazolylazo)-2,6-diaminopyridine. **Khimiya.** 23(5): 66-69.
- Clarke, M. J. 2003. Ruthenium metallopharmaceuticals. **Coor. Chem. Rev.** 236: 209-233.
- Connors, K.A. 1987. **Binding Constants.** John Wiley and Sons, Inc., New York.
- Corral, E., A. C.G. Hotze, D.M. Tooke, A.L. Spek and J. Reedijk. 2006. Ruthenium polypyridyl complexes containing the bischelating ligand 2,2'-azobispyridine.

Synthesis, characterization and crystal structures. **Inorg. Chim. Acta.** 359: 830-838.

Dwyer, F.P., H.A. Goodwin and E.C. Gyarfas. 1963. Mono- and Bis-(2,2'-bipyridine) and (1,10-phenanthroline) Chelates of Ruthenium and Osmium. I. Monochelates of Bivalent, Tervalent, and Quadrivalent Ruthenium. **Aust. J. Chem.** 16(1): 42-50.

El-Gogary, T.M. and G. Koehler. 2007. Interaction of psoralens with DNA-bases (I). An ab initio quantum chemical, density functional theory and second-order Møller-Plesset perturbational study. **J. Mol. Struct. (Theochem).** 808: 97-109.

Fletcher, J.M., B.F. Greenfield, C.J. Hardy, D. Scagill and J.L. Woodhead. 1961. Ruthenium red. **J. Chem. Soc.** 2000-2006.

Foresman, J.B. and Æ. Frisch. 1995-96. **Exploring Chemistry with Electronic Structure Methods.** 2nd ed. Gaussian, Inc., Pittsburgh.

Garcia, M.F., D.V. Gonzalez and T.C.R. Gonzalez. 1982. Analytical Applications of 3-(2'-thiazolylazo)-2,6-diaminopyridine: Spectrophotometric Determination of Palladium. **Microchem. J.** 27(2): 194-199.

Garg, B.S., R.K. Sharma, N. Bhojak and S. Mittal. 1999. Chelating Resins and Their Applications in the Analysis of Trace Metal Ions. **Microchem. J.** 61: 94-114.

Garza-Ortiz, A., H. den Dulk, J. Brouwer, H. Kooijman, A.L. Spek and J. Reedijk. 2007. The synthesis, chemical and biological properties of dichloro(azpy) gold(III) chloride (azpy = 2-(phenylazo)pyridine) and the gold-induced conversion of the azpy ligand to the chloride of the novel tricyclic pyrido[2,1-c][1,2,4]benzotriazin-11-ium cation. **J. Inorg. Biochem.** 101: 1922-1930.

- Ghosh, J.P., J. Pramanick and H.R. Das. 1981. Preconcentration and properties of a new chelating resin containing 2-nitroso-1-naphthol. **Talanta**. 28(12): 957-959.
- Gibb, T.C., R. Greatrex, and N.N. Greenwood. 1980. A novel case of magnetic relaxation in the ^{99}Ru Mössbauer spectrum of Na_3RuO_4 . **J. Solid State Chem.** 31(2): 153-169.
- Glasel, J.A. 1995. Validity of Nucleic Acid Purities Monitored by A260/A280 Absorbance Ratios. **Biotechniques**. 18(1): 62-63.
- Goldberg, R.N. and L.G. Hepler. 1968. Thermochemistry and oxidation potentials of platinum group metals and their compounds. **Chem. Rev.** 68(2): 229-252.
- Gonzalez, V.D., M.J. Sanchez and F.M. Garcia. 1986. Complexation equilibria and spectrophotometric determination of cobalt with 3-(2'-thiazolylazo)-2,6-diaminobenzene and 3-(2'-thiazolylazo)-2,6-diaminopyridine. **Quim. Anal. (Barcelona)**. 5(3):335-341.
- Gottlieb, H.E., V. Kotlyar and A. Nudelman. 1997. NMR Chemical Shifts of Common Laboratory Solvents as Trace Impurities. **J. Org. Chem.** 62:7512-7515.
- Greenwood, N.N. and A. Earnshaw. 1997. **Chemistry of the elements**. 2nd ed. Butterworth-Heinemann, Oxford.
- Han, D., H. Wang and N. Ren. 2004. Molecular modeling study on the binding mode of polypyridyl transition Ru metal complexes with B-DNA. **J. Mol. Struct. (Theochem)**. 711: 185-192.
- Harris, D.C. 1999. **Quantitative chemical analysis**. 5th ed. W. H. Freeman, New York.

- Hao, Y.M. and H.X. Shen. 2000. Simple and sensitive determination of nucleic acids using palladium(II) complex with 2-(2-thiazolylazo)-5-dimethylaminobenzoic acid. **Anal. Chim. Acta.** 422: 159-166.
- Held, P. G. 2001. **Nucleic Acid Purity Assessment Using A260/A280 Ratios.**
Available Source:
http://www.biotek.com/products/tech_res_detail.php?id=43, August 22, 2007.
- Hotze, A.C.G., A.H. Velders, F. Ugozzoli, M. Biagini-Cingi, A.M. Manotti-Lanfredi, J.G. Haasnoot and J. Reedijk. 2000. Synthesis, Characterization, and Crystal Structure of α -[Ru(azpy)₂(NO₃)₂] (azpy = 2-(Phenylazo)pyridine) and the Products of Its Reactions with Guanine Derivatives. **Inorg. Chem.** 39: 3838-3844.
- Hyde, K.R., E.W. Hooper, J. Waters and J.M. Fletcher. 1965. α - and β -ruthenium trichloride. **J. Less Common Met.** 8(6): 428-434.
- Jensen, B.R. 1960. 1-(2'-Thiazolylazo)-2-oxyaryl compounds as complexometric metal indicators. **Acta. Chem. Scand.** 14: 927-932.
- Kettle, S.F.A. 1998. **Physical inorganic chemistry: a coordination chemistry approach.** Spektrum Academic Publishers, Oxford.
- Landing, W.H., C. Haraldsson and N. Paxéus. 1986. Vinyl Polymer Agglomerate Based Transition Metal Cation Chelating Ion-Exchange Resin Containing the 8-hydroxyquinoline Functional Group. **Anal. Chem.** 58: 3031-3035.
- Likussar, W. and D.F. Boltz. 1971. Theory of Continuous Variation Plots and a New Method for Spectrophotometric Determination of Extraction and Formation Constants. **Anal. Chem.** 43(10): 1265-1272.

- Lee, C.H., M.Y. Suh, K.S. Joe, T.Y. Eom and W. Lee. 1997. A chelating resin containing 4-(2-thiazolylazo)resorcinol as the functional group. Chromatographic application to the preconcentration and separation of some trace metal ions including uranium. **Anal. Chim. Acta.** 351: 57-63.
- Lee, R., H. Williams, T. Nathaniel, W. Brenda and K.J. Brewer. 2003. Synthesis, Characterization, and DNA Binding Properties of a Series of Ru, Pt Mixed-Metal Complexes. **Inorg. Chem.** 42: 4394-4400.
- Lee, W., S.E. Lee, C.H. Lee, Y.S. Kim and Y.I. Lee. 2001. A chelating resin containing 1-(2-thiazolylazo)-2-naphthol as the functional group; synthesis and sorption behavior for trace metal ions. **Microchem. J.** 70: 195-203.
- Lemos, V.A., E.S. Santos, M.S. Santos, and R.T. Yamaki. 2007. Thiazolylazo dyes and their application in analytical methods. **Microchim. Acta.** 158: 189-204.
- _____, R.E. Santellib, M.S. de Carvalhoc and S.L.C. Ferreira. 2000. Application of polyurethane foam loaded with BTAC in an on-line preconcentration system: cadmium determination by FAAS. **Spectrochim. Acta. Part B: Atomic Spectroscopy.** 55(9): 1497-1502.
- Luoma, E.V. and C.H. Brubaker Jr. 1966. On the rapid electron exchange between ruthenate and perruthenate ions in basic solutions. **Inorg. Chem.** 5(9): 1618-1619.
- Ma, W.X., F. Liu, K. A. Li, W. Chen and S. Y. Tong. 2000. Preconcentration, separation and determination of trace Hg(II) in environmental samples with aminopropylbenzoylazo-2-mercaptobenzothiazole bonded to silica gel. **Anal. Chim. Acta.** 416(2): 191-196.
- Miessler, G.L. and D.A. Tarr. 2004. **Inorganic Chemistry.** 3rd ed. Pearson Education International, New Jersey.

- Mubarak, A.T., A.Z. El-Sonbati and S.M. Ahmed. 2007. Supramolecular structural and spectral perspectives of novel ruthenium(III) azodye complex. **J. Coord. Chem.** 60(17): 1877-1890.
- Mura, P., M. Camalli, L. Messori, F. Piccioli, P. Zanello and M. Corsini. 2004. Synthesis, Structure Characterization, Solution Chemistry, and Preliminary Biological Studies of the Ruthenium(III) Complexes [TzH][*trans*-RuCl₄(Tz)₂] and [TzH][*trans*-RuCl₄(DMSO)(Tz)]·(DMSO), the Thiazole Analogues of Antitumor ICR and NAMI-A. **Inorg. Chem.** 43: 3863-3870.
- Parasuk, W. 2003. Structures of some Metal Complexes of 3-(2'-Thiazolylazo)-2,6-diaminopyridine. pp. 41. **7th Annual National Symposium on Computational Science and Engineering.** Faculty of Science, Chulalongkorn University. Bangkok.
- Park, Y.J., K.H. Jung, K.K. Park and T.Y. Eom. 1993. Hydrophobic effects of *o*-phenanthroline and 2,2-bipyridine on adsorption of metal(II) ions onto silica gel surface. **J. Colloid Interface Sci.** 160(2): 324-331.
- Pavia, D.L., G.M. Lampman and G.S. Kriz. 2001. **Introduction to Spectroscopy.** 3rd ed. Thomson Learning, Inc., Victoria.
- Perez, P., L. Maria, M.J. Sanchez, J.J. Arias, V. Gonzalez and F.M. Garcia. 1987. Complexes of copper(II) with 3-(2'-thiazolylazo)-2,6-diaminopyridine and 3-(4'-methyl-2'-thiazolylazo)-2,6-diaminopyridine. Spectrophotometric determination of copper. **Quim. Anal. (Barcelona).** 6(3): 355-361.
- Poowanathai, N. 2003. **Recovery of silver as silver nitrate from silver chloride and photographic process waste.** M.S. Thesis, Kasetsart University.

- Pu, Q., Z. Su, Z. Hu, X. Chang and M. Yang. 1995. 2-mercaptobenzothiazole-bonded silica gel as selective adsorbent for preconcentration of gold, platinum and palladium prior to their simultaneous inductively coupled plasma optical emission spectrophotometric determination. **J. Anal. At. Spectrom.** 13: 249-253.
- Purohit, R. and S. Devi. 1995. Determination of trace amounts of nickel by chelating ion exchange and on-line enrichment in flow injection spectrophotometry. **The Analyst.** 120: 555-559.
- Ramesh, A., K.R. Mohan and K. Seshaiiah. 2002. Preconcentration of trace metals on Amberlite XAD-4 resin coated with dithiocarbamates and determination by inductively coupled plasma-atomic emission spectrometry in saline matrices. **Talanta.** 57(2): 243-252.
- Rengaraj, S., K.H. Yeon and S.H. Moon. 2001. Removal of chromium from water and wastewater by ion exchange resins. **J. Hazard. Mater.** 87(1-3): 273-287.
- Ronconi, L. and P.J. Sadler. 2007. Using coordination chemistry to design new medicines. **Coord. Chem. Rev.** 251: 1633-1648.
- Rungrojwittayakul, S. 2004. **Separation of Lead and Cobalt ions From Solution by 2-(2'-thiazolylazo)-p-cresol Chelating Resin.** M.S. Thesis, Kasetsart University.
- Sahni, S. and J. Reedijk. 1984. Coordination Chemistry of Chelating Resins and Ion Exchangers. **Coord. Chem. Rev.** 59: 1-139.
- Salazar, C.S. and M.I. Toral. 2004. Study of stability physical chemical of 3-[2'-thiazolylazo]-2,6-diaminopyridine and the formation of 3-[N,N-ethyl-methazo]-2,6-diaminopyridine as new ligand chromophore. **J. Chil. Chem. Soc.** 49(2): 169-172.

- Selig, H., W.A. Sunder, F.A. Disalvo and W.E. Falconer. 1978. Hydrolysis reactions of transition metal hexafluorides in liquid hydrogen fluoride: oxonium salts with Pt, Ir and Ru. **J. Fluorine Chem.** 11(1): 39-50.
- Sharov, K.S. and V.M. Ivanov. 2003. Protolytic equilibria of 3-(2-thiazolylazo)-2,6-diaminopyridine in aqueous solutions and organic solvents. **Moscow University Chemistry Bulletin.** 44(6): 397.
- _____ and _____. 2005a. Complex Formation in the 3-(2-Thiazolylazo)-2,6-Diaminopyridine-Palladium(II) System. **Russ. J. Inorg. Chem.** 50(1): 113-119.
- _____ and _____. 2005b. Thermodynamic and Kinetic Characteristics of the Complex Formation of 3-(2-Thiazolylazo)-2,6-Diaminopyridine with Rhodium(III). **Russ. J. Inorg. Chem.** 50(1): 120-127.
- Shraydeh, B.F., Z.A.Z. Abu and M.A. Hannoun. 1986. Spectrophotometric determination of trace amounts of mercury with 3-(2'-thiazolylazo)-2,6-diaminopyridine and gelatin. **Spectrosc. Lett.** 19(8): 929-937.
- Solomon, T.W.G. and C.B. Fryhle. 2002. **Organic Chemistry.** 7th ed. upgrade, John Wiley & Sons, Inc., New York.
- Svendsen, R. and W. Lund. 2000. Speciation of Cu, Fe and Mn in beer using ion exchange separation and size-exclusion chromatography in combination with electrothermal atomic absorption spectrometry. **Analyst.** 125: 1933-1937.
- Taveema, P. 2005. **Complex formation between 3-(2'-thiazolylazo)-2,6-diaminopyridine with Palladium(II) and Gold(III) and its application as reagent for determination of gold(III).** M.S. Thesis, Kasetsart University.

- Terada, K. and H. Kawamura. 1991. Preconcentration of Gold(III), Palladium(II) and Ruthenium(III) with Dithiocarbamate-Chitin. **Anal. Sci.** 7: 71-73.
- _____, K. Morimoto and T. Kiba. 1980. Preconcentration of silver(I), gold(III) and palladium(II) in sea water with p-dimethylaminobenzylidemerhodamine supported on silica gel. **Anal. Chim. Acta.** 116(1): 127-135.
- _____, K. Matsumoto and Y. Taniguchi. 1983. Preconcentration of palladium(II) from water with thionalide loaded on silica gel. **Anal. Chim. Acta.** 147: 411-415.
- Toral, M.I., P. Richter, L. Nelson, M.T. Escudero and C. Soto. 2000. Simultaneous determination of platinum and palladium by second derivative spectrophotometry using 3-(2'-thiazolylazo)-2,6-diaminopyridine as chromophore ligand. **Anal. Lett.** 33(1): 93-109.
- _____, C. Paipa, J. Narváez and P. Richter. 2002. Simultaneous determination of iron and ruthenium by preconcentration on sulfopropyl sephadex cation exchanger. **Microchem. J.** 73: 317-324.
- Ueda, K., Y. Koshino and Y. Yamamoto. 1985. Preconcentration of uranium in seawater with heterocyclic azo dyes supported on silica gel. **Anal. Lett.** 18(A18): 2345-2359.
- Veerachalee, N. 2007. **Determination of Cobalt(III) by Complexation with 3-(2'-thiazolylazo)-2,6-diaminopyridine and Preparation of Chelating Resin to separate Cobalt(III).** M.S. Thesis, Kasetsart University.
- Velders, A.H., K. van der Schilden, A.C.G. Hotze, J. Reedijk, H. Kooijman and A.L. Spek. 2004. Dichlorobis(2-phenylazopyridine)ruthenium(II) complexes: characterization, spectroscopic and structural properties of four isomers. **Dalton Trans.** 448-455.

- Wade, L.G. 1999. **Organic Chemistry**. 4th ed. Prentice Hall International, New Jersey.
- Waller, F. J. 1986. Catalysis with Metal Cation-Exchanged Resins. **Cat. Rev.** 28(1): 1-12.
- Xiong, Z. and P. Yang. 2002. Studies of the interaction between sheared DNA and Λ - or Δ -[Ru(phen)₂dppz]ⁿ⁺ by molecular modeling. **J. Mol. Struct. (Theochem)**. 582: 107-117.
- Yadav, G. D. and H. B. Kulkarni. 2000. Ion-exchange resin catalysis in the synthesis of isopropyl lactate. **React. Funct. Polym.** 44(2): 153-165.
- Zachariasen, H. and F.E. Beamish. 1962. Separation of Ruthenium from Base Metals by Cation Exchange. **Anal. Chem.** 34(8): 964-966.

APPENDICES

APPENDIX A

Calculation of stability constant by continuous variation method

A stability constant (K_f) of the complex can be evaluated from measurements of the deviations from the theoretical straight line, which represent the curve that would result if the reaction between the ligand and the metal produced to completion.



$$K_f = \frac{[\text{Ru}(\text{TADAP})_2]^{3+}}{[\text{Ru}][\text{TADAP}]^2}$$

When $V_{\text{Ru}^{3+}} = 0.0075$ ml, $V_{\text{TADAP}} = 0.175$ ml, $A = 0.6918$ and $A_{\text{ex}} = 0.72$

$$C_{\text{Ru}} = [\text{Ru}^{3+}] + [\text{Ru}(\text{TADAP})_2]^{3+}$$

$$[\text{Ru}^{3+}] = C_{\text{Ru}} - [\text{Ru}(\text{TADAP})_2]^{3+}$$

$$C_{\text{TADAP}} = [\text{TADAP}] + [\text{Ru}(\text{TADAP})_2]^{3+}$$

$$[\text{TADAP}] = C_{\text{TADAP}} - [\text{Ru}(\text{TADAP})_2]^{3+}$$

$$[\text{Ru}^{3+}] = 4.821 \times 10^{-3} \text{ M and } [\text{TADAP}] = 4.545 \times 10^{-3} \text{ M}$$

So, initial concentration of C_{Ru} and C_{TADAP} are

$$C_{\text{Ru}} = \frac{(0.075 \times 10^{-3})(4.8209 \times 10^{-3})}{25 \times 10^{-3}} = 1.4463 \times 10^{-5} \text{ M}$$

$$C_{\text{TADAP}} = \frac{(0.175 \times 10^{-3})(4.545 \times 10^{-3})}{25 \times 10^{-3}} = 3.1815 \times 10^{-5} \text{ M}$$

If the complex is stable, two straight lines are intercepted and thus the complex concentration is equal to the original concentration of metal ion.

$$[\text{M}] = C_{\text{M}} - [\text{ML}_2] = C_{\text{M}} - \frac{A}{A_{\text{ex}}} C_{\text{M}} \quad \text{when } [\text{ML}_2] = \frac{A}{A_{\text{ex}}} C_{\text{M}}$$

$$[L] = C_L - [ML_2] = C_L - \frac{A}{A_{\text{ex}}} C_L \quad \text{when } [ML_2] = \frac{A}{A_{\text{ex}}} C_L$$

$$[\text{Ru}(\text{TADAP})_2^{3+}]_{\text{ex}} = C_{\text{Ru}}$$

$$A_{\text{ex}} = \epsilon b [\text{Ru}(\text{TADAP})_2^{3+}]_{\text{ex}} = \epsilon b C_{\text{Ru}}$$

but

$$A = \epsilon b [\text{Ru}(\text{TADAP})_2^{3+}]$$

$$\frac{A}{A_{\text{ex}}} = \frac{\epsilon b [\text{Ru}(\text{TADAP})_2^{3+}]}{\epsilon b C_{\text{Ru}}}$$

So,

$$[\text{Ru}(\text{TADAP})_2^{3+}] = \frac{A}{A_{\text{ex}}} C_{\text{Ru}}$$

Thus,

$$K_f = \frac{\frac{A}{A_{\text{ex}}} C_{\text{Ru}}}{(C_{\text{Ru}} - \frac{A}{A_{\text{ex}}} C_{\text{Ru}})(C_{\text{TADAP}} - \frac{A}{A_{\text{ex}}} C_{\text{Ru}})}$$

So,

$$K_f = \frac{0.69/0.72}{(1 - (0.69/0.72))(3.1815 \times 10^{-5} - (0.69/0.72)1.4463 \times 10^{-5})}$$

$$K_f = 7.48 \times 10^{10}$$

APPENDIX B

Calculation of stability constant by Benesi-Hildebrand's equation

The determination of equilibrium constant, K, the Benesi-Hildebrand equation was applied from equilibrium reaction of complex.



The equilibrium constant for the above reaction is defined by the equation

$$K = \frac{[ML_2]}{([M]-[ML_2])([L]-[ML_2])^2} \quad \text{--- (2)}$$

Where [ML] is molar concentration of the complex, [M]-[ML] is molar concentration of free metal ion and [L]-[ML] is molar concentration of free ligand.

From Beer's law, the true molar extinction coefficient, ϵ_0 , of the complex at the wavelength of maximum absorption will then be given by the equation

$$\epsilon_0 = \frac{A}{cb} = \frac{A}{[ML_2]b}$$

$$[ML_2] = \frac{A}{\epsilon_0 b} \quad \text{--- (3)}$$

In this reaction, ligand is added in excess. Therefore, [L] is much more than [ML]. The [ML] can be eliminated and the equation (2) can be arranged and obtained as the relationship;

$$K = \frac{[ML_2]}{([M]-[ML_2])([L]-[ML_2])^2}$$

$$K = \frac{A/\epsilon b}{([M]-A/\epsilon b)(L)^2}$$

$$K = \frac{A}{\epsilon b[M][L]^2 - [L]^2 A}$$

$$A = K\epsilon b[M][L]^2 - K[L]^2 A$$

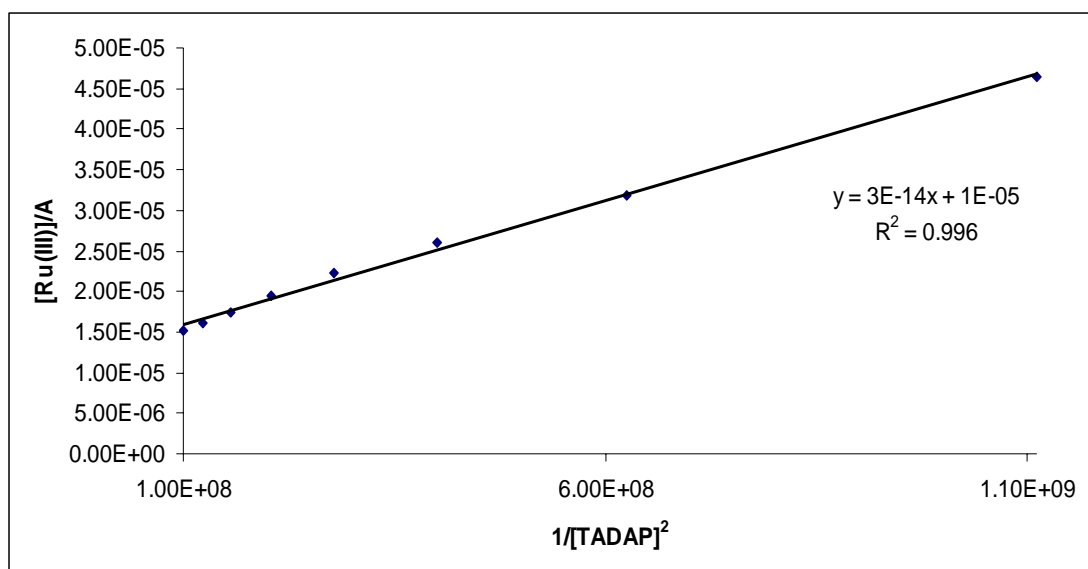
$$K\epsilon b[M][L]^2 = A + K[L]^2A$$

$$K\epsilon b[M][L]^2 = A(1 + K[L]^2)$$

$$\frac{[M]b}{A} = \frac{1}{K\epsilon[L]^2} + \frac{1}{\epsilon} \quad \text{--- (4)}$$

The equation (4) is “Benesi-Hildebrand equation” which is in the form of the linear equation, $y = mx + c$.

For the experiment, the concentration of ruthenium(III) is fixed while the concentrations of ligand are varied. The relationship between $[M]/A$ and $1/[L]^2$ are plotted as shown in Appendix Figure A1.



Appendix Figure A1 The relationship between $[Ru(III)]/A$ and $1/[TADAP]^2$.

The stability constant was obtained from the slope and y -intercept.

$$\text{Slope} = 1/K\epsilon = 3 \times 10^{-14}$$

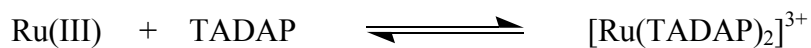
$$y\text{-intercept} = 1/\epsilon = 1 \times 10^{-5}$$

$$\text{Stability constant (K)} = y\text{-intercept/slope} = 3.33 \times 10^8$$

APPENDIX C

Determination of stabilization energies by quantum chemical calculation and the output data of all complexes optimized by Gaussian 03

For the calculation of stabilization energy of complex between ruthenium(III) and TADAP, $[\text{Ru}(\text{TADAP})_2]^{3+}$, the reaction of complex formation should be



The molecular structures of all reactants and products were created on GaussView version 3.0 and their cartesian coordinates were used as input structures on Gaussian03. The quantum chemical calculations were carried out at B3LYP (Lee, Yang and Parr correlation functional) level with 6-31G* basis set for all atoms and SDD (Stuttgart/Dresden) basis set for ruthenium atom. The stabilization energy, E, of the complex $[\text{Ru}(\text{TADAP})_2]^{3+}$ was calculated as followed:

$$\begin{aligned} E &= (E_{\text{product}}) - (E_{\text{reactant}}) \\ &= [(E_{\text{complex}})] - [(E_{\text{Ru(III)}}) + 2(E_{\text{TADAP}})] \\ &= [(-2166.76043217)] - \\ &\quad [(-92.6782252) + 2(-1036.3310676)] \\ E &= -1.2464812 \text{ atomic unit} \\ &= -782.18 \text{ kcal/mol} \end{aligned}$$

Appendix Table C1 Potential energies and stabilization energies of all species obtained at B3LYP level with 6-31G* and SDD basis sets.

Atoms, molecules and complexes	Potential Energies (a.u.)	Stabilization Energies (a.u.)	Stabilization Energies (kcal/mol)
Ru(III)	-92.8518159	-	-
Cl ⁻	-460.2522333	-	-
H ₂ O	-76.4089533	-	-
TADAP	-1036.331068	-	-
Adenine	-467.2901688	-	-
Guanine	-542.5046641	-	-
[Ru(TADAP)] ³⁺	-1130.150934	-0.9680503	-607.46
[Ru(TADAP)Cl] ²⁺	-1590.903888	-1.4687707	-921.67
[Ru(TADAP)H ₂ O] ³⁺	-1206.644499	-1.0526624	-660.56
[Ru(TADAP) ₂] ³⁺	-2166.760432	-1.2464812	-782.18
[Ru(TADAP) ₂ Cl ₂] ⁺	-3087.927796	-1.9093784	-1198.15
[Ru(TADAP) ₂ (H ₂ O) ₂] ³⁺	-2319.602927	-1.27106960	-797.61
[Ru(TADAP) ₂ Cl] ²⁺	-2627.35916	-1.59297550	-999.61
[Ru(TADAP) ₂] ³⁺ -5coor	-2166.740517	-1.22656560	-769.68
[Ru(TADAP) ₂ H ₂ O] ³⁺	-2243.125825	-1.20292079	-754.84
[Ru(TADAP) ₂] ³⁺ -A*	-2634.133996	-1.32987650	-834.51
[Ru(TADAP) ₂ Cl] ²⁺ -A*	-3094.737588	-1.68123445	-1054.99
[Ru(TADAP) ₂] ³⁺ -G**	-2709.329439	-1.31082406	-822.55
[Ru(TADAP) ₂ Cl] ²⁺ -G**	-3169.934955	-1.66410651	-1044.24
[Ru(TADAP) ₂ H ₂ O] ³⁺ -A*	-2710.506496	-1.29342275	-811.64
[Ru(TADAP) ₂ H ₂ O] ³⁺ -G**	-2785.672866	-1.24529719	-781.44

*A = Adenine base

**G = Guanine base

1. The example of input data

1.1 TADAP

%chk=TADAP001.chk

#B3LYP/6-31G* opt

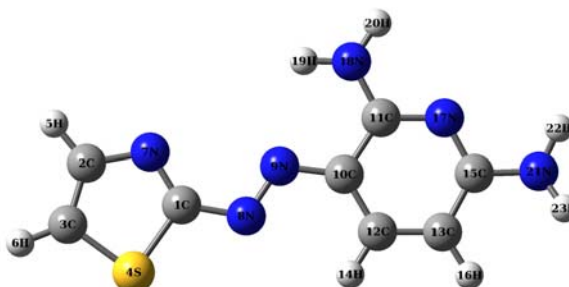
-----24-04-07-----

0 1

H	-3.06841703	5.03088116	5.16009199
C	-2.01166243	5.28521698	5.10748062
C	-1.31569117	6.02344067	6.03877561
S	-1.02717556	4.80454341	3.84412275
H	-1.73782934	6.44895227	6.95096769
N	0.05930845	6.17496272	5.66812781
C	0.33336924	5.54430555	4.47484947
N	1.22393712	5.51669731	4.02083876
N	2.11450748	5.48909077	3.56683088
C	3.42364517	5.44850968	2.89943947
C	3.80943243	6.48252629	2.02692530
C	4.30995039	4.39128630	3.11340845
N	4.99253322	6.50908028	1.38308517
N	2.91529574	7.61969531	1.76564834
C	5.54058689	4.40212978	2.45449523
H	4.04299597	3.56502046	3.78750316
C	5.83569463	5.48090539	1.60085652
H	3.35637615	8.46601932	2.06428325
H	2.72096714	7.67274189	0.78614658
H	6.26628492	3.59086481	2.59441609
N	7.11652418	5.54334758	0.88219337
H	7.86730453	5.58070293	1.54168917
H	7.21686702	4.73039766	0.30857119

2. The output data of the optimized structures

2.1 TADAP



Appendix Figure C2 The optimized structure of TADAP.

Appendix Table C2 The standard orientation of TADAP.

	X	Y	Z		X	Y	Z
C	-7.72254	1.224	0.0000	C	-10.05814	-3.91668	1.20709
C	-5.81994	2.55627	0.0000	H	-8.92624	-2.33592	2.16065
C	-6.8264	3.49632	0.00081	C	-10.46258	-4.48406	-0.00124
S	-8.33703	2.77917	0.0008	H	-10.38046	-4.36259	2.15932
H	-4.75073	2.77569	-0.00057	N	-10.05338	-3.91798	-1.20926
H	-6.68699	4.57556	0.00146	N	-8.80860	-2.18846	-2.4806
N	-6.34531	1.224	0.00000	H	-8.13576	-2.78522	-2.91782
N	-8.57989	0.02991	-0.00069	H	-9.59955	-2.08042	-3.08287
N	-8.05518	-1.13102	0.00115	N	-11.32035	-5.67784	-0.00266
C	-8.83537	-2.21764	0.00042	H	-10.79404	-6.46685	0.3143
C	-9.23948	-2.78538	-1.20823	H	-12.09885	-5.52965	0.60724
C	-9.24479	-2.78315	1.20795				

Appendix Table C3 The optimized bond length of TADAP.

bond	distance (Å)	bond	distance (Å)	bond	distance (Å)	bond	distance (Å)
1,4	1.7675	3,4	1.7301	11,17	1.3422	15,17	1.3373
1,7	1.3107	3,6	1.0811	11,18	1.3522	15,21	1.3686
1,8	1.3878	8,9	1.2787	12,13	1.3746	18,19	1.0106
2,3	1.3708	9,10	1.3745	12,14	1.0849	18,20	1.0079
2,5	1.0851	10,11	1.4334	13,15	1.4236	21,22	1.0106
2,7	1.3673	10,12	1.4109	13,16	1.0858	21,23	1.009

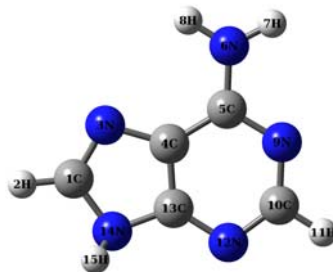
Appendix Table C4 The optimized bond angle of TADAP.

angle	degree	angle	degree	angle	degree	angle	degree
4,1,7	114.54	1,4,3	88.57	17,11,18	117.45	17,15,21	115.91
4,1,8	115.10	1,7,2	110.45	10,12,13	120.16	11,17,15	118.07
7,1,8	130.35	1,8,9	113.69	10,12,14	118.16	11,18,19	118.28
3,2,5	124.31	8,9,10	116.47	13,12,14	121.67	11,18,20	118.86
3,2,7	116.75	9,10,11	115.70	12,13,15	117.84	19,18,20	121.12
5,2,7	118.93	9,10,12	126.98	12,13,16	121.76	15,21,22	116.18
2,3,4	109.68	11,10,12	117.30	15,13,16	120.38	15,21,23	119.23
2,3,6	128.40	10,11,17	122.83	13,15,17	123.77	22,21,23	116.74
4,3,6	121.91	10,11,18	119.70	13,15,21	120.28		

Appendix Table C5 The optimized torsion angle of TADAP.

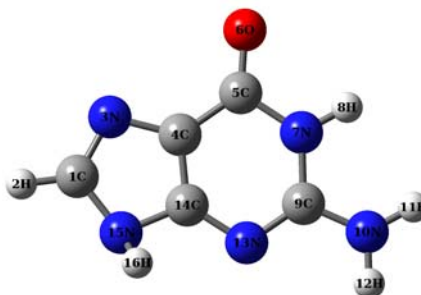
angle	degree	angle	degree	angle	degree	angle	degree
7,1,4,3	-0.05	2,3,4,1	0.03	11,10,12,13	-0.44	14,12,13,16	0.41
8,1,4,3	-179.95	6,3,4,1	-179.98	11,10,12,14	179.84	12,13,15,17	0.57
4,1,7,2	0.06	1,8,9,10	-179.44	10,11,17,15	-0.18	12,13,15,21	-177.60
8,1,7,2	179.93	8,9,10,11	-179.34	18,11,17,15	178.81	16,13,15,17	179.76
4,1,8,9	-179.33	8,9,10,12	1.22	10,11,18,19	-6.70	16,13,15,21	1.57
7,1,8,9	0.79	9,10,11,17	-178.87	10,11,18,20	-171.87	13,15,17,11	-0.42
5,2,3,4	179.95	9,10,11,18	2.15	17,11,18,19	174.26	21,15,17,11	177.82
5,2,3,6	-0.02	12,10,11,17	0.61	17,11,18,20	9.09	13,15,21,22	-167.90
7,2,3,4	-0.01	12,10,11,18	-178.36	10,12,13,15	-0.09	13,15,21,23	-19.69
7,2,3,6	-179.99	9,10,12,13	178.97	10,12,13,16	-179.27	17,15,21,22	13.77
3,2,7,1	-0.03	9,10,12,14	-0.72	14,12,13,15	179.59	17,15,21,23	161.98
5,2,7,1	179.99						

2.2 Adenine

**Appendix Figure C3** The optimized structure of adenine.**Appendix TableC6** The standard orientation of adenine.

	X	Y	Z		X	Y	Z
C	2.280037	-0.741138	-0.036845	N	-1.933290	0.520244	0.009671
H	3.288357	-1.126138	0.001456	C	-1.285610	1.681788	-0.005308
N	1.190413	-1.449937	-0.018840	H	-1.839464	2.608957	-0.003589
C	0.173166	-0.502702	-0.011319	N	0.014129	1.911479	-0.023231
C	-1.222161	-0.615489	0.007150	C	0.705844	0.752158	-0.025369
N	-1.869193	-1.788828	0.022187	N	2.063021	0.611554	-0.041883
H	-2.878915	-1.808587	0.035194	H	2.613962	0.899940	0.741250
H	-1.347158	-2.653454	0.020514				

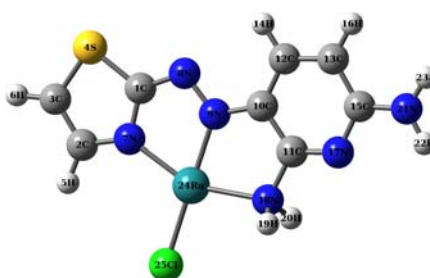
2.3 Guanine



Appendix Figure C4 The optimized structure of guanine.

Appendix Table C7 The standard orientation of guanine.

	X	Y	Z		X	Y	Z
C	-2.700928	-0.547440	-0.024835	C	1.670641	-0.556657	-0.007401
H	-3.746669	-0.817176	-0.033181	N	2.949087	-0.958121	-0.007670
N	-2.220120	0.671039	-0.009620	H	3.770662	-0.370667	-0.011336
C	-0.842443	0.486376	-0.006759	H	3.108815	-1.955251	-0.025553
C	0.213357	1.435840	0.007525	N	0.680512	-1.444587	-0.018608
O	0.145398	2.663888	0.020893	C	-0.542750	-0.850259	-0.016347
N	1.464589	0.807817	0.005021	N	-1.734241	-1.532256	-0.032304
H	2.273735	1.395371	0.012866	H	-1.335772	-2.177789	0.619239

2.4 $[\text{Ru}(\text{TADAP})\text{Cl}]^{2+}$ 

Appendix Table C8 The standard orientation of $[\text{Ru}(\text{TADAP})\text{Cl}]^{2+}$.

	X	Y	Z		X	Y	Z
C	-2.02166	1.06685	-0.0003	H	1.48502	2.92275	-0.00053
C	-3.66381	-0.48414	-0.00036	C	4.19633	0.81877	-0.0003
C	-4.41108	0.71076	-0.00029	H	3.97751	3.00937	-0.00083
S	-3.42972	2.09841	-0.0001	N	3.57445	-0.41462	-0.00011
H	-4.09209	-1.48192	-0.00042	N	1.60658	-1.75338	0.00024
H	-5.4961	0.78847	-0.00037	H	1.93805	-2.29787	0.81162
N	-2.33256	-0.28777	-0.00041	H	1.93869	-2.29856	-0.81043
N	-0.77041	1.50305	-0.00014	N	5.51528	0.79252	-0.00043
N	0.09385	0.50712	-0.00025	H	6.01273	-0.10229	-0.00034
C	1.44883	0.74107	-0.00022	H	6.08504	1.64113	-0.00039
C	2.2872	-0.44015	-0.00005	Ru	-0.54709	-1.34456	-0.00046
C	2.07818	2.01363	-0.00041	Cl	-1.7338	-3.25333	0.0649
C	3.45148	2.0581	-0.00052				

Appendix Table C9 The optimized bond length of $[\text{Ru}(\text{TADAP})\text{Cl}]^{2+}$.

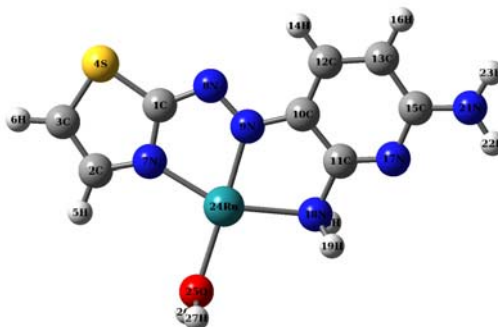
bond	distance (Å)	bond	distance (Å)	bond	distance (Å)	bond	distance (Å)
1,4	1.7519	3,6	1.0842	11,17	1.2948	15,21	1.3281
1,7	1.3777	7,24	2.0878	11,18	1.4693	18,19	1.028
1,8	1.3214	8,9	1.3464	12,13	1.3708	18,20	1.028
2,3	1.398	9,10	1.3656	12,14	1.0841	18,24	2.1861
2,5	1.0836	9,24	2.0119	13,15	1.4383	21,22	1.0178
2,7	1.3474	10,11	1.4347	13,16	1.0856	21,23	1.016
3,4	1.7099	10,12	1.4199	15,17	1.3723	24,25	2.2407

Appendix Table C10 The optimized bond angle of $[\text{Ru}(\text{TADAP})\text{Cl}]^{2+}$.

angle	degree	angle	degree	angle	degree	angle	degree
4,1,7	113.00	2,7,24	137.46	10,12,14	120.05	19,18,20	104.74
4,1,8	124.52	1,8,9	109.52	13,12,14	121.74	19,18,24	112.24
7,1,8	122.47	8,9,10	118.14	12,13,15	119.26	20,18,24	112.23
3,2,5	125.300	8,9,24	121.61	12,13,16	120.89	15,21,22	119.70
3,2,7	113.99	10,9,24	120.23	15,13,16	119.83	15,21,23	122.45
5,2,7	120.70	9,10,11	114.94	13,15,17	122.42	22,21,23	117.84
2,3,4	112.28	9,10,12	127.12	13,15,21	121.93	7,24,9	75.59
2,3,6	126.44	11,10,12	117.93	17,15,21	115.64	7,24,18	154.33
4,3,6	121.26	10,11,17	124.75	11,17,15	117.42	7,24,25	105.40
1,4,3	88.97	10,11,18	116.46	11,18,19	108.91	9,24,18	78.74
1,7,2	111.73	17,11,18	118.78	11,18,20	108.91	9,24,25	178.99
1,7,24	110.79	10,12,13	118.20	11,18,24	109.61	18,24,25	100.25

Appendix Table C11 The optimized torsion angle of $[\text{Ru}(\text{TADAP})\text{Cl}]^{2+}$.

plane	degree	plane	degree	plane	degree	plane	degree
7,1,4,3	-0.01	1,7,24,18	-0.34	12,10,11,17	0.03	12,13,15,21	-179.98
8,1,4,3	179.95	1,7,24,25	179.84	12,10,11,18	-179.96	16,13,15,17	-179.98
4,1,7,2	0.01	2,7,24,9	179.94	9,10,12,13	179.96	16,13,15,21	0.01
4,1,7,24	-179.99	2,7,24,18	179.63	9,10,12,14	-0.02	13,15,17,11	-0.01
8,1,7,2	-179.95	2,7,24,25	-0.16	11,10,12,13	-0.02	21,15,17,11	179.99
8,1,7,24	0.03	1,8,9,10	179.99	11,10,12,14	179.98	13,15,21,22	-179.99
4,1,8,9	-179.95	1,8,9,24	-0.05	10,11,17,15	-0.01	13,15,21,23	0.00
7,1,8,9	0.01	8,9,10,11	-179.95	18,11,17,15	179.98	17,15,21,22	-0.00
5,2,3,4	179.99	8,9,10,12	0.05	10,11,18,19	-123.29	17,15,21,23	179.99
5,2,3,6	-0.01	24,9,10,11	0.08	10,11,18,20	123.00	11,18,24,7	0.44
7,2,3,4	0.00	24,9,10,12	-179.89	10,11,18,24	-0.13	11,18,24,9	0.13
7,2,3,6	-179.98	8,9,24,7	0.05	17,11,18,19	56.70	11,18,24,25	-179.75
3,2,7,1	-0.01	8,9,24,18	179.91	17,11,18,20	-56.99	19,18,24,7	121.61
3,2,7,24	-179.99	8,9,24,25	-173.93	17,11,18,24	179.86	19,18,24,9	121.30
5,2,7,1	-179.99	10,9,24,7	-179.99	10,12,13,15	0.00	19,18,24,25	-58.58
5,2,7,24	0.01	10,9,24,18	-0.12	10,12,13,16	-179.99	20,18,24,7	-120.72
2,3,4,1	0.00	10,9,24,25	6.02	14,12,13,15	179.98	20,18,24,9	-121.02
6,3,4,1	179.99	9,10,11,17	-179.95	14,12,13,16	0.00	20,18,24,25	59.083
1,7,24,9	-0.04	9,10,11,18	0.04	12,13,15,17	0.02		

2.5 $[\text{Ru}(\text{TADAP})\text{H}_2\text{O}]^{3+}$ **Appendix Figure C6** The optimized structure of $[\text{Ru}(\text{TADAP})\text{H}_2\text{O}]^{3+}$.

Appendix Table C12 The standard orientation of $[\text{Ru}(\text{TADAP})\text{H}_2\text{O}]^{3+}$.

	X	Y	Z		X	Y	Z
H	-1.74902	-1.54073	-0.00039	C	4.36266	-0.602	-0.00056
C	-3.55104	-0.18383	0.00163	H	4.38497	-2.79305	-0.00383
C	-4.17281	-1.43593	0.00128	N	3.62112	0.55265	0.00181
C	-3.04416	-2.72044	-0.00031	N	1.50872	1.65036	0.00512
C	-4.06461	0.77035	0.00244	H	1.76377	2.22708	-0.80672
N	-5.24041	-1.62484	0.00178	H	1.76128	2.22158	0.82162
N	-2.20484	-0.24063	0.00057	N	5.68063	-0.43864	-0.00115
N	-0.46223	-1.84135	-0.00066	H	6.07241	0.50078	0.00008
H	0.26464	-0.70802	0.00028	H	6.32714	-1.2224	-0.00279
H	1.62602	-0.81578	0.00025	Ru	-0.60819	1.10464	0.00032
S	2.33183	0.43331	0.00227	O	-1.12895	3.06384	0.21658
C	2.39102	-2.01193	-0.00178	H	-2.06771	3.21203	0.02933
C	3.75777	-1.90694	-0.00218	H	-0.68552	3.78784	-0.24979
C	1.89298	-2.97489	-0.00312				

Appendix Table C13 The optimized bond length of $[\text{Ru}(\text{TADAP})\text{H}_2\text{O}]^{3+}$.

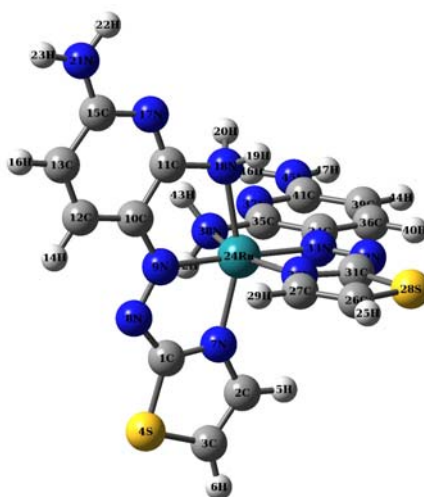
bond	distance (Å)	bond	distance (Å)	bond	distance (Å)	bond	distance (Å)
1,4	1.7444	7,24	2.091	12,13	1.3725	18,20	1.0306
1,7	1.3806	8,9	1.3187	12,14	1.0852	18,24	2.2005
1,8	1.3276	9,10	1.3697	13,15	1.4458	21,22	1.0225
2,3	1.4057	9,24	2.0071	13,16	1.0867	21,23	1.021
2,5	1.0841	10,11	1.4433	15,17	1.3806	24,25	2.1551
2,7	1.3471	10,12	1.4206	15,21	1.3199	25,26	0.9774
3,4	1.7004	11,17	1.2889	18,19	1.0301	25,27	0.9773
3,6	1.0867	11,18	1.4741				

Appendix Table C14 The optimized bond angle of $[\text{Ru}(\text{TADAP})\text{H}_2\text{O}]^{3+}$.

angle	degree	angle	degree	angle	degree	angle	degree
4,1,7	113.47	1,8,9	111.04	12,13,15	119.21	15,21,22	120.17
4,1,8	124.358	8,9,10	119.57	12,13,16	120.86	15,21,23	122.66
7,1,8	122.12	8,9,24	120.76	15,13,16	119.91	22,21,23	117.16
3,2,5	124.70	10,9,24	119.64	13,15,17	122.32	7,24,9	76.43
3,2,7	113.81	9,10,11	114.85	13,15,21	121.99	7,24,18	152.20
5,2,7	121.47	9,10,12	126.93	17,15,21	115.67	7,24,25	102.87
2,3,4	112.43	11,10,12	118.21	11,17,15	117.49	9,24,18	78.92
2,3,6	126.30	10,11,17	124.63	11,18,19	108.49	9,24,25	175.96
4,3,6	121.25	10,11,18	116.49	11,18,20	108.69	18,24,2	102.57
1,4,3	89.01	17,11,18	118.87	11,18,24	108.27	24,25,26	126.42
1,7,2	111.25	10,12,13	118.07	19,18,20	104.13	24,25,27	125.41
1,7,24	109.50	10,12,14	120.49	19,18,24	114.93	26,25,27	107.57
2,7,24	139.24	13,12,14	121.42	20,18,24	112.08		

Appendix Table C15 The optimized torsion angle of $[\text{Ru}(\text{TADAP})\text{H}_2\text{O}]^{3+}$.

plane	degree	plane	degree	plane	degree	plane	degree
7,1,4,3	-0.29	2,7,24,9	176.98	9,10,12,14	-0.96	21,15,17,11	179.28
8,1,4,3	177.55	2,7,24,18	148.80	11,10,12,13	-1.95	13,15,21,22	-179.75
4,1,7,2	0.55	2,7,24,25	-7.09	11,10,12,14	178.96	13,15,21,23	0.02
4,1,7,24	-179.68	1,8,9,10	178.67	10,11,17,15	-0.69	17,15,21,22	-0.19
8,1,7,2	-177.34	1,8,9,24	-2.69	18,11,17,15	178.30	17,15,21,23	179.58
8,1,7,24	2.41	8,9,10,11	-173.26	10,11,18,19	-136.57	11,18,24,7	39.32
4,1,8,9	-177.71	8,9,10,12	6.67	10,11,18,20	110.77	11,18,24,9	11.43
7,1,8,9	-0.04	24,9,10,11	8.08	10,11,18,24	-11.21	11,18,24,25	-164.74
5,2,3,4	179.37	24,9,10,12	-171.97	17,11,18,19	44.33	19,18,24,7	160.80
5,2,3,6	-0.17	8,9,24,7	3.13	17,11,18,20	-68.30	19,18,24,9	132.90
7,2,3,4	0.36	8,9,24,18	170.16	17,11,18,24	169.70	19,18,24,25	-43.26
7,2,3,6	-179.18	8,9,24,25	-77.52	10,12,13,15	0.28	20,18,24,7	-80.55
3,2,7,1	-0.58	10,9,24,7	-178.23	10,12,13,16	-179.16	20,18,24,9	-108.45
3,2,7,24	179.76	10,9,24,18	-11.20	14,12,13,15	179.34	20,18,24,25	75.37
5,2,7,1	-179.6	10,9,24,25	101.10	14,12,13,16	-0.10	7,24,25,26	78.30
5,2,7,24	0.71	9,10,11,17	-177.75	12,13,15,17	1.36	7,24,25,27	-111.57
2,3,4,1	-0.03	9,10,11,18	3.22	12,13,15,21	-179.10	9,24,25,26	158.02
6,3,4,1	179.54	12,10,11,17	2.30	16,13,15,17	-179.17	9,24,25,27	-31.85
1,7,24,9	-2.67	12,10,11,18	-176.72	16,13,15,21	0.35	18,24,25,26	-90.45
1,7,24,18	-30.85	9,10,12,13	178.10	13,15,17,11	-1.15	18,24,25,27	79.67
1,7,24,25	173.24						

2.6 $[\text{Ru}(\text{TADAP})_2]^{3+}$ **Appendix Figure C7** The optimized structure of $[\text{Ru}(\text{TADAP})_2]^{3+}$.

Appendix Table C16 The standard orientation of $[\text{Ru}(\text{TADAP})_2]^{3+}$.

	X	Y	Z		X	Y	Z
C	-0.895743	-1.618810	-2.195862	H	-1.423268	-3.860900	3.520562
C	1.234101	-2.322529	-1.947527	C	-0.835206	-3.114744	2.999602
C	0.834931	-3.115310	-2.999176	C	-1.234298	-2.322093	1.947826
S	-0.801582	-2.808863	-3.447700	S	0.801335	-2.808383	3.448081
H	2.211920	-2.341202	-1.483603	H	-2.212122	-2.340743	1.483912
H	1.422919	-3.861607	-3.520018	N	-0.266862	-1.471316	1.486479
N	0.266733	-1.471611	-1.486294	C	0.895595	-1.618489	2.196098
N	-2.010275	-0.898483	-1.939932	N	2.010179	-0.898276	1.940099
N	-1.802728	-0.097018	-0.933113	N	1.802736	-0.096987	0.933114
C	-2.792451	0.752175	-0.506743	C	2.792529	0.752070	0.506642
C	-2.441029	1.600151	0.580737	C	2.441216	1.599842	-0.581039
C	-4.099624	0.882379	-1.050628	C	4.099654	0.882361	1.050621
C	-4.942890	1.815745	-0.509848	N	3.221820	2.497696	-1.104994
H	-4.407369	0.253622	-1.879292	N	1.085884	1.451250	-1.156161
C	-4.480863	2.631298	0.580938	C	4.942970	1.815635	0.509756
H	-5.948440	1.949590	-0.896264	H	4.407322	0.253752	1.879425
N	-3.221599	2.498067	1.104638	C	4.481030	2.631024	-0.581190
N	-1.085635	1.451666	1.155758	H	1.196443	1.141455	-2.128506
H	-1.196085	1.142272	2.128244	H	0.681826	2.390566	-1.243721
H	-0.681503	2.390992	1.242877	H	5.948485	1.949544	0.896238
N	-5.253684	3.556783	1.139462	N	5.253897	3.556424	-1.139790
H	-4.900526	4.115413	1.911280	H	4.900806	4.114932	-1.911729
H	-6.203678	3.730590	0.827091	H	6.203865	3.730280	-0.827366
Ru	0.000013	-0.066687	-0.000030				

Appendix Table C17 The optimized bond length of $[\text{Ru}(\text{TADAP})_2]^{3+}$.

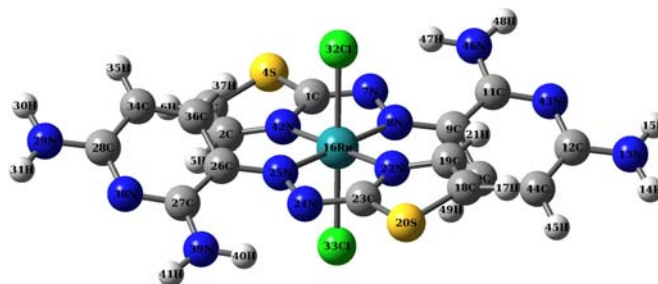
bond	distance (Å)	bond	distance (Å)	bond	distance (Å)	bond	distance (Å)
1,4	1.7298	11,17	1.3000	24,33	2.0301	34,36	1.4218
1,7	1.3699	11,18	1.4798	24,38	2.1954	35,37	1.3000
1,8	1.3515	12,13	1.3692	25,26	1.0835	35,38	1.4798
2,3	1.3762	12,14	1.0848	26,27	1.3762	36,39	1.3692
2,5	1.0825	13,15	1.4382	26,28	1.7243	36,40	1.0848
2,7	1.3684	13,16	1.0855	27,29	1.0825	37,41	1.3703
3,4	1.7243	15,17	1.3703	27,30	1.3684	38,42	1.0265
3,6	1.0835	15,21	1.3288	28,31	1.7298	38,43	1.0263
7,24	2.0625	18,19	1.0265	30,31	1.3699	39,41	1.4382
8,9	1.3035	18,20	1.0263	31,32	1.3515	39,44	1.0855
9,10	1.3720	18,24	2.1954	32,33	1.3035	41,45	1.3288
9,24	2.0301	21,22	1.0161	33,34	1.372	45,46	1.0161
10,11	1.4231	21,23	1.0150	34,35	1.4231	45,47	1.0150
10,12	1.4218	24,30	2.0625				

Appendix Table C18 The optimized bond angle of [Ru(TADAP)₂]³⁺.

angle	degree	angle	degree	angle	degree	angle	degree
4,1,7	113.7405	13,12,14	121.4739	18,24,30	91.5806	33,34,36	126.9426
4,1,8	123.2719	12,13,15	119.2263	18,24,33	101.973	35,34,36	117.6968
7,1,8	122.9876	12,13,16	120.9282	18,24,38	92.5013	34,35,37	124.8378
3,2,5	125.423	15,13,16	119.8447	30,24,33	76.9062	34,35,38	117.6025
3,2,7	114.2516	13,15,17	122.0017	30,24,38	156.1227	37,35,38	117.5595
5,2,7	120.3218	13,15,21	121.7961	33,24,38	79.2323	34,36,39	118.5271
2,3,4	111.8199	17,15,21	116.2021	25,26,27	127.3541	34,36,40	119.9981
2,3,6	127.3542	11,17,15	117.7047	25,26,28	120.8249	39,36,40	121.4739
4,3,6	120.8248	11,18,19	107.4475	27,26,28	111.8199	35,37,41	117.7046
1,4,3	89.1798	11,18,20	107.5674	26,27,29	125.4227	24,38,35	108.528
1,7,2	111.0076	11,18,24	108.5275	26,27,30	114.2518	24,38,42	110.0867
1,7,24	109.6773	19,18,20	103.7582	29,27,30	120.3219	24,38,43	118.8828
2,7,24	139.2767	19,18,24	110.0912	26,28,31	89.1799	35,38,42	107.4464
1,8,9	110.0396	20,18,24	118.8793	24,30,27	139.277	35,38,43	107.5689
8,9,10	120.3796	15,21,22	120.0022	24,30,31	109.6771	42,38,43	103.7578
8,9,24	120.37	15,21,23	122.2923	27,30,31	111.0075	36,39,41	119.2263
10,9,24	119.2408	22,21,23	117.7042	28,31,30	113.7404	36,39,44	120.9283
9,10,11	115.3496	7,24,9	76.9061	28,31,32	123.2716	41,39,44	119.8447
9,10,12	126.9423	7,24,18	156.123	30,31,32	122.9879	37,41,39	122.0018
11,10,12	117.6968	7,24,30	94.1403	31,32,33	110.0396	37,41,45	116.202
10,11,17	124.8378	7,24,33	101.9013	24,33,32	120.3696	39,41,45	121.7961
10,11,18	117.6026	7,24,38	91.5774	24,33,34	119.241	41,45,46	120.0022
17,11,18	117.5594	9,24,18	79.2329	32,33,34	120.3797	41,45,47	122.2923
10,12,13	118.5272	9,24,30	101.8988	33,34,35	115.3493	46,45,47	117.7042
10,12,14	119.998	9,24,38	101.9758				

Appendix Table C19 The optimized torsion angle of $[\text{Ru}(\text{TADAP})_2]^{3+}$.

plane	degree	plane	degree	plane	degree	plane	degree
7,1,4,3	0.19	10,9,33,34	-88.94	20,18,24,38	-23.21	26,28,31,30	0.19
8,1,4,3	-179.87	9,10,11,17	177.98	7,24,30,27	-77.22	26,28,31,32	-179.87
4,1,7,2	-0.24	9,10,11,18	-1.84	7,24,30,31	100.18	24,30,31,28	-178.43
4,1,7,24	-178.44	12,10,11,17	-0.88	9,24,30,27	0.24	24,30,31,32	1.62
8,1,7,2	179.82	12,10,11,18	179.28	9,24,30,31	177.65	27,30,31,28	-0.24
8,1,7,24	1.62	9,10,12,13	-178.2	18,24,30,27	79.57	27,30,31,32	179.82
4,1,8,9	178.94	9,10,12,14	1.37	18,24,30,31	-103.01	28,31,32,33	178.93
7,1,8,9	-1.13	11,10,12,13	0.42	33,24,30,27	-178.49	30,31,32,33	-1.13
5,2,3,4	179.27	11,10,12,14	-179.90	33,24,30,31	-1.08	31,32,33,24	0.01
5,2,3,6	-0.34	10,11,17,15	0.64	38,24,30,27	179.37	31,32,33,34	178.86
7,2,3,4	-0.03	18,11,17,15	-179.52	38,24,30,31	-3.21	24,33,34,35	0.20
7,2,3,6	-179.64	10,11,18,19	-116.62	7,24,33,32	-90.89	24,33,34,36	178.94
3,2,7,1	0.17	10,11,18,20	132.21	7,24,33,34	90.23	32,33,34,35	-178.66
3,2,7,24	177.57	10,11,18,24	2.39	18,24,33,32	89.47	32,33,34,36	0.07
5,2,7,1	-179.16	17,11,18,19	63.53	18,24,33,34	-89.39	33,34,35,37	177.97
5,2,7,24	-1.77	17,11,18,20	-47.62	30,24,33,32	0.64	33,34,35,38	-1.85
2,3,4,1	-0.09	17,11,18,24	-177.44	30,24,33,34	-178.23	36,34,35,37	-0.89
6,3,4,1	179.55	10,12,13,15	0.17	38,24,33,32	179.76	36,34,35,38	179.28
1,7,24,9	-1.08	10,12,13,16	179.86	38,24,33,34	0.89	33,34,36,39	-178.29
1,7,24,18	-3.22	14,12,13,15	-179.48	7,24,38,35	-103.50	33,34,36,40	1.37
1,7,24,30	100.18	14,12,13,16	0.20	7,24,38,42	13.83	35,34,36,39	0.42
1,7,24,33	177.65	12,13,15,17	-0.43	7,24,38,43	133.24	35,34,36,40	-179.90
1,7,24,38	-103.01	12,13,15,21	179.65	9,24,38,35	179.55	34,35,37,41	0.64
2,7,24,9	-178.51	16,13,15,17	179.87	9,24,38,42	-63.11	38,35,37,41	-179.52
2,7,24,18	179.36	16,13,15,21	-0.03	9,24,38,43	56.29	34,35,38,24	2.40
2,7,24,30	-77.23	13,15,17,11	0.03	18,24,38,35	100.03	34,35,38,42	-116.61
2,7,24,33	0.24	21,15,17,11	179.94	18,24,38,42	-142.63	34,35,38,43	132.22
2,7,24,38	79.56	13,15,21,22	179.76	18,24,38,43	-23.23	37,35,38,24	-177.43
1,8,9,10	178.86	13,15,21,23	0.18	30,24,38,35	0.42	37,35,38,42	63.54
1,8,9,24	0.01	17,15,21,22	-0.14	30,24,38,42	117.76	37,35,38,43	-47.61
8,9,10,11	-178.66	17,15,21,23	-179.72	30,24,38,43	-122.83	34,36,39,41	0.17
8,9,10,12	0.07	11,18,24,7	0.44	33,24,38,35	-1.68	34,36,39,44	179.86
24,9,10,11	0.21	11,18,24,9	-1.67	33,24,38,42	115.65	40,36,39,41	-179.48
24,9,10,12	178.95	11,18,24,30	-103.49	33,24,38,43	-124.94	40,36,39,44	0.20
8,9,24,7	0.64	11,18,24,33	179.56	25,26,27,29	-0.33	35,37,41,39	0.03
8,9,24,18	179.76	11,18,24,38	100.04	25,26,27,30	-179.64	35,37,41,45	179.94
8,9,24,30	-90.88	19,18,24,7	117.78	28,26,27,29	179.27	36,39,41,37	-0.43
8,9,24,38	89.47	19,18,24,9	115.66	28,26,27,30	-0.03	36,39,41,45	179.65
10,9,24,7	-178.23	19,18,24,30	13.85	25,26,28,31	179.55	44,39,41,37	179.87
10,9,24,18	0.88	19,18,24,33	-63.09	27,26,28,31	-0.08	44,39,41,45	-0.03
10,9,24,30	90.23	19,18,24,38	-142.61	26,27,30,24	177.56	37,41,45,46	-0.14
10,9,24,38	-89.40	20,18,24,7	-122.81	26,27,30,31	0.17	37,41,45,47	-179.72
8,9,33,32	-89.81	20,18,24,9	-124.93	29,27,30,24	-1.77	39,41,45,46	179.76
8,9,33,34	90.61	20,18,24,30	133.25	29,27,30,31	-179.16	39,41,45,47	0.18
10,9,33,32	90.61	20,18,24,33	56.30				

2.7 [Ru(TADAP)₂Cl₂]⁺**Appendix Figure C8** The optimized structure of [Ru(TADAP)₂Cl₂]⁺.**Appendix Table C20** The standard orientation of [Ru(TADAP)₂Cl₂]⁺.

	X	Y	Z		X	Y	Z
C	0.474725	2.800133	-0.098502	C	-3.133153	-0.581014	0.106052
C	-1.645333	2.679828	-0.816034	C	-4.322873	-1.254834	-0.406790
C	-1.500669	4.034943	-0.802952	C	-5.690931	0.475108	0.293880
S	0.088947	4.484342	-0.262041	N	-6.941612	0.976449	0.336274
H	-2.524110	2.141456	-1.137464	H	-7.162805	1.814079	0.852602
H	-2.224089	4.784483	-1.090226	H	-7.697907	0.432613	-0.056156
N	1.736104	2.370717	0.124753	Cl	-0.041117	0.427957	2.319967
N	1.860144	1.079279	-0.058852	Cl	0.041009	-0.427687	-2.319883
C	3.133119	0.580956	-0.105997	C	-4.604505	1.179888	0.906193
C	3.351707	-0.650372	-0.787132	H	-4.781373	2.091383	1.467153
C	4.322895	1.254634	0.406893	C	-3.351853	0.650359	0.787081
C	5.690792	-0.475405	-0.293876	H	-2.506440	1.121366	1.273009
N	6.941450	-0.976740	-0.336478	N	-5.536159	-0.692894	-0.334076
H	7.162445	-1.814960	-0.851922	N	-4.266222	-2.444514	-1.021373
H	7.697722	-0.433389	0.056654	H	-3.408805	-2.979432	-1.014562
Ru	0.000031	0.000064	0.000059	H	-5.127450	-2.818353	-1.397355
H	2.224141	-4.784432	1.090084	N	-0.540578	1.982669	-0.385503
C	1.500742	-4.034865	0.802826	N	5.536117	0.692545	0.334212
C	1.645403	-2.679754	0.815997	C	4.604312	-1.180009	-0.906293
S	-0.088811	-4.484236	0.261697	H	4.781104	-2.091432	-1.467394
H	2.524149	-2.141392	1.137530	N	4.266389	2.444287	1.021544
N	0.540627	-1.982556	0.385569	H	3.409030	2.979295	1.014826
C	-0.474645	-2.800018	0.098425	H	5.127636	2.817944	1.397662
N	-1.736043	-2.370647	-0.124805	H	2.506252	-1.121272	-1.273092
N	-1.860160	-1.079242	0.058951				

Appendix Table C21 The optimized bond length of $[\text{Ru}(\text{TADAP})_2\text{Cl}_2]^+$.

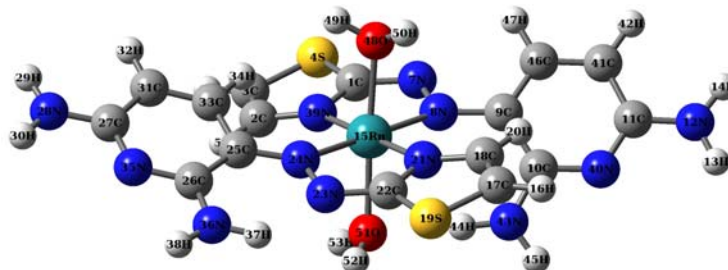
bond	distance (Å)	bond	distance (Å)	bond	distance (Å)	bond	distance (Å)
1,4	1.7355	10,49	1.0829	18,19	1.3629	28,29	1.3481
1,7	1.351	11,43	1.3391	18,20	1.7382	28,34	1.4325
1,42	1.3347	11,46	1.3402	19,21	1.0795	28,38	1.3351
2,3	1.3629	12,13	1.3481	19,22	1.3755	29,30	1.0085
2,5	1.0795	12,43	1.3351	20,23	1.7355	29,31	1.0108
2,42	1.3755	12,44	1.4325	22,23	1.3347	34,35	1.0848
3,4	1.7382	13,14	1.0085	23,24	1.351	34,36	1.3652
3,6	1.0806	13,15	1.0108	24,25	1.3103	36,37	1.0829
7,8	1.3103	16,22	2.0908	25,26	1.3678	39,40	1.0106
8,9	1.3679	16,25	2.1514	26,27	1.4603	39,41	1.0114
8,16	2.1513	16,32	2.3594	26,36	1.424	44,45	1.0848
9,10	1.424	16,33	2.3594	27,38	1.3391	46,47	1.0106
9,11	1.4603	16,42	2.0908	27,39	1.3402	46,48	1.0114
10,44	1.3652	17,18	1.0806				

Appendix Table C22 The optimized bond angle of $[\text{Ru}(\text{TADAP})_2\text{Cl}_2]^+$.

angle	degree	angle	degree	angle	degree	angle	degree
4,1,7	122.1094	13,12,43	116.5946	21,19,22	119.6192	28,29,31	118.8063
4,1,42	113.891	13,12,44	120.479	18,20,23	88.9519	30,29,31	118.784
7,1,42	123.4407	43,12,44	122.9256	16,22,19	138.2465	28,34,35	120.7164
3,2,5	125.812	12,13,14	121.9063	16,22,23	110.1463	28,34,36	117.8902
3,2,42	114.5641	12,13,15	118.8111	19,22,23	111.5829	35,34,36	121.375
5,2,42	119.6201	14,13,15	118.7897	20,23,22	113.8913	26,36,34	121.2012
2,3,4	110.9238	8,16,22	104.9028	20,23,24	122.1078	26,36,37	118.0861
2,3,6	128.0301	8,16,32	87.1929	22,23,24	123.4421	34,36,37	120.5623
4,3,6	121.0394	8,16,33	92.8089	23,24,25	112.2402	27,38,28	119.8479
1,4,3	88.9519	8,16,42	75.0978	16,25,24	114.1227	27,39,40	120.1726
1,7,8	112.2402	22,16,25	75.0963	16,25,26	128.5276	27,39,41	117.5548
7,8,9	116.8716	22,16,32	89.7241	24,25,26	116.8707	40,39,41	121.96
7,8,16	114.1257	22,16,33	90.2804	25,26,27	125.314	1,42,2	111.5834
9,8,16	128.5247	25,16,32	92.8078	25,26,36	118.3177	1,42,16	110.1465
8,9,10	118.3168	25,16,33	87.1904	27,26,36	116.2204	2,42,16	138.2462
8,9,11	125.3146	25,16,42	104.9032	26,27,38	121.6999	11,43,12	119.8479
10,9,11	116.2207	32,16,42	90.2773	26,27,39	122.4248	10,44,12	117.8899
9,10,44	121.2013	33,16,42	89.7182	38,27,39	115.83	10,44,45	121.3749
9,10,49	118.0864	17,18,19	128.0309	29,28,34	120.4785	12,44,45	120.7167
44,10,49	120.5619	17,18,20	121.0389	29,28,38	116.5951	11,46,47	120.1738
9,11,43	121.6994	19,18,20	110.9237	34,28,38	122.9257	11,46,48	117.5551
9,11,46	122.4264	18,19,21	125.8124	28,29,30	121.9003	47,46,48	121.9598
43,11,46	115.8288	18,19,22	114.5645				

Appendix Table C23 The optimized torsion angle of $[\text{Ru}(\text{TADAP})_2\text{Cl}_2]^+$.

plane	degree	plane	degree	plane	degree	plane	degree
7,1,4,3	169.52	8,9,10,44	177.92	19,22,42,1	-2.02	20,23,24,25	166.73
42,1,4,3	-2.17	8,9,10,49	2.35	19,22,42,2	179.99	22,23,24,25	4.16
4,1,7,8	-166.73	11,9,10,44	2.10	23,22,42,1	180.00	23,24,25,16	-19.15
42,1,7,8	4.16	11,9,10,49	-173.45	23,22,42,2	2.02	23,24,25,26	-168.09
4,1,42,2	3.21	8,9,11,43	179.33	22,16,25,24	-20.13	16,25,26,27	152.49
4,1,42,16	-175.34	8,9,11,46	1.88	22,16,25,26	168.14	16,25,26,36	-32.10
7,1,42,2	-168.36	10,9,11,43	-5.17	32,16,25,24	-109.09	24,25,26,27	-19.02
7,1,42,16	13.08	10,9,11,46	177.37	32,16,25,26	79.18	24,25,26,36	156.37
5,2,3,4	-178.12	9,10,44,12	1.58	33,16,25,24	70.90	25,26,27,38	-179.34
5,2,3,6	0.93	9,10,44,45	-176.85	33,16,25,26	-100.81	25,26,27,39	-1.88
42,2,3,4	1.16	49,10,44,12	177.04	42,16,25,24	159.86	36,26,27,38	5.17
42,2,3,6	-179.78	49,10,44,45	-1.40	42,16,25,26	-11.85	36,26,27,39	-177.37
3,2,42,1	-2.81	9,11,43,12	4.24	8,16,42,1	-16.36	25,26,36,34	-177.92
3,2,42,16	175.14	46,11,43,12	-178.14	8,16,42,2	165.66	25,26,36,37	-2.35
5,2,42,1	176.51	9,11,46,47	-9.91	25,16,42,1	163.63	27,26,36,34	-2.10
5,2,42,16	-5.52	9,11,46,48	176.37	25,16,42,2	-14.33	27,26,36,37	173.45
2,3,4,1	0.53	43,11,46,47	172.50	32,16,42,1	70.66	26,27,38,28	-4.23
6,3,4,1	-178.59	43,11,46,48	-1.21	32,16,42,2	-107.31	39,27,38,28	178.15
1,7,8,9	168.09	43,12,13,14	-175.06	33,16,42,1	-109.34	26,27,39,40	9.91
1,7,8,16	-19.15	43,12,13,15	-3.21	33,16,42,2	72.67	26,27,39,41	-176.38
7,8,9,10	-156.35	44,12,13,14	4.64	17,18,19,21	-0.93	38,27,39,40	-172.49
7,8,9,11	19.04	44,12,13,15	176.49	17,18,19,22	179.78	38,27,39,41	1.20
16,8,9,10	32.10	13,12,43,11	179.52	20,18,19,21	178.12	34,28,29,30	-4.73
16,8,9,11	-152.49	44,12,43,11	-0.17	20,18,19,22	-1.15	34,28,29,31	-176.44
7,8,16,22	-159.87	13,12,44,10	177.52	17,18,20,23	178.59	38,28,29,30	174.98
7,8,16,32	-70.90	13,12,44,45	-4.01	19,18,20,23	-0.53	38,28,29,31	3.27
7,8,16,33	109.08	43,12,44,10	-2.78	18,19,22,16	-175.13	29,28,34,35	4.02
7,8,16,42	20.12	43,12,44,45	175.66	18,19,22,23	2.80	29,28,34,36	-177.51
9,8,16,22	11.85	8,16,22,19	14.33	21,19,22,16	5.53	38,28,34,35	-175.67
9,8,16,32	100.82	8,16,22,23	-163.63	21,19,22,23	-176.51	38,28,34,36	2.78
9,8,16,33	-79.18	25,16,22,19	-165.66	18,20,23,22	2.17	29,28,38,27	-179.53
9,8,16,42	-168.14	25,16,22,23	16.36	18,20,23,24	-169.52	34,28,38,27	0.17
7,8,25,24	-180.00	32,16,22,19	-72.68	16,22,23,20	175.33	28,34,36,26	-1.58
7,8,25,26	8.27	32,16,22,23	109.34	16,22,23,24	-13.09	28,34,36,37	-177.04
9,8,25,24	-8.27	33,16,22,19	107.31	19,22,23,20	-3.21	35,34,36,26	176.86
9,8,25,26	180.00	33,16,22,23	-70.65	19,22,23,24	168.36	35,34,36,37	1.40

2.8 $[\text{Ru}(\text{TADAP})_2(\text{H}_2\text{O})_2]^{3+}$ **Appendix Figure C9** The optimized structure of $[\text{Ru}(\text{TADAP})_2(\text{H}_2\text{O})_2]^{3+}$.**Appendix Table C24** The standard orientation of $[\text{Ru}(\text{TADAP})_2(\text{H}_2\text{O})_2]^{3+}$.

	X	Y	Z		X	Y	Z
C	-0.544656	2.924348	0.041561	N	7.053495	0.726782	-0.594603
C	1.557907	2.889214	0.796678	H	7.292541	1.623452	-0.998893
C	1.338409	4.250036	0.768055	H	7.812923	0.110344	-0.321590
S	-0.236917	4.627107	0.197452	C	4.693829	1.164015	-0.854978
H	2.476846	2.419891	1.120192	H	4.885614	2.126001	-1.319011
H	2.031052	5.031920	1.055048	C	3.428690	0.706383	-0.662344
N	-1.779824	2.453112	-0.181839	H	2.584800	1.307004	-0.976446
N	-1.883317	1.160495	0.003293	N	5.602564	-0.902642	0.064348
C	-3.194703	0.718004	-0.131553	N	4.294360	-2.625349	0.717418
C	-3.752501	-0.309158	0.760717	H	3.405724	-3.105548	0.771086
C	-5.813765	-0.183684	-0.265748	H	5.166522	-3.102093	0.926288
N	-7.055040	-0.653225	-0.356195	N	0.506170	2.128529	0.361098
H	-7.355692	-1.399517	0.264998	N	-5.000308	-0.746990	0.637927
H	-7.740277	-0.264448	-0.994878	C	-5.388658	0.903273	-1.129177
Ru	-0.006294	0.111271	0.023713	H	-6.079542	1.341011	-1.842933
H	-2.343384	-4.677050	-0.793648	N	-3.042194	-0.787581	1.789563
C	-1.595212	-3.927129	-0.572588	H	-2.100335	-0.486391	2.005860
C	-1.718607	-2.570982	-0.644236	H	-3.516771	-1.414653	2.431619
S	-0.004790	-4.386209	-0.051876	C	-4.093418	1.340673	-1.034170
H	-2.610701	-2.043756	-0.951230	H	-3.731867	2.143717	-1.665911
N	-0.585941	-1.866585	-0.282317	O	-0.048032	0.456455	-2.094890
C	0.423470	-2.704772	0.026100	H	0.800995	0.659596	-2.527817
N	1.690477	-2.298417	0.241658	H	-0.433083	-0.285320	-2.597557
N	1.877591	-1.004476	-0.005900	O	-0.062730	-0.259738	2.165453
C	3.164999	-0.589148	-0.108418	H	0.427572	-1.054132	2.453322
C	4.373548	-1.392766	0.217785	H	0.260041	0.476640	2.718472
C	5.795859	0.312310	-0.450227				

Appendix Table C25 The optimized bond length of $[\text{Ru}(\text{TADAP})_2(\text{H}_2\text{O})_2]^{3+}$.

bond	distance (Å)	bond	distance (Å)	bond	distance (Å)	bond	distance (Å)
1,4	1.7374	11,12	1.3302	19,22	1.7369	31,32	1.0851
1,7	1.3407	11,40	1.34	21,22	1.3478	31,33	1.3591
1,39	1.3563	11,41	1.4518	22,23	1.3479	33,34	1.0824
2,3	1.3787	12,13	1.0165	23,24	1.3306	36,37	1.0115
2,5	1.0814	12,14	1.0142	24,25	1.3566	36,38	1.0157
2,39	1.3691	15,21	2.0836	25,26	1.4875	41,42	1.0855
3,4	1.7174	15,24	2.1897	25,33	1.4334	41,46	1.3704
3,6	1.0833	15,39	2.1085	26,35	1.332	43,44	1.0122
7,8	1.3099	15,48	2.1469	26,36	1.3324	43,45	1.0152
8,9	1.3906	15,51	2.1744	27,28	1.332	46,47	1.0838
8,15	2.1505	16,17	1.0821	27,31	1.4504	48,49	0.9744
9,10	1.4705	17,18	1.3636	27,35	1.3335	48,50	0.9753
9,46	1.4178	17,19	1.7353	28,29	1.0122	51,52	0.9769
10,40	1.3281	18,20	1.0808	28,30	1.0155	51,53	0.9758
10,43	1.3386	18,21	1.3821				

Appendix Table C26 The optimized bond angle of $[\text{Ru}(\text{TADAP})_2(\text{H}_2\text{O})_2]^{3+}$.

angle	degree	angle	degree	angle	degree	angle	degree
4,1,7	121.5073	11,12,14	122.5465	19,22,21	114.0231	31,33,34	119.8536
4,1,39	114.6255	13,12,14	117.804	19,22,23	122.0591	26,35,27	120.8931
7,1,39	123.1457	8,15,21	102.6458	21,22,23	123.5788	26,36,37	120.7504
3,2,5	124.7416	8,15,39	75.3372	22,23,24	113.3023	26,36,38	117.4079
3,2,39	114.8022	8,15,48	83.9853	15,24,23	111.8387	37,36,38	121.376
5,2,39	120.4531	8,15,51	94.0111	15,24,25	131.4121	1,39,2	110.1272
2,3,4	111.6938	21,15,24	75.74	23,24,25	116.437	1,39,15	109.5939
2,3,6	127.2378	21,15,48	90.1303	24,25,26	126.0882	2,39,15	140.2789
4,3,6	121.0684	21,15,51	88.5951	24,25,33	118.7158	10,40,11	119.6119
1,4,3	88.6879	24,15,39	106.2933	26,25,33	115.0583	11,41,42	120.4374
1,7,8	113.3329	24,15,48	94.8935	25,26,35	121.7074	11,41,46	118.3263
7,8,9	112.0126	24,15,51	87.0599	25,26,36	122.2573	42,41,46	121.2262
7,8,15	114.4467	39,15,48	90.5044	35,26,36	116.0045	10,43,44	123.4784
9,8,15	131.9747	39,15,51	90.6843	28,27,31	120.2921	10,43,45	117.3083
8,9,10	121.4098	16,17,18	128.0175	28,27,35	117.5277	44,43,45	118.9217
8,9,46	121.3168	16,17,19	120.7718	31,27,35	122.1783	9,46,41	120.204
10,9,46	116.9124	18,17,19	111.2107	27,28,29	122.813	9,46,47	119.0144
9,10,40	122.0447	17,18,20	125.0834	27,28,30	119.2122	41,46,47	120.755
9,10,43	120.9793	17,18,21	114.7686	29,28,30	117.9366	15,48,49	117.0647
40,10,43	116.8582	20,18,21	120.1479	27,31,32	120.3725	15,48,50	113.2033
12,11,40	117.6416	17,19,22	89.0457	27,31,33	118.0345	49,48,50	105.8766
12,11,41	119.8072	15,21,18	138.6118	32,31,33	121.5765	15,51,52	114.5811
40,11,41	122.5511	15,21,22	110.3873	25,33,31	122.0281	15,51,53	114.8892
11,12,13	119.5784	18,21,22	110.9005	25,33,34	118.0495	52,51,53	106.2977

Appendix Table C27 The optimized torsion angle of $[\text{Ru}(\text{TADAP})_2(\text{H}_2\text{O})_2]^{3+}$.

plane	degree	plane	degree	plane	degree	plane	degree
7,1,4,3	168.48	8,9,46,47	3.18	24,15,39,1	163.77	18,21,22,23	170.92
39,1,4,3	-2.07	10,9,46,41	-5.48	24,15,39,2	-16.11	19,22,23,24	166.77
4,1,7,8	-166.58	10,9,46,47	176.37	48,15,39,1	68.52	21,22,23,24	-6.13
39,1,7,8	3.15	9,10,40,11	-4.419	48,15,39,2	-111.36	22,23,24,15	20.20
4,1,39,2	2.77	43,10,40,11	171.66	51,15,39,1	-109.08	22,23,24,25	-165.47
4,1,39,15	-177.14	9,10,43,44	-0.56	51,15,39,2	71.02	15,24,25,26	163.68
7,1,39,2	-167.60	9,10,43,45	173.15	8,15,48,49	142.46	15,24,25,33	-20.80
7,1,39,15	12.46	40,10,43,44	-176.69	8,15,48,50	-93.94	23,24,25,26	-9.28
5,2,3,4	-179.97	40,10,43,45	-2.97	21,15,48,49	-114.83	23,24,25,33	166.22
5,2,3,6	0.06	40,11,12,13	1.32	21,15,48,50	8.75	24,25,26,35	178.93
39,2,3,4	0.65	40,11,12,14	178.19	24,15,48,49	-39.13	24,25,26,36	-3.16
39,2,3,6	-179.29	41,11,12,13	-178.56	24,15,48,50	84.45	33,25,26,35	3.27
3,2,39,1	-2.17	41,11,12,14	-1.70	39,15,48,49	67.26	33,25,26,36	-178.82
3,2,39,15	177.71	12,11,40,10	179.95	39,15,48,50	-169.14	24,25,33,31	-176.81
5,2,39,1	178.42	41,11,40,10	-0.15	49,48,51,52	-64.86	24,25,33,34	0.16
5,2,39,15	-1.68	12,11,41,42	0.49	49,48,51,53	59.75	26,25,33,31	-0.81
2,3,4,1	0.76	12,11,41,46	-178.36	50,48,51,52	59.12	26,25,33,34	176.15
6,3,4,1	-179.28	40,11,41,42	-179.39	50,48,51,53	-176.25	25,26,35,27	-3.20
1,7,8,9	175.22	40,11,41,46	1.74	8,15,51,52	153.03	36,26,35,27	178.77
1,7,8,15	-17.29	8,15,21,18	10.93	8,15,51,53	-83.43	25,26,36,37	8.62
7,8,9,10	-140.40	8,15,21,22	-164.89	21,15,51,52	50.45	25,26,36,38	-179.09
7,8,9,46	32.48	24,15,21,18	-167.94	21,15,51,53	173.98	35,26,36,37	-173.36
15,8,9,10	54.98	24,15,21,22	16.22	24,15,51,52	-25.33	35,26,36,38	-1.08
15,8,9,46	-132.12	48,15,21,18	-72.92	24,15,51,53	98.19	31,27,28,29	-1.18
7,8,15,21	-162.53	48,15,21,22	111.23	39,15,51,52	-131.61	31,27,28,30	-178.88
7,8,15,39	18.34	51,15,21,18	104.73	39,15,51,53	-8.08	35,27,28,29	178.32
7,8,15,48	-73.75	51,15,21,22	-71.10	16,17,18,20	-0.59	35,27,28,30	0.62
7,8,15,51	108.00	18,21,39,1	-4.83	16,17,18,21	179.26	28,27,31,32	2.74
9,8,15,21	1.77	18,21,39,2	174.20	19,17,18,20	179.47	28,27,31,33	-178.70
9,8,15,39	-177.33	22,21,39,1	-179.73	19,17,18,21	-0.67	35,27,31,32	-176.73
9,8,15,48	90.55	22,21,39,2	-0.68	16,17,19,22	179.44	35,27,31,33	1.80
9,8,15,51	-87.67	21,15,24,23	-20.39	18,17,19,22	-0.61	28,27,35,26	-178.89
7,8,24,23	177.46	21,15,24,25	166.38	17,18,21,15	-173.78	31,27,35,26	0.60
7,8,24,25	3.30	39,15,24,23	158.75	17,18,21,22	2.03	27,31,33,25	-1.53
9,8,24,23	-19.07	39,15,24,25	-14.46	20,18,21,15	6.07	27,31,33,34	-178.45
9,8,24,25	166.75	48,15,24,23	-109.28	20,18,21,22	-178.10	32,31,33,25	176.99
8,9,10,40	-179.56	48,15,24,25	77.49	17,19,22,21	1.81	32,31,33,34	0.07
8,9,10,43	4.50	51,15,24,23	68.89	17,19,22,23	-171.72	11,41,46,9	1.35
46,9,10,40	7.24	51,15,24,25	-104.31	15,21,22,19	174.55	11,41,46,47	179.46
46,9,10,43	-168.68	8,15,39,1	-15.12	15,21,22,23	-12.02	42,41,46,9	-177.49
8,9,46,41	-178.67	8,15,39,2	164.98	18,21,22,19	-2.49	42,41,46,47	0.61

APPENDIX D

Nucleic Acid Purity Assessment Using A260/A280 Ratios

A common practice in molecular biology is to perform a quick assessment of the purity of nucleic acid samples by determining the ratio of spectrophotometric absorbance of the sample at 260 nm to that of 280 nm. The basis of this test rests on the Beer-Lambert Law:

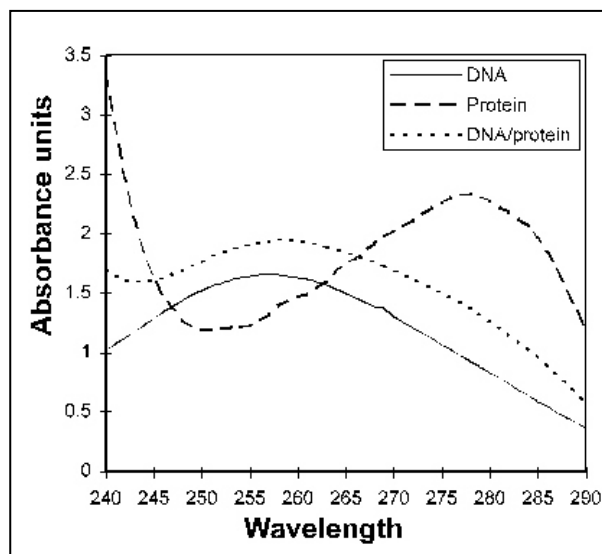
$$A = \epsilon C b \quad \text{--- (1)}$$

Where the absorbance (A) is the product of the extinction coefficient (ϵ), the concentration of the sample (C), and the optical pathlength (b). With an optical pathlength of 1 cm, which is commonly used in spectrophotometers, the pathlength can be ignored and extinction coefficients can be explained as an absorbance value at a specific concentration as seen in the equation below.

$$\epsilon = A/C \quad \text{--- (2)}$$

The commonly accepted average extinction coefficients for 1 mg/ml nucleic acid solutions at 260 nm and 280 nm is 20 and 10 respectively. Similarly the extinction coefficient values at 260 nm and 280 nm at a concentration of 1 mg/ml are 0.57 and 1.00 respectively for proteins. Thus in relative terms, nucleic acid samples would be expected to have a higher absorbance at 260 nm than at 280 nm, while with a protein sample, the inverse would be true. Using these extinction coefficients, pure nucleic acid samples would have an A_{260}/A_{280} ratio of 2.0, while protein would be 0.57. Samples that contain a mixture of protein and DNA would of course be influenced by both macromolecules. The theoretical A_{260}/A_{280} ratio for samples that contain a mixture of protein and nucleic acid can be estimated by using the following formula:

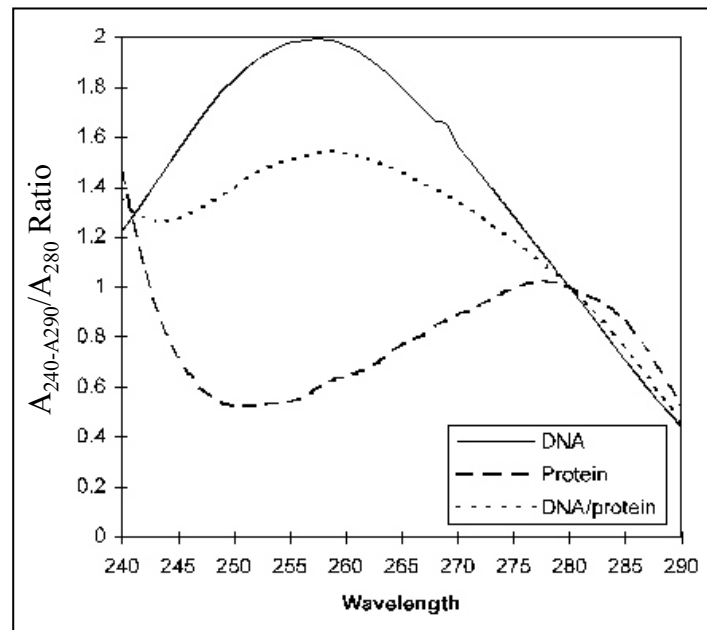
$$\frac{A_{260}}{A_{280}} = \frac{(\epsilon_{260}p \times (\%P) + \epsilon_{260}n \times (\%N))}{(\epsilon_{280}p \times (\%P) + \epsilon_{280}n \times (\%N))} \quad \text{--- (3)}$$



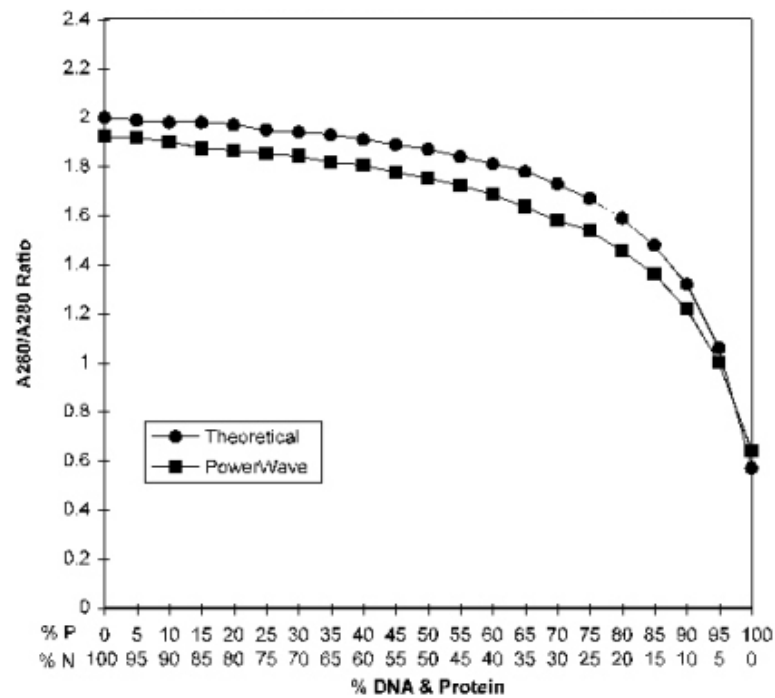
Appendix Figure D10 Absorbance profiles of DNA and protein samples from 240 nm to 290 nm.

The data depicted in Appendix Figure D10 demonstrates the positioning of peak absorbance of pure DNA and protein solutions, as well as a mixture of the two macromolecules. The peak in absorbance for DNA was at 257 nm and for protein was at 277 nm. A 10:1(w/w) mixture DNA/protein results in a peak absorbance at 259 nm and an absorbance profile very similar in shape as that demonstrated by pure DNA with a small increase at wavelength below 240 nm and represents a sum of the two absorbance patterns of the macromolecules.

A_{280} ratio measurements were then calculated by dividing the absorbance determination at each wavelength by the A_{280} determination for that sample as shown in Appendix Figure D11. It was found that samples containing only protein demonstrate a peak at 280 nm, reflecting the maximal absorbance of proteins at this wavelength. The sample containing a mixture of DNA and protein demonstrates a profile very similar to that of pure DNA in shape, but with values that are much lower, despite having equivalent amounts of nucleic acid in both samples.



Appendix Figure D11 A_{280} ratio of samples containing DNA and/or protein at wavelengths from 240 nm to 290 nm.



Appendix Figure D12 Comparison of theoretical A_{260}/A_{280} ratios with those determined using the PowerWave 200 scanning microplate spectrophotometer.

The absorbance of various mixtures of DNA and protein were determined at 260 nm and 280 nm. Subsequently the A_{260}/A_{280} ratios were determined for each mixture and compared to the theoretical value calculated from the extinction coefficients. Filled circles indicates theoretical ratios while filled boxed denote experimentally determined ratios. When the A_{260}/A_{280} ratio is determined for a range of different DNA/protein mixtures one finds that the ratio is relatively insensitive to the addition of protein to pure nucleic acid. As demonstrated in Appendix Figure D12 as increasing percentages of protein are measured little change is seen in the A_{260}/A_{280} ratio until the percentage of protein is approximately 75%. Interestingly, even when equal amounts of nucleic acid and protein by weight are determined a ratio of 1.75, is still returned. DNA or protein only samples were found to have A_{260}/A_{280} ratios of 1.92 and 0.64, respectively.

It is important to note that the A_{260}/A_{280} ratio is only an indication of purity rather than a precise answer. Pure DNA and RNA preparations have expected A_{260}/A_{280} ratios of ≥ 1.8 and ≥ 2.0 respectively and are based on the extinction coefficients of nucleic acids at 260 nm and 280 nm. There are several factors that may affect A_{260}/A_{280} ratios. The 260 nm measurements are made very near the peak of the absorbance spectrum for nucleic acids, while the 280 nm measurement is located in a portion of the spectrum that has a very steep slope. As a result, very small differences in the wavelength in and around 280 nm will effect greater changes in the A_{260}/A_{280} ratio than small differences at 260 nm. Consequently, different instruments will result in slightly different A_{260}/A_{280} ratios on the same solution due to the variability of wavelength accuracy between instruments. Individual instruments, however, should give consistent results. Concentration can also affect the results, as dilute samples will have very little difference between the absorbance at 260 nm and that at 280 nm. With very small differences, the detection limit and resolution of the instrument measurements begin to become much more significant. The type(s) of protein present in a mixture of DNA and protein can also affect the A_{260}/A_{280} ratio determination. Absorbance in the UV range of proteins is primarily the result of aromatic ring structures. Proteins are composed of 22 different amino acids of which only three contain aromatic side chains. Thus the amino acid sequence of proteins would be

expected to have a tremendous influence on the ability of a protein to absorb light at 280 nm.

APPENDIX E

Calculation of the percentage of elements of TADAP

Molecular formula of TADAP is $C_8H_8N_6S$. From molecular weight of TADAP (220.254 g/mol), the percentage of elements of TADAP can be determined as followed:

$$\begin{aligned}\text{Percentage of carbon} &= \frac{\text{number of carbon} \times \text{atomic weight of carbon}}{\text{Molecular weight of TADAP}} \times 100 \\ &= \frac{8 \times 12.011}{220.254} \times 100 \\ &= 43.64\%\end{aligned}$$

$$\begin{aligned}\text{Percentage of hydrogen} &= \frac{\text{number of hydrogen} \times \text{atomic weight of hydrogen}}{\text{Molecular weight of TADAP}} \times 100 \\ &= \frac{8 \times 1.008}{220.254} \times 100 \\ &= 3.66\%\end{aligned}$$

$$\begin{aligned}\text{Percentage of nitrogen} &= \frac{\text{number of nitrogen} \times \text{atomic weight of nitrogen}}{\text{Molecular weight of TADAP}} \times 100 \\ &= \frac{6 \times 14.007}{220.254} \times 100 \\ &= 38.16\%\end{aligned}$$

$$\begin{aligned}\text{Percentage of sulfur} &= \frac{\text{number of sulfur} \times \text{atomic weight of sulfur}}{\text{Molecular weight of TADAP}} \times 100 \\ &= \frac{1 \times 32.066}{220.254} \times 100 \\ &= 14.56\%\end{aligned}$$

CIRRICULUM VITAE

NAME : Mr. Ratanon Chotima

BIRTH DATE : August 22, 1983

BIRTH PLACE : Chanthaburi, Thailand

EDUCATION	<u>YEAR</u>	<u>INSTITUTE</u>	<u>DEGREE/DIPLOMA</u>
	2006	Kasetsart Univ.	B.Sc. (Chemistry)

POSITION/TITLE : Postgraduated student

WORKPLACE : Faculty of Science, Kasetsart University

SCHOLARSHIP/AWARDS :

- Development and Promotion of Science and Technology Talents Project (DPST)
- Center for Innovation in Chemistry: Postgraduate Education and Research Program in Chemistry (PERCH-CIC)
- Outstanding Poster Award at PACCON 2008 (Pure and Applied Chemistry International Conference) 31 Jan – 2 Feb 2008